MEMOIRS

OF THE

COLLEGE OF SCIENCE

UNIVERSITY OF KYOTO

THE
PHYSICAL
SOCIETY

SERIES A

VOL. XXV, NOs. 3 & 4.

December 1949

KYOTO

Memoirs of the College of Science, University of Kyoto, Series A,
Vol. XXV, Nos. 3 & 4, Article 17, 1949.

On a Method of Plunging of R_2 with Symmetric Projective Connexion into a Projective Space S_4.

By

Joyo Kanitani

(Received May 24, 1948)

1. According to the result of a previous paper[1], a two-dimensional space R_2 with a symmetric projective connexion $d\omega_\alpha^\beta = \Gamma_{\alpha i}^\beta dx^i$ $(\alpha, \beta = 0, 1, 2)$ can be so plunged into a four-dimensional projective space S_4 that the space R_2 becomes a ruled surface in S_4. In this paper we investigate another way of plunging of R_2 into S_4.

By assumption we have

$$\Gamma_{ij}^\beta = \Gamma_{ji}^\beta \quad (\beta = 0, 1, 2, i, j = 1, 2),$$

and we may suppose always that

$$d\omega_0^0 = 0, \quad d\omega_0^1 = dx^1, \quad d\omega_0^2 = dx^2.$$

Consider a dominant projective connexion $d\Omega_\sigma^\tau = H_{\sigma i}^\tau dx^i$ $(\sigma, \tau = 0, 1, 2, 3, 4)$ subjected to the condition[2]

$$\left.\begin{aligned} &H_{\alpha i}^\beta = \Gamma_{\alpha i}^\beta \ (\alpha, \beta, = 0, 1, 2\,;\ i = 1, 2), \\ &H_{0i}^p = 0 \ (p = 3, 4\,;\ i = 1, 2) \end{aligned}\right\} \tag{1}$$

$$\left.\begin{aligned} H_{11}^3 &= 1, & H_{11}^4 &= 0, \\ H_{12}^3 &= 0, & H_{12}^4 &= 0, \\ H_{22}^3 &= 0, & H_{22}^4 &= 1. \end{aligned}\right\} \tag{2}$$

1. J. Kanitani: Sur l'espace à connexion projective majorante, II, Jap. Jour. of Math. **19**, 395 (1948).

2. We denote by α, β, γ the suffixes which take the values 0, 1, 2; by $h, i, j, , k, l, m$ those which take the values 1, 2; by σ, τ, ρ those which take the values 0, 1, 2, 3, 4; by p, q, r those which take the values 3, 4.

We shall now prove that H_{pi}^{τ} $(\tau = 0, 1, 2, 3, 4\ ;\ i = 1, 2\ ;\ p = 3, 4)$ can be so determined that the tensor of curvature $T_{\sigma ij}^{\tau}$ of the connexion $d\Omega_{\sigma}^{\tau}$ becomes zero.

2. Put

$$R_{\sigma ij}^{\tau} = \frac{\partial H_{\sigma i}^{\tau}}{\partial x^{j}} - \frac{\partial H_{\sigma j}^{\tau}}{\partial x^{i}} + H_{\sigma i}^{\gamma} H_{\gamma j}^{\tau} - H_{\sigma j}^{\gamma} H_{\gamma i}^{\tau},$$

$$(\sigma, \tau = 0, 2, 3, 4\ ;\ i, j = 1, 2)$$

so that[3] for $\alpha, \beta = 0, 1, 2$ $R_{\alpha ij}^{\beta}$ becomes the tensor of curvature of the given connexion $d\omega_{\alpha}^{\beta}$ while we have, when $\sigma \leqq 2$, $\tau > 2$,

$$R_{012}^{3} = R_{012}^{4} = 0, \qquad R_{h12}^{3} = -\Gamma_{h2}^{1}, \qquad R_{h11}^{4} = \Gamma_{h1}^{2} \qquad (h = 1, 2).$$

The equation $T_{\alpha 12}^{\tau} = 0$ can be written as[4]

$$R_{\alpha 12}^{\tau} + \Gamma_{\alpha 1}^{q} \Gamma_{q2}^{\tau} - \Gamma_{\alpha 2}^{q} \Gamma_{q1}^{\tau} = 0.$$

We get therefore

$$\Gamma_{32}^{\tau} = R_{121}^{\tau}, \qquad \Gamma_{41}^{\tau} = R_{212}^{\tau} \qquad (\tau = 0, 1, 2, 3\ 4).$$

If we substitute these values of Γ_{32}^{τ}, Γ_{41}^{τ}, the equation $\Gamma_{p12}^{\sigma} = 0$ becomes

$$\left.\begin{aligned} \frac{\partial \Gamma_{31}^{\sigma}}{\partial x^{2}} &= \frac{\partial R_{121}^{\sigma}}{\partial x^{1}} - \Gamma_{31}^{\alpha} \Gamma_{\alpha 2}^{\sigma} - \Gamma_{31}^{3} R_{121}^{\sigma} - \Gamma_{31}^{4} \Gamma_{42}^{\sigma} \\ &\quad + R_{121}^{\alpha} \Gamma_{\alpha 1}^{\sigma} + R_{121}^{3} \Gamma_{31}^{\sigma} + R_{121}^{4} R_{212}^{\sigma}, \\ \frac{\partial \Gamma_{42}^{\sigma}}{\partial x^{1}} &= \frac{\partial R_{212}^{\sigma}}{\partial x^{2}} + R_{212}^{\alpha} \Gamma_{\alpha 2}^{\sigma} + R_{212}^{3} R_{121}^{\sigma} + R_{212}^{4} \Gamma_{42}^{\sigma} \\ &\quad - \Gamma_{42}^{\alpha} \Gamma_{\alpha 1}^{\sigma} - \Gamma_{42}^{3} \Gamma_{31}^{\sigma} - \Gamma_{42}^{4} R_{212}^{\sigma}. \end{aligned}\right\} \qquad (3)$$

Thus the functions Γ_{31}^{σ}, Γ_{42}^{σ} are determined as solutions of this system of simultaneous partial differential equations. Now suppose that the functions Γ_{ij}^{α} $(\alpha = 0, 1, 2\ ;\ i, j = 1, 2)$ are analytic in the vicinity of x_0^i. Let $\Phi_{31}^{\sigma}(x^1)$ and $\Phi_{42}^{\sigma}(x^2)$ be arbitrary functions which are analytic in the vicinity of x_0^1 and x_0^2 respectively. Then the system (3) admits one and only one system of solutions Γ_{31}^{σ}, Γ_{42}^{σ} $(\sigma = 0, 1, 2, 3, 4)$ such that Γ_{31}^{σ} are reduced to $\Phi_{31}^{\sigma}(x^1)$ when $x^2 = x_0^2$, while Γ_{42}^{σ} are reduced to $\Phi_{42}^{\sigma}(x^2)$ when $x^1 = x_0^1$.

3. By the said convention, the summation is made from 0 to 2 with respect to γ.

4. The summation is made from 3 to 4 with respect to q.

This can be proved by the method of dominant function. Put

$$x = x^1 - x_0^1, \qquad y = y^1 - y_0^1,$$

$$Z^\sigma(x, y) = \Gamma_{31}^\sigma(x + x_0^1, y + x_0^2) - \Phi_{31}^\sigma(x + x_0^1),$$

$$W^\sigma(x, y) = \Gamma_{42}^\sigma(x + x_0^1, y + x_0^2) - \Phi_{42}^\sigma(y + x_0^2).$$

Then the system of equations (3) can be written in the form:

$$\frac{\partial Z^\sigma}{\partial y} = F_1(x, y, Z^\sigma, W^\tau), \qquad \frac{\partial W^\sigma}{\partial x} = F_2(x, y, Z^\sigma, W^\tau). \tag{4}$$

$$(\sigma, \tau = 0, 1, 2, 3, 4)$$

Making use of these equations and

$$Z^\sigma(x, 0) = W^\sigma(0, y) = 0,$$

we can evaluate the successive partial derivatives of Z^σ, W^σ for $x = y = 0$ in only one way. To verify the convergency of Taylor's series with the coefficients thus determined, we consider the system of equations

$$\frac{\partial Z^\sigma}{\partial y} = \frac{M}{1 - \frac{1}{\rho}(x + y + Z^0 + W^0 + \cdots + Z^5 + W^5)},$$

$$\frac{\partial W^\sigma}{\partial x} = \frac{M}{1 - \frac{1}{\rho}(x + y + Z^0 + W^0 + \cdots + Z^5 + W^5)},$$

where ρ, M are the constants such that

$$|F_1| < M, \ |F_2| < M \text{ for } |x| + |y| + |Z^0| + \cdots\cdots + |W^5| < \rho.$$

If we put

$$Z^\sigma = W^\sigma = f(x + y), \qquad x + y = u,$$

this system are reduced to the ordinary differential equation

$$\frac{df}{du} = \frac{M}{1 - \frac{1}{\rho}(u + 10f)},$$

which admits an analytical solution satisfying the condition $f(0) = 0$.

3. Conversely, suppose that, in a four-dimensional projective space S_4, there exists a surface V_2 whose generic point A_0 are defined by

$$dA_\sigma = H^\tau_{\sigma i}\, dx^i\, A_\tau ,$$

where $H^\beta_{\alpha i}$, H^p_{0i} ($\alpha, \beta = 0, 1, 2$; $i = 1, 2$; $p = 3, 4$) are subjected to the condition (1) and

$$|A_0\ A_1\ A_2\ A_3\ A_4| \neq 0 .$$

Let B^σ_τ be algebraic complement of A^τ_σ, divided by this determinant. We can take B^σ_0, B^σ_1, B^σ_2, B^σ_3, B^σ_4 as coordinates of the hyper-plane

$$B^\sigma = A_0 \cdots A_{\sigma-1}\ A_{\sigma+1} \cdots A_4 ,$$

and we have

$$dB^\sigma = - H^\sigma_{\tau i}\, dx^i\, B^\tau .$$

A hyper-plane passing through the tangent plane $A_0 A_1 A_2$ of V_2 at A is expressed by $\nu_p B^p$. When we associate such hyper-plane to every point A_0 of V_2, the characteristic of the envelope of the hyper-planes along a curve C on V_2 is the intersection of the hyper-planes $\nu_p B^p$, $d(\nu_p B^p)$. This intersection will coincide with the tangent plane $A_0 A_1 A_2$ if and only if

$$\nu_p H^p_{1i}\, dx^i = 0, \qquad \nu_p H^p_{2i}\, dx^i = 0.$$

Eliminating ν_3, ν_4 from these equations we get

$$\begin{vmatrix} H^3_{11}\, dx^1 + H^3_{12}\, dx^2 & H^3_{21}\, dx^1 + H^3_{22}\, dx^2 \\ H^4_{11}\, dx^1 + H^4_{12}\, dx^2 & H^4_{21}\, dx^1 + H^4_{22}\, dx^2 \end{vmatrix} = 0 .$$

If the osculating planes at a point A_0 of the curves lying on V_2 and passing through A_0 are not all contained in a hyper-plane, there exist two families of curves satisfying this equation. We shall call them characteristic curves of V_2. Taking these curves as parameter curves and performing a transformation of the form

$$A_3 = \mu^3_3 A^1_3 + \mu^4_3 A^1_4 , \qquad A_4 = \mu^3_4 A^1_3 + \mu^4_4 A^1_4 ,$$

we can deduce the equations (2).

Hence we have the following proposition.

A space $\boldsymbol{R}_2$ *with a symmetric projective connexion can be so plunged into* $\boldsymbol{S}_4$ *that* $\boldsymbol{R}_2$ *becomes a surface* V_2 *and a net of curves arbitrarily given upon* $\boldsymbol{R}_2$ *becomes the net of characteristic curves of* V_2.

Since $\Phi_{31}^{\sigma}(x^1)$ and $\Phi_{42}^{\sigma}(x^2)$ to which Γ_{31}^{σ}, Γ_{42}^{σ} are reduced for $x^2 = x_0^2$ and $x^1 = x_0^1$ respectively may be arbitrary functions, we can say as follows:

Let C, C' *be any two geodesics on* $\boldsymbol{R}_2$ *passing through a point and having distinct tangents at this point. Then the space* $\boldsymbol{R}_2$ *can be so plunged into* $\boldsymbol{S}_4$ *that the curves* C, C' *become conics on* V_2.

Memoirs of the College of Science, University of Kyoto, Series A,
Vol. XXV, Nos. 3 & 4, Article 18, 1949.

Basis-Theorem concerning Differential Polynomials

By

Kôtaro Okugawa

(Received May 18, 1948)

---

1. Differential polynomials. Let x be the independent complex variable and $y_1, \cdots, y_n$ the indeterminate analytic functions of x. We denote by y_{ij} the j th derivative of y_i $(i = 1, \cdots, n\,;\ j = 0, 1, 2, \cdots)$. The algebraic properties of the following two kinds of *differential polynomials* of $y_1, \cdots \cdots, y_n$ are important in the theory of systems of ordinary differential equations in the unknown functions $y_1, \cdots, y_n$:

1^0) Let $\mathfrak{F}$ be an arbitrary field which is constituted of functions, meromorphic in a fixed open domain D of the x-plane, and which is closed with respect to the differentiation. Any polynomial of y_{ij} $(i = 1, \cdots, n\,;\ j = 0, 1, 2, \cdots)$ with coefficients from $\mathfrak{F}$ is called an *algebraic differential polynomial*. We shall denote by $\mathfrak{P}_0$ the totality of all such polynomials.

2^0) Let $\mathfrak{A}$ be the totality of all functions of $x, y_1, \cdots, y_n$ which are analytic at $(x, y_1, \cdots, y_n) = (0, 0, \cdots, 0)$. Any polynomial of y_{ij} $(i = 1, \cdots \cdots, n\,;\ j = 1, 2, \cdots)$ with coefficients in $\mathfrak{A}$ will be called a *differential pseudopolynomial*. The totality of all such polynomials will be denoted by $\mathfrak{P}$.

Both $\mathfrak{P}_0$, $\mathfrak{P}$ are integral domains which are closed with respect to the differentiation.[1]

2. Basis-theorem. One of the first results, concerning these rings $\mathfrak{P}_0$ and $\mathfrak{P}$, is *the basis-theorem of Ritt.*

Let Σ be any subset of $\mathfrak{P}$ $(\mathfrak{P}_0)$. A finite subset Φ of Σ is called a *basis* of Σ if and only if there exists, for every element G of Σ, a positive integer p such that G^p is a linear combination of the elements of Φ and

1. The introductory monograph on these subjects: Ritt, J. F., Differential Equations from the Algebraic Standpoint, Amer. Math. Soc. Colloq. Publ., vol. **14**, New York, 1932. Also see his paper: Ritt, Algebraic aspects of the theory of differential equations, Semicent. Publ., Amer. Math. Soc., vol. **II** (1938). Our paper concerns directly with Ritt, Systems of differential equations, I. Theory of ideals, Amer. Journ. of Math., **60** (1938). 535—548; this paper will be quoted by RII in the following lines.

their derivatives of various orders, where the coefficients of the linear combination are elements of $\mathfrak{P}$ ($\mathfrak{P}_0$) and p may vary in accordance with the element G.

The *basis-theorem* asserts that *any subset of* $\mathfrak{P}$ ($\mathfrak{P}_0$) *has a basis.*

In the algebraic proofs[2] of the theorem, assumption is made of the existence of the " incomplete system ", which turns out not to exist, and certain lemmas are established under this assumption and led to a contradiction. In this paper, we shall try a direct proof of the theorem.

In what follows, the descriptions will be limited to $\mathfrak{P}$; but, similar discussions could be done concerning $\mathfrak{P}_0$ and in this case the discussions would be much simpler, because we should not have to deal with elements which are not polynomials (in the ordinary sense) of $y_1, \cdots, y_n$.[3]

3. Reduction of the proof. In order to prove the basis-theorem, looking upon x as another dependent variable, *it is sufficient to prove it in the ring which is the totality of all differential polynomials that do not contain* x *effectively.*

Let $\mathfrak{A}'$ be the totality of all functions of $y_1, \cdots, y_n$ which are analytic at $(y_1, \cdots, y_n) = (0, \cdots, 0)$. Let $\mathfrak{P}'$ be the totality of all polynomials of y_{ij} $(i = 1, \cdots, n\ ;\ j = 1, 2, \cdots)$ with coefficients from $\mathfrak{A}'$, then $\mathfrak{P}'$ is an integral domain which is closed with respect to the differentiation. *We have only to prove the existence of the basis for every subset* Σ *of* $\mathfrak{P}'$. Let (Σ) be the ideal[4] which is generated by Σ in $\mathfrak{P}'$. We can see that the *existence of the basis (in the sense of* § 2*) of the ideal* (Σ) *leads us to that of the set* Σ.

Now, let us fix an *ordering* of the elements of $\mathfrak{P}'$ by means of the method in RII, and call an ideal *regular* if it is *regular* as a subset of $\mathfrak{P}'$ in the sense of RII. Then we see that, *in order to prove the existence of the basis for the ideal, it is sufficient to prove it for the regular ideal of* $\mathfrak{P}'$.

4. Ranking of regular ideals. We can prove that every regular non-zero ideal of $\mathfrak{P}'$ has a *basic set*, i. e., any one of the *ascending sets* of minimal rank in the ideal. Let Σ, Σ' be two regular non-zero ideals of $\mathfrak{P}'$. If a basic set of Σ is *of lower rank* (as an ascending set) than a basic set of Σ', we call Σ *of lower rank* than Σ'. This definition of

2. Raudenbush, H. W., Ideal theory and algebraic differential equations. Trans. Amer. Math. Soc., **36** (1934), 361—368; Ritt, the last paper of the footnote 1.

3. Under the restriction of the space, we shall use the concepts in RII without repeating their definitions; also, we describe only the outlines of our proofs.

4. In this paper, we mean by " ideal " one that is closed with respect to the differentiation.

the rank is independent of the choice of a basic set from a regular ideal. If the *index* of Σ is smaller than that of Σ', then Σ is necessarily of lower rank than Σ'. In this ordering of the regular ideals, the minimal condition is satisfied. Therefore, *in order to prove the existence of the basis for regular ideals, we can rely on the induction with respect to this ranking.* The unit-ideal, which is the regular ideal of the lowest rank, has plainly the basis 1.

Now, let Σ be a regular ideal of $\mathfrak{P}'$ of the index j, and *assume that every regular ideal of lower index or of lower rank than Σ has the basis.* In § 6 we shall prove, under this assumption, that Σ must have the basis. If this would be established, then by induction, the proof of the basis-theorem would be completed. Meanwhile, let $(A) = (A_1, \cdots, A_s)$ be a basic set of Σ, and denote by S_i, I_i *the separant* and *the initial* of A_i $(i = 1, 2, \cdots, s)$. Then, both S_i, I_i are necessarily *reduced with respect to the ascending set* (A).

Under our assumption, we can prove that the ideals (Σ, S_i), (Σ, I_i), which are generated by Σ and S_i, by Σ and I_i respectively, and which are not necessarily regular, must have the bases $(i = 1, \cdots, s)$.

5. A lemma. Applying a lemma of Raudenbush,[5] we can prove:

Lemma. Let Σ be an ideal of $\mathfrak{P}'$, and let G, H two elements of $\mathfrak{P}'$ such that the ideals (Σ, G), (Σ, H) have the bases. And, let their bases be

$$\begin{aligned} &(1) \qquad B_1, \cdots, B_m, G, \\ &(2) \qquad B_1, \cdots, B_m, H, \end{aligned} \qquad (B_i \in \Sigma \ (i = 1, \cdots, m))$$

respectively (where we can assume that $B_1, \cdots, B_m$ in (1), (2) are common to both sets). Then the set

$$B_1, \cdots, B_m, GH$$

is a basis of the ideal (Σ, GH).

6. The proof of the basis-theorem. Let Σ be a regular non-zero ideal of $\mathfrak{P}'$ of the index j, and let $(A) = (A_1, \cdots, A_s)$ be a basic set of Σ.[6] Put

$$T = S_1 \cdots S_s \ I_1 \cdots I_s,$$

5. See footnote 2. The lemma asserts that, if the product GH of two differential polynomials G, H is a linear combination of a set $P_1, \cdots, P_r$ of differential polynomials and their derivatives, so are the sufficiently large powers of $(dG/dx)\,H$.

6. We can take (A) such that the first $n - j$ elements $A, \cdots, A_{n-j}$ are regular series of the classes $j + 1, \cdots, n$ respectively and that A_i is a polynomial in $y_{j+1}, \cdots, y_{j+i}$ for every i $(1 \leqq i \leqq n - j)$.

where S_i, I_i are the separant and the initial of A_i $(i=1, \cdots, s)$. Now, as it was mentioned in § 4, we assume that all regular ideals of the indices $< j$ or of lower ranks than Σ have the bases, and deduce that Σ itself must have the basis.

It was already remarked in § 4 that all ideals (Σ, S_i) and (Σ, I_i) $(i=1, \cdots, s)$ have the bases. Hence, according to the lemma of § 5, the ideal (Σ, T) has the basis. Let

$$B_1, \cdots, B_m, T$$

be a basis of (Σ, T). Then, it can be shown that

$$A_1, \cdots, A_s, \ B_1, \cdots, B_m$$

is a basis of Σ.

(Proof) Let F be any element of Σ. Write F as a polynomial in y_{ij} $(i=1, \cdots, n\ ;\ j=1, 2, \cdots)$ with series as its coefficients:

$$F = \sum_{k=1}^{\lambda} G_k Y_k,$$

where Y_k's are distinct monomials of y_{ij} $(i=1, \cdots, n\ ;\ j=1, 2, \cdots)$ which are effectively contained in F and coefficients G_k are series. Applying to G_k Späth's theorem and algebraic division by A_{ij} we arrive at the equalities:

$$G_k = H_{kp} A_p + \cdots + H_{k1} A_1 + G'_k \ (k=1, 2, \cdots, \lambda), \ (p=n-j),$$

where $A_1, \cdots, A_p$ are those elements of the basic set (A) of Σ that are *regular series* of the classes $j+1, \cdots, n$ respectively, and where $H_{kp}, \cdots \cdots, H_{k1}, G'_k$ are series of $\mathfrak{P}'$, and G'_k $(k=1, 2, \cdots, \lambda)$ are polynomials in $y_{j+1}, \cdots, y_n$. Therefore, we have

$$F = H_p A_p + \cdots + H_1 A_1 + F',$$

where $H_1, \cdots, H_p, F'$ are elements of $\mathfrak{P}'$ and F' is a polynomial of $y_{j+1}, \cdots \cdots, y_n$ and y_{ik} $(i=1, 2, \cdots, n\ ;\ k=1, 2, \cdots)$ from Σ.

Since F' is an element of (Σ, T), there exists a positive integer q such that

$$(F')^q = \sum_{i,h} P_{ih} (d^i B_h / dx^i) + \sum_{k=0}^{r} Q_k (d^k T / dx^k) \qquad (1)$$

$$(P_{ih}, Q_k \in \mathfrak{P}').$$

While, let F'' be *the remainder* of F' with respect to the ascending set (A), then

$$T_1F' \equiv F''\,(A),$$

where T_1 is a power product of S_i, $I_i\,(i=1,\cdots,s)$ and F'' is an element of Σ reduced with respect to the ascending set (A); the congruence means modulo the ideal generated by $A_1,\cdots,A_s$. If F'' were not zero, Σ would have an ascending set of lower rank than the basic set (A); this would be a contradiction. Thus, T_1F' must be a linear combination of the elements of (A) and their derivatives. Hence, for sufficiently large integer t, $(TF')^t$ must be a linear combination of the elements of (A) and their derivatives.

Therefore, by the lemma of Raudenbush, there is a positive integer ν such that

$$(F'T)^\nu,(F'(dT/dx))^\nu,(F'(d^2T/dx^2))^\nu,\cdots,(F'(d^rT/dx^r))^\nu$$

are linear combinations of the elements of (A) and their derivatives.

Now, multiplying (1) by F'' and taking the $\{(r+1)(\nu-1)+1\}$th power of it, we see that $((F')^{q+1})^{(r+1)(\nu-1)+1}$ is a linear combination of the elements of (A) and their derivatives.

Memoirs of the College of Science, University of Kyoto, Series A,
Vol. XXV, Nos. 3 & 4, Article 19, 1949.

Linear Conditions at a Point

By

Kôtaro Okugawa

(Received May 18, 1948)

In algebraic geometry the "behavior", at a point O, of a curve or a surface is a fundamental notion. By this word is mostly meant the infinitely near base condition, and this is always a set of linear conditions for the coefficients of the equation of a curve or a surface. In this report we shall deal with the linear conditions in general; therefore the infinitely near base conditions are included in our "linear conditions."

Let O be a point of an n-dimensional affine space, $Ox_1x_2\cdots x_n$ a coordinate system in the space, and $R = K[x_1, x_2, \cdots, x_n]$ the ring of polynomials of the current coordinates $x_1, x_2, \cdots, x_n$ with coefficients from the field K.

A homogeneous condition for the coefficients $a_{i_1i_2\cdots i_n}$ of a polynomial $f(x) = \sum a_{i_1i_2\cdots i_n} x_1^{i_1} x_2^{i_2}\cdots x_n^{i_n}$ can be regarded as a condition for the corresponding hypersurface f; $f(x) = 0$. While, conditions for the coefficients of a polynomial, if its degree is not assigned, are rather attached to the coefficients of a formal power series than to those of a polynomial. Hence, we shall mainly consider the ring $\overline{R} = K[[x_1, x_2, \cdots, x_n]]$ of formal power series of $x_1, x_2, \cdots, x_n$ with coefficients from K.

A formal power series $f(x) = \sum \alpha_{i_1i_2\cdots i_n} x_1^{i_1} x_2^{i_2}\cdots x_n^{i_n}$ can be represented by an infinite sequence $(\alpha) = (\alpha_{i_1i_2\cdots i_n})$ (i's running throughout all non-negative integers), where $\alpha_{i_1i_2\cdots i_n}$ precedes $\alpha_{j_1i_2\cdots j_n}$ when the corresponding n-tuples $(i_1, i_2, \cdots, i_n)$ and $(j_1, j_2, \cdots, j_n)$ are such that, either 1^0) $i_1 + i_2 + \cdots + i_n < j_1 + j_2 + \cdots + j_n$, or 2^0) $i_1 + i_2 + \cdots + i_n = j_1 + j_2 + \cdots + j_n$ and the first non-zero difference among $i_k - j_k$ $(k = 1, 2, \cdots, n)$ is positive; in either case we call $(i_1, i_2, \cdots, i_n) < (j_1, j_2, \cdots, j_n)$.

A linear homogeneous equation

$$\sum_{(i_1, i_2, \cdots, i_n) \leq (p_1, p_2, \cdots, p_n)} a_{i_1i_2\cdots i_n} \xi_{i_1i_2\cdots i_n} = 0 \quad (a_{i_1i_2\cdots i_n} \in K) \tag{1}$$

in the unknown $\xi_{i_1i_2\cdots i_n}$ (where the n-tuple $(p_1, p_2, \cdots, p_n)$ is an arbitrary

n-tuple, designating the upper limit of the range of the summation) is called a *linear condition* for the power series of $\bar{R}$.

Let $f(x) = \sum \alpha_{i_1 i_2 \cdots i_n} x_1^{i_1} x_2^{i_2} \cdots x_n^{i_n}$ be a series of R. If $\xi_{i_1 i_2 \cdots i_n} = \alpha_{i_1 i_2 \cdots i_n}$ satisfies the equation (1), i. e. if

$$\sum_{(i_1, i_2, \cdots, i_n) \leq (p_1, p_2, \cdots, p_n)} a_{i_1 i_2 \cdots i_n} \alpha_{i_1 i_2 \cdots i_n} = 0 , \tag{2}$$

then we say that *the series* $f(x)$ *satisfies linear condition* (1).

Let (E):

$$\sum_{(i_1, i_2, \cdots, i_n) \leq (p_1^{(\lambda)}, p_2^{(\lambda)}, \cdots, p_n^{(\lambda)})} a_{i_1 i_2 \cdots i_n} \xi_{i_1 i_2 \cdots i_n} = 0$$

(λ running throughout a set of indices) be a set of linear conditions. If the series $f(x)$ satisfies every condition of the set (E), we say that $f(x)$ *satisfies the linear condition* (E).

The linear condition (1) can be represented by an infinite sequence $(a) = (a_{i_1 i_2 \cdots i_n})$, where we mean $a_{i_1 i_2 \cdots i_n} = 0$ for every n-tuple $(i_1, i_2, \cdots, i_n) > (p_1, p_2, \cdots, p_n)$. That the series (α) satisfies the linear condition (a), we shall denote it by the notation $(a) \perp (\alpha)$. Moreover, that the series (α) satisfies the linear condition (E), we shall denote it by $(E) \perp (\alpha)$.

Thus, the ring $\bar{R}$ can be regarded as a K-module of all infinite dimensional vectors (α): and the totality $\mathfrak{M}$ of all linear conditions as a K-module of all infinite dimensional vectors (a), where all but a finite number of components $a_{i_1 i_2 \cdots i_n}$ are zeros.

1. Module-theoretical preliminaries. Given a subset (E) of $\mathfrak{M}$, we denote by $\mathfrak{A}_{(E)}$ the totality of all series (α) such that $(E) \perp (\alpha)$; $\mathfrak{A}_{(E)}$ is the set of all series satisfying the linear condition (E), and it is a submodule of R. If M is the submodule of $\mathfrak{M}$ which is generated by (E), then we see that $\mathfrak{A}_M = \mathfrak{A}_{(E)}$. Therefore, in what follows, we shall deal only with submodules of $\mathfrak{M}$.

Now, let $\mathfrak{A}$ be a submodule of $\bar{R}$. If any enumerable set $(\alpha^{(\lambda)}_{i_1 i_2 \cdots i_n})$ $(\lambda = 1, 2, \cdots)$ of series of R such that there exists, for every n-tuple $(i_1, i_2, \cdots, i_n)$, a positive integer $r(i_1, i_2, \cdots, i_n)$ which has the property that $\alpha^{(\lambda)}_{i_1 i_2 \cdots i_n} = 0$ for all $\lambda > r(i_1, i_2, \cdots, i_n)$, has the sum-series

$$\sum_{\lambda=1}^{\infty} (\alpha^{(\lambda)}_{i_1 i_2 \cdots i_n}) = (\sum_{\lambda=1}^{r(i_1, i_2, \cdots, i_n)} \alpha^{(\lambda)}_{i_1 i_2 \cdots i_n})$$

in $\mathfrak{A}$, then we call $\mathfrak{A}$ a *permissible submodule* of $\bar{R}$. We can prove that, if M is any submodule of $\mathfrak{M}$, $\mathfrak{A}_M$ is a permissible submodule of $\bar{R}$.

Given a submodule $\mathfrak{A}$ of R, we denote by $M_{\mathfrak{A}}$ the totality of all linear

conditions (a) of $\mathfrak{M}$ such that $(a) \mid \mathfrak{A}$, i. e., (a) is satisfied by every series of $\mathfrak{A}$. We see that $M_{\mathfrak{A}}$ is a submodule of $\mathfrak{M}$.

It can be proved, by somewhat long but easy discussions which we have no space to describe here, that the correspondences $M \rightarrow \overline{\mathfrak{A}}_M$ and $\mathfrak{A} \rightarrow M_{\overline{\mathfrak{A}}}$, between the set of all submodules M of $\mathfrak{M}$ and the set of all *permissible* submodules $\mathfrak{A}$ of $\overline{R}$, are mutually inverses, and moreover that the correspondence is dual isomorphism between the lattice of all submodules of $\mathfrak{M}$ and the lattice of all *permissible* submodules of $\overline{R}$. The orderings in both of these lattices are the usual set-theoretical inclusion-orders.

2. Linear condition at a point. We are to be concerned with the linear condition which can be named "linear condition at the point O." For such condition it is natural to hope that, if a hypersurface f satisfies the condition, then the product hypersurface $f \cdot g$ also satisfies it for any hypersurface g. If a submodule M of $\mathfrak{M}$ is such that, if a series $f(x)$ of R satisfies the condition M, so does the product $f(x) \cdot g(x)$ for any series $g(x)$ of R, then M is called a *linear condition at* O or a *D-submodule* of $\mathfrak{M}$.

We now enter into the stage where properties of $\overline{R}$, as a ring, are to be investigated. Hereafter, it is convenient to use Macauley's notation concerning the *inverse system*.[1] Namely, we represent a linear condition $(a_{i_1 i_2 \cdots i_n})$ by a polynomial:

$$\varphi(x^{-1}) = \varphi(x_1^{-1}, x_2^{-1}, \cdots, x_n^{-1}) = \sum a_{i_1 i_2 \cdots i_n} x_1^{-i_1} x_2^{-i_2} \cdots x_n^{-i_n}.$$

Thus, $\mathfrak{M}$ can be regarded as a K-module of all such polynomials.

By the definition, M is a D-submodule of $\mathfrak{M}$ if and only if $\overline{\mathfrak{A}}_M$ is an ideal in $\overline{R}$. Since $\overline{\mathfrak{A}}_M$ is a permissible submodule, this is the same thing as that $x_r \cdot f(x)$ $(r = 1, 2, \cdots, n)$ are all contained in $\overline{\mathfrak{A}}_M$, provided $f(x)$ is contained in $\overline{\mathfrak{A}}_M$. From this we can deduce that M is a D-submodule of $\mathfrak{M}$ if and only if the *x_r-derivative*

$$x_r \cdot \varphi(x^{-1}) = \sum a_{i_1 i_2 \cdots i_n} x_1^{-i_1} x_2^{-i_2} \cdots x_{r-1}^{-i_{r-1}} x_r^{-(i_r - 1)} x_{r+1}^{-i_{r+1}} \cdots x_n^{-i_n}$$

(where every term of at least one positive exponent is omitted out) is contained in M, provided $\varphi(x^{-1})$ is a polynomial in M.

Let us call any ideal of R which is a permissible submodule of R a *permissible ideal*. It can be proved that the lattice of all D-submodules M of $\mathfrak{M}$ and the lattice of all permissible ideals of $\overline{R}$ are sublattices

1. Macauley, The Algebraic Theory of Modular Systems, 1916.

of the lattice of submodules of $\mathfrak{M}$ and the lattice of permissible submodules of $\overline{R}$ respectively, and that they are dual isomorphic by the correspondence $M \rightarrow \mathfrak{A}_M$, $\mathfrak{A} \rightarrow M_{\mathfrak{A}}$.

We see that every 0-dimensional and every $(n-1)$-dimensional ideal of $\overline{R}$ is permissible ideal. Furthermore, it can be proved that $\mathfrak{A}_M$ is 0-dimensional ideal if and only if the corresponding D-submodule M of $\mathfrak{M}$ has a finite module-basis.

3. 0-Dimensional ideals. If we desire to use properly the word "linear condition at O," it is natural to limit our consideration only on those D-submodules M of $\mathfrak{M}$ such that $\mathfrak{A}_M$ are 0-dimensional ideals, i. e. on D-submodules M which have finite module-bases.

Let M be a D-submodule of $\mathfrak{M}$ which has a finite module-basis and $\mathfrak{A}$ the corresponding 0-dimensional ideal. It can be proved, on account of the dual isomorphism, that since $\mathfrak{A}$ decomposes into an intersection of a finite number s of irreducible ideals $\mathfrak{A}_1, \mathfrak{A}_2, \cdots, \mathfrak{A}_s$, M decomposes into a module-sum of s additively irreducible D-submodules $M_1, M_2, \cdots M_s$ which correspond to $\mathfrak{A}_1, \mathfrak{A}_2, \cdots, \mathfrak{A}_s$ respectively, although the decomposition is not uniquely determined.

We see that every monomial $x_1^{m_1} x_2^{m_2} \cdots x_n^{m_n}$ can be used as an operator of successive derivation of any polynomial $\varphi(x^{-1})$ of $\mathfrak{M}$, and moreover, that every element of $\overline{R}$ can be regarded as such operator. We call the result $g(x) \cdot \varphi(x^{-1})$ of operating $g(x)$ upon $\varphi(x^{-1})$ the $g(x)$-derivative of $\varphi(x^{-1})$.

Let $\varphi(x^{-1})$ be a polynomial of $\mathfrak{M}$. We denote by $(\varphi(x^{-1}))$ the totality of all $g(x)$-derivatives of $\varphi(x^{-1})$, $g(x)$ running throughout all series of $\overline{R}$. It is a D-submodule of $\mathfrak{M}$, and we call it a *principal D-submodule* of $\mathfrak{M}$. It can be proved that a D-submodule of $\mathfrak{M}$ is (additively) irreducible if and only if it is principal.

By these descriptions we see that the principal D-submodules of $\mathfrak{M}$ are the prototypes of the linear conditions at O and that they correspond to the irreducible 0-dimensional ideals of $\overline{R}$ belonging to the unique maximal prime ideal $\mathfrak{P} = (x_1, x_2, \cdots, x_n)$.

If we take intersections with R of the ideals of $\overline{R}$, we can conclude that there is a reversible one-to-one correspondence between D-submodules, which has finite module-basis, and primary ideals of R belonging to the prime ideal $\mathfrak{P} = (x_1, x_2, \cdots, x_n)$ (which corresponds to the point O in question); and that, in this correspondence, to a principal D-submodule corresponds an irreducible ideal belong to $\mathfrak{P}$.

Memoirs of the College of Science, University of Kyoto, Series A,
Vol. XXV, Nos. 3 & 4, Article 20, 1949.

A Wave-mechanical Treatment of the Electron Oscillation

By

Isao Takahashi

(Received March 16, 1948)

1. Introduction

The wave-mechanical treatment of an electron oscillation was made by Schuster[1] for the first time. His case where plane parallel electrodes were assumed was that the cathode and the anode were situated symmetrically relative to the grid and no anode d. c. voltage was applied. He adopted cylindrical functions for the exact wave functions, and obtained graphically the differences of the energies (proper values), in order to derive the frequency formulas in accordance with classical ones for his case, but he did not consider any transition probability.

The author[2] tried to solve the same problem for the case where the distances of the cathode and the anode from the grid were not necessarily equal to each other, the anode d. c. voltage being applied.

The author solved the wave equation with the aid of Jeffrey's approximation method (W. K. B. method) and derived the equation to determine the proper values. The differences of the energies (proper values) were shown to give the frequency formulas for B. K. wave and dwarf waves. In his calculation, the author limited the wave function within the space between the cathode and the plane where potential energy vanishes between the grid and the anode. But, an alternative is that the space is extended beyond the cathode and the anode with the potential gradient preserved, as is shown with the dotted lines in Fig. 2 and we make use of the quantum condition expressed by the integration between two classical reflecting points in W. K. B. method. The results

1. Ann. d. Phy. **76**, 1930.

2. The first part of "On the Electron Oscillation of Barkhausen and Kurz" lectured by W. Nakayama and its abstract in Nippon Sugaku-Butsurigakkaishi, **5** (1931), 214.

of the proper values in both assumptions, however, agree approximately, as is shown below, when the energy of electron is sufficiently small against eV_g, where V_g is the grid d. c. voltage. In this paper, the transition probabilities are calculated subject to the former assumption.

2. Unperturbed functions

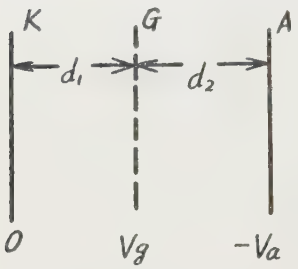

Fig. 1

K : cathode
G : grid
A : anode
d : distances between electrodes
V : d. c. voltages

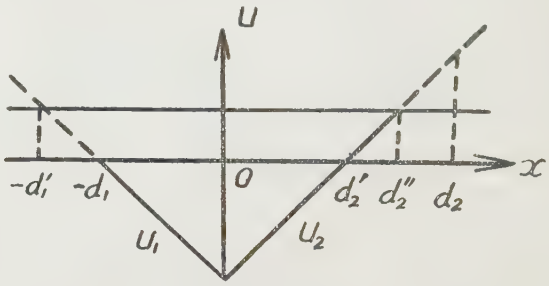

Fig. 2

U : potential energy of an electron
W : proper value
$-d_1, d_2$: points of zero potential
$-d_1', d_2''$: classical reflecting points

Since we assume that the potential is linear between electrodes as shown in Fig. 2, the wave functions satisfy the following equations :

$$\frac{d^2\psi_1}{dx^2} + \kappa^2(W - U_1)\,\psi_1 = 0 \quad \text{between K and G ;}$$

$$\frac{d^2\psi_2}{dx^2} + \kappa^2(W - U_2)\,\psi_2 = 0 \quad \text{between G and A ,}$$

where $\kappa^2 = \dfrac{8\pi^2 m}{h^2} \sim 1.67 \times 10^{28}$ and

$$W - U_1 = W + eV_g + a_1 x = W' + a_1 x ,$$
$$W - U_2 = W + eV_g - a_2 x = W' - a_2 x$$

with $W' = W + eV_g$, $a_1 = eV_g/d_1$, $a_2 = e\,(V_g + V_a)/d_2$.

The approximate solutions between $-d_1$ and d_2' are

$$\psi_{\substack{1\\2}} = (W' \pm a_{\substack{1\\2}} x)^{-\frac{1}{4}} \left\{ A_{\substack{1\\2}} e^{i\kappa \int_0^x (W' \pm a_{\frac{1}{2}} x)^{1/2} dx} + B_{\substack{1\\2}} e^{-i\kappa \int_0^x (W' \pm a_{\frac{1}{2}} x)^{1/2} dx} \right\} , \quad (1)$$

where suffixes 1 and 2 correspond respectively to + and − of the double signs.

At $x = 0$, for the derivatives of ψ,

$$\psi_{\frac{1}{2}}' = i\kappa (W'' \pm a_{\frac{1}{2}} x)^{-\frac{1}{4}} \left\{ A_{\frac{1}{2}} e^{i\kappa \int_0^x} - B_{\frac{1}{2}} e^{-i\kappa \int_0^x} \right\} \qquad (2)$$

holds good, because of the extraordinarily large value of κ.

The boundary conditions of ψ_1 and ψ_2 are

$$\psi_1 = 0 \qquad \text{at} \quad x = -d_1 ,$$

$$\psi_1 = \psi_2 , \quad \psi_1' = \psi_2' \quad \text{at} \quad x = 0 ,$$

$$\psi_2 = 0 \qquad \text{at} \quad x = d_2' ,$$

which give

$$A_1 = A_2 = A , \quad B_1 = B_2 = B ,$$

and

$$\frac{2\kappa}{3} (W'^{3/2} - W^{3/2}) \left(\frac{1}{a_1} + \frac{1}{a_2} \right) = n\pi , \qquad (3)$$

n being any positive integer. Corresponding to the large value of the left-hand side of (3), n must be very large. The quantum condition in W. K. B. method:

$$\int_{-d_1'}^{d_2''} \kappa \sqrt{W - U}\, dx = \left(n + \frac{1}{2} \right) n$$

gives, instead of (3),

$$\frac{2\kappa}{3} W'^{3/2} \left(\frac{1}{a_1} + \frac{1}{a_2} \right) = \left(n + \frac{1}{2} \right) \pi . \qquad (4)$$

For large values of n and $eV_g \gg W$, the above two expressions (3) and (4) agree with each other. The difference of energy can be given as differential ΔW in the equation:

$$\kappa \left(\frac{1}{a_1} + \frac{1}{a_2} \right) (W'^{1/2} - W^{1/2}) \Delta W = \Delta n \pi , \qquad (5)$$

for $\Delta n \ll n$ which is very large.

When we apply the frequency condition:

$$\nu = \frac{\Delta W}{h} ,$$

the classical wave length formulas for B. K. wave and dwarf waves can be derived from (5). Thus,

$$\lambda = \frac{c}{\nu} = c\sqrt{\frac{8m}{eV_g}\frac{(d_1+d_2)V_g + d_1 V_g}{V_g + V_a}}\frac{1}{\Delta n}.$$

Equation (1) is transformed so as to adapt the boundary conditions and the subsequent calculation, as follows:

$$\psi_{n_2^1} = C_{n_2^1}(W_n' \pm a_1 x)^{-\frac{1}{4}}\left\{e^{i\kappa I n_2^1} - e^{-i\kappa I n_2^1}\right\}, \tag{6}$$

with $C_{n1} = C_{n2}\cos n\pi$, where

$$I_{n_2^1} = \pm\frac{2\kappa}{3a_2^1}\left\{(W_n' \pm a_2^1 x)^{3/2} - W_n^{3/2}\right\}. \tag{7}$$

In order to show the orthogonality of ψ_n's and to normalize ψ_n, we put

$$(W_n' \pm a_2^1 x)^{3/2} = y. \tag{8}$$

Then, we get

$$x = \pm\frac{1}{a_2^1}(y^{2/3} - y_0^{2/3}), \quad dx = \pm\frac{2}{3a_2^1}y^{-1/3}dy,$$

with $y_1 = W_n^{3/2}$, $y_0 = W_n'$ and

$$I_{n_2^1} = \pm\alpha_2^1(y - y_1), \quad I_{m_2^1} = I_{n_2^1} - \Delta I_2^1, \quad \Delta I_2^1 = \pm\beta_2^1(y^{1/3} - y_1^{1/3}),$$

where $\alpha_2^1 = \frac{2\kappa}{3a_2^1}$, $\beta_2^1 = \frac{\kappa}{a_2^1}\Delta W$.

Hence, putting $(W_n^{3/2} \pm a_2^1 x)^{-1/4} = (y^{2/3} - \Delta W)^{-1/4} \fallingdotseq y^{-1/6}$, we have

$$\int_{-d_1}^{d_2'}\psi_n^*\psi_m dx$$

$$= C_{n1}^* C_{m1}\left(+\frac{2}{3a_1}\right)\int_{y_1}^{y_0} y^{-\frac{2}{3}}(e^{-i\Delta I_1} - e^{-2iIn_1}e^{i\Delta I_1} - e^{2iIn_1}e^{-i\Delta I_1} + e^{i\Delta I_1})\,dy$$

$$+ C_{n2}^* C_{m2}\left(-\frac{2}{3a_2}\right)\int_{y_0}^{y_1} y^{-\frac{2}{3}}(e^{-i\Delta I_2} - e^{-2iIn_2}e^{i\Delta I_2} - e^{2iIn_2}e^{-i\Delta I_2} + e^{i\Delta I_2})\,dy.$$

Since, in this integral, $e^{\pm 2iI_n}$ oscillate very rapidly, we may take their mean value which is equal to 0. Therefore

$$\int_{-a_1}^{a_2'} \psi_n^* \psi_m dx = C_{n1}^* C_{m1} \left(+ \frac{4}{3a_1} \right) \int_{y_1}^{y_0} y^{-2/3} \cos(\Delta I_1)\, dy + C_{n2}^* C_{m2} \left(- \frac{4}{3a_2} \right) \int_{y_0}^{y_1} y^{-2/3} \cos(\Delta I_2)\, dy . \qquad (9)$$

If we make the transformation:

$$y^{\frac{1}{3}} = z , \qquad (10)$$

then we have

$$\int_{-a_1}^{a_2'} \psi_n^* \psi_m dx = C_{n1}^* C_{m1} \left(+ \frac{4}{a_1} \right) \int_{z_1}^{z_0} \cos\left\{ + \beta_1 (z - z_1) \right\} dz + C_{n2}^* C_{m2} \left(- \frac{4}{a_2} \right) \int_{z_0}^{z_1} \cos\left\{ - \beta_2 (z - z_1) \right\} dz ,$$

with $z_1 = y_1^{1/3} = W_n^{1/2}$, $z_0 = y_0^{1/3} = W_n'^{1/2}$.

According as $\Delta n = n - m$ is even or odd,

$$\left. \begin{aligned} \sin\{\beta_1 (z_0 - z_1)\} &= \mp \sin\{\beta_2 (z_0 - z_1)\} , \\ \cos\{\beta_1 (z_0 - z_1)\} &= \pm \cos\{\beta_2 (z_0 - z_1)\} , \end{aligned} \right\} \qquad (11)$$

because of (5) expressed in the form $\beta_1 (z_0 - z_1) + \beta_2 (z_0 - z_1) = \Delta n \pi$, and moreover

$$C_{n1}^* C_{m1} = \pm C_{n2}^* C_{m2} , \qquad (12)$$

corresponding to Δn being even or odd.

Thus, we have finally

$$\int_{-a_1}^{a_2} \psi_n^* \psi_m dx = 0 , \qquad \text{for } n \neq m \qquad (13)$$

and the condition of normalization $\int_{-a_1}^{a_2} \psi_n^* \psi_n dx = 1$ gives

$$| C_{n2} |^2 = \frac{1}{4 (W_n'^{1/2} - W_n^{1/2}) \left(\frac{1}{a_1} + \frac{1}{a_2} \right)} . \qquad (14)$$

3. Transition

We can calculate the transition probabilities between two energy states as in the case of an atom. We assume that the oscillating field is an oscillating statical field, but we have to take into account that the oscillating field between K and G is generally not equal to that between G and A, both in amplitude and in sense. Therefore, we cannot take formally $|\int_{-d_1}^{d_2}\psi_n^* x\,\psi_m dx|^2$ to give the measure of transition probability. We thus proceed to treat a perturbation problem with the perturbing potentials u_1 and u_2 such that

$$u_1 = (-f_1 x - g)\sin\omega t\,, \quad u_2 = (f_2 x - g)\sin\omega t\,, \tag{15}$$

with $f_1 = \frac{ev_1}{d_1}$, $f_2 = \frac{e(v_1+v_2)}{d_2}$, $ev_1 = g$, where $v_1\sin\omega t$ and $-v_2\sin\omega t$ are oscillating voltages on the grid and on the anode respectively as shown in Fig. 3.

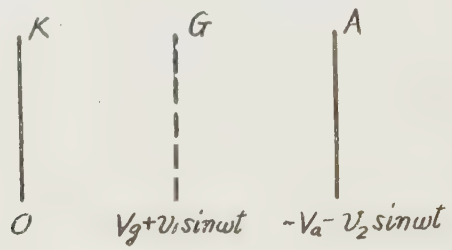

Fig. 3.

We have to solve the following unstationary wave equation:

$$\left\{-\frac{1}{\kappa^2}\frac{\partial^2}{\partial x^2} + U + u\right\}\Psi = i\hbar\frac{\partial}{\partial t}\Psi\,,$$

where

$$\Psi = \sum_m a_m(t)\Psi_m\,, \quad \Psi_m = \psi_m e^{-\frac{iW_m}{\hbar}t}$$

a_m's being determined by the equations:

$$i\hbar a_n = \sum_m U_{nm}a_m\,, \qquad U_{nm} = \int_{-d_1}^{d_2'}\Psi_n^* U\Psi_m dx\,.$$

Assuming U in the form:

$$U_{\frac{1}{2}} = (\mp f_{\frac{1}{2}}x - g)(e^{i\omega t} - e^{-i\omega t})/2i\,,$$

we obtain

$$U_{nm} = \frac{1}{2i}\left\{e^{\frac{t}{\hbar}(Wn - Wm + \hbar\omega)} - e^{\frac{t}{\hbar}(Wn - Wm - \hbar\omega)}\right\} \int_{-a_1}^{a_2'} (\mp f_{\frac{1}{2}} x)\, \psi_n^* \psi_m dx .$$

With the aid of the transformations (8) and (10), we have

$$\begin{aligned} U_{nm}^{(0)} &= \int_{-a_1}^{a_2'} \psi_n^* (\mp f_{\frac{1}{2}} x)\, \psi_m dx \\ &= 4 C_{n2}^* C_{m2} \\ &\quad \times \left\{ \mp \frac{f_1}{(\kappa \Delta W)^2} \left[2z_0 \cos\{\beta_1 (z_0 - z_1)\} - 2z_1 - \frac{2}{\beta_1} \sin\{\beta_1 (z_0 - z_1)\} \right] \right. \\ &\quad \left. + \frac{f_2}{(\kappa \Delta W)^2} \left[2z_1 - 2z_0 \cos\{\beta_2 (z_0 - z_1)\} + \frac{2}{\beta_2} \sin\{\beta_2 (z_0 - z_1)\} \right] \right\} , \end{aligned}$$

where $-$ or $+$ of the double signs in front of f_1 should be taken according as Δn is even or odd.

Since the ratio $z_1 : 1/\beta$ is nearly equal to the ratio $W_n^{1/2} : W_n'^{1/2}$, we can neglect z_1 in the above expression and therefore, by use of (11), we get

$$\begin{aligned} U_{nm}^{(0)} = \frac{8 C_{n2}^* C_{m2}}{(\kappa \Delta W)^2} \left\{ - (f_1 + f_2) z_0 \cos\{\beta_2 (z_0 - z_1)\} \right. \\ \left. + \left(\frac{f_2}{\beta_2} - \frac{f_1}{\beta_1} \right) \sin\{\beta_2 (z_0 - z_1)\} \right\} . \end{aligned}$$

If we put

$$\frac{f_2}{\beta_2} - \frac{f_1}{\beta_1} = R \cos\varphi , \qquad (f_1 + f_2) z_0 = R \sin\varphi ,$$

then we have

$$U_{nm}^{(0)} = \frac{8 C_{n2}^* C_{m2}}{(\kappa \Delta W)^2} R \sin\{\beta_2 (z_0 - z_1) - \varphi\} , \tag{16}$$

where

$$\tan\varphi = (f_1 + f_2) z_0 \Big/ \left(\frac{f_2}{\beta_2} - \frac{f_1}{\beta_1} \right) ,$$

and

$$R^2 = \left(\frac{f_2}{\beta_2} - \frac{f_1}{\beta_1} \right)^2 + (f_1 + f_2)^2 z_0^2 ,$$

Since $\beta_2(z_0 - z_1) = \dfrac{\Delta n\pi}{1 + a_2/a_1}$, because of (5), the forbidden transitions are given by $\dfrac{\Delta n\pi}{1 + a_2/a_1} - \varphi = N\pi$, namely:

$$1 + \frac{a_2}{a_1} = \frac{\Delta n}{N + \varphi/\pi}, \tag{17}$$

where N is an integer. Thus, it is found that the forbidden transitions are characterized by the tube dimensions, applied d. c. voltages, and external circuit relations which are implied in β_1 and β_2.

4. Conclusion

In this paper, the author has calculated the measure of the transition probability and has shown the possibility of the occurrence of B. K. wave and the dwarf waves and that of the forbidden transition.

Memoirs of the College of Science, University of Kyoto, Series A,
Vol. XXV, Nos. 3 & 4, Article 21, 1949.

On the Electronic Admittance in Reflex Klystron. I

By

Isao Takahashi and **Kenji Mitani**

(Received August 24, 1949)

Introduction

The possibility of oscillation of the klystron, including the case of the reflex klystron, has been discussed by many authors, [3, 4, 7] * but in their calculations, the effect of the transit time of electron in the resonator gap and the effect of the oscillatory voltage on the electron motion in the drift space have been neglected. We have calculated the interelectrode admittance of the reflex klystron, taking these effects into consideration. The method of calculation is similar to that which the senior author (I. T.) has adopted in the case of B. K. oscillation.[2]

In the case of reflex klystron too as in the case of B. K. oscillation, we could demonstrate the production of the negative conductance.

The Velocity of Electron in Each Space

The sectional view of the reflex klystron in principle is shown in Fig. 1 (a).

F : filament
R : cavity resonator
G_1, G_2 : grids forming the gap of cavity resonator
d : the distance between G_1 and G_2
A : repeller
D : the distance between G_2 and A

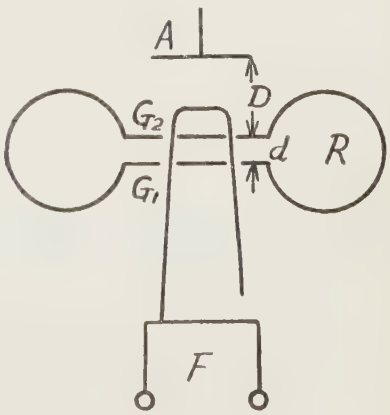

Fig. 1. (a)

* These numbers indicate the numbers of papers listed at the end of this paper.

Fig. 1 (b) shows the potential distribution in this klystron; V_0 is the accelerating voltage; $v_g e^{j\omega t}$ is the oscillatory one which G_2 has against G_1, and $-V_a$ is the voltage of A against G_1, consequently the repelling voltage acting between G_2 and A is $-(V_a + v_g e^{j\omega t})$.

In the following, we consider the induced current flowing into G_2 by way of the resonator from G_1.

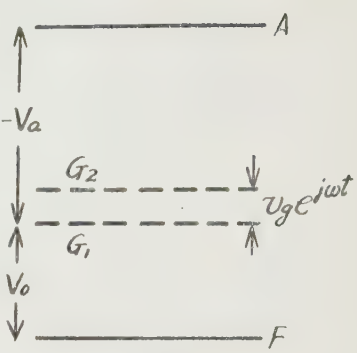

Fig. 1. (b)

First we calculate the velocity of electron in each space. The velocity u_0 which the electron has when it reaches G_1 starting from the filament, is

$$u_0 = \sqrt{\frac{2eV_0}{m}}, \tag{1}$$

where m is the mass of an electron and $-e$ its charge.

(a) From G_1 to G_2.

The equation of motion is

$$m\frac{du_1}{dt} = e\frac{v_g}{d}e^{j\omega t}.$$

From this equation, we get the velocity u_1 in the resonator gap:

$$u_1(t, t_0) = u_0 + \frac{\alpha_1}{j\omega}(e^{j\omega t} - e^{j\omega t_0}), \tag{2}$$

where

$$\alpha_1 \equiv \frac{e}{m}\frac{v_g}{d}, \tag{3}$$

and t_0 is the instant at which the electron passes through G_1.

The instant t_1 at which the electron reaches G_2 can be put:

$$t_1 = t_0 + T_1 + \delta T_1, \tag{4}$$

where T_1 is the transit time from G_1 to G_2 when $v_g = 0$, namely

$$T_1 = \frac{d}{u_0}. \tag{5}$$

And the deviation δT_1 from T_1 is calculated in the first approximation as:

$$\delta T_1(t_0) = \frac{\alpha_1}{\omega^2 u_0} e^{j\omega t_0}(e^{j\omega T_1} - 1 - j\omega T_1) . \qquad (6)$$

Thus, the velocity which the electron has when it reaches G_2, becomes, in the first approximation,

$$u_1(t_1) = u_1(t_1, t_0) = u_0 + \frac{\alpha_1}{j\omega} e^{j\omega t_0}(e^{j\omega T_1} - 1) .$$

(b) From G_2 to A and again to G_2.

The equation of motion is

$$m\frac{du_2}{dt} = -\frac{e}{D} V_a(1 + Re^{j\omega t}) , \text{ where } R = \frac{v_g}{V_a} . \qquad (7)$$

From this equation, the velocity u_2 in this space is

$$u_2(t, t_0) = u_1(t_1) - \alpha_2(t - t_1) - \frac{\alpha_2 R}{j\omega}(e^{j\omega t} - e^{j\omega (t_0 + T_1)}) , \qquad (8)$$

where

$$\alpha_2 \equiv \frac{e}{m}\frac{V_a}{D} . \qquad (9)$$

The instant, when the electron comes back to G_2, can be put

$$t_2 = t_1 + T_2 + \delta T_2 = t_0 + (T_1 + \delta T_1) + (T_2 + \delta T_2) , \qquad (10)$$

where T_2 is the transit time from G_2 to G_2 before A, when $v_g = 0$, that is

$$T_2 = \frac{2u_0}{\alpha_2} . \qquad (11)$$

δT_2 is the deviation from T_2 caused by v_g, and is calculated from (8) as:

$$\delta T_2(t_0) = \frac{2\alpha_1}{j\omega\alpha_2} e^{j\omega t_0}(e^{j\omega T_1} - 1) + \frac{2R}{\omega^2 T_2} e^{j\omega (t_0 + T_1)}(e^{j\omega T_2} - 1 - j\omega T_2) . \qquad (12)$$

Accordingly, the velocity which the electron has when it is back to G_2, is

$$u_2(t_2) = u_2(t_2, t_0)$$

$$= -u_0 \frac{\alpha_1}{j\omega} e^{j\omega t_0}(e^{j\omega T_1} - 1)$$

$$+ R\frac{\alpha_2}{\omega^2 T_2} e^{j\omega(t_0+T_1)}\left\{(-2 + j\omega T_2)e^{j\omega T_2} + 2 + j\omega T_2\right\} . \quad (13)$$

(c) From G_2 to G_1.

By solving the equation of motion, $m\frac{du_3}{dt} = e\frac{v_g}{d}e^{j\omega t}$, the velocity of the electron moving from G_2 to G_1 is found to be equal to

$$u_3(t, t_0) = u_2(t_2) + \frac{\alpha_1}{j\omega}(e^{j\omega t} - e^{j\omega(t_0+T_1+T_2)}) . \quad (14)$$

If we put the time t_3 when the electron comes back to G_1, as follows:

$$t_3 = t_2 + T_1 + \delta T_3 , \quad (15)$$

we get, by integrating (14), the following form for δT_3:

$$\delta T_3(t_0) = -e^{j\omega(T_1+T_2)}\delta T_1(t_0) + \frac{\alpha_1}{\omega^2 u_0}(j\omega T_1)e^{j\omega t_0}(e^{j\omega T_1} - 1)$$

$$+ R\frac{\alpha_2}{\omega^2 u_0}\frac{T_1}{T_2}e^{j\omega(t_0+T_1)}\left\{(-2 + j\omega T_2)e^{j\omega T_2} + 2 + j\omega T_2\right\} . \quad (16)$$

Induced Current in the Resonator Gap

We calculate the induced current flowing into G_2 by way of the resonator from G_1, caused by electron motion in like manner as in the previous papers.[1, 2]

The induced current J_1 caused by the repelled electrons is

$$J_1 = \frac{ne}{d}\int_{t_0''}^{t_0'} u_3\, dt_0 , \quad (17)$$

where n is the number of electrons emitted per unit time by F to contribute to the oscillation. t_0' is the t_0 of the electrons which pass through G_2 at t on their way back from before A and t_0'' the t_0 of the electrons which come back to G_1 at t on their way back too.

We have

$$t_0' = t - T_1 - T_2 - \delta T_1(t_0') - \delta T_2(t_0') \fallingdotseq t - T_1 - T_2 - \delta T_1' - \delta T_2',$$

$$t_0'' = t - 2T_1 - T_2 - \delta T_1(t_0'') - \delta T_2(t_0'') - \delta T_3(t_0'')$$

$$\fallingdotseq t - 2T_1 - T_2 - \delta T_1'' - \delta T_2'' - \delta T_3'' ,$$

with

$$\delta T_1' \equiv \delta T_1(t - T_1 - T_2), \qquad \delta T_2' \equiv \delta T_2(t - T_1 - T_2),$$
$$\delta T_1'' \equiv \delta T_1(t - 2T_1 - T_2), \qquad \delta T_2'' \equiv \delta T_2(t - 2T_1 - T_2),$$
$$\delta T_3'' \equiv \delta T_3(t - 2T_1 - T_2).$$

Then we get, to the first approximation,

$$\begin{aligned} J_1 = &- ne + \frac{ne\alpha_1}{d\omega^2} e^{j\omega t}\Big[2 - j\omega T_1 - (2 + j\omega T_1) e^{-j\omega T_1} \\ &+ (2 - j\omega T_2) e^{-j\omega T_2} + (2 + 2j\omega T_1 - j\omega T_2) e^{-j\omega(T_1 + T_2)} \\ &+ (-4 - 2j\omega T_1 + 2j\omega T_2) e^{-j\omega(T_1 + T_2)}\Big] \\ &+ \frac{ne\alpha_2 R}{d\omega^2} e^{j\omega t}\Big[1 - e^{-j\omega T_2} - j\omega T_2 e^{-j\omega T_2} - e^{-j\omega T_1} \\ &+ e^{-j\omega(T_1 + T_2)} + j\omega T_2 e^{-j\omega(T_1 + T_2)} \\ &- \frac{T_1}{T_2}\Big\{(-2 + j\omega T_2) e^{-j\omega T_1} + (2 + j\omega T_2) e^{-j\omega(T_1 + T_2)}\Big\} \\ &+ \frac{1}{j\omega T_2}\Big\{(-2 + j\omega T_2) + (2 + j\omega T_2) e^{-j\omega T_2}\Big\}(1 - e^{-j\omega T_1})\Big], \end{aligned} \tag{18}$$

Similarly, the induced current J_2 caused by the electrons moving from G_1 to G_2 is

$$J_2 = \frac{ne}{d} \int_{t_0'''}^{t} u_1 dt_0, \tag{19}$$

where t_0''' is the t_0 of the electrons which pass through G_2 at t on their way to A. Therefore

$$t_0''' = t - T_1 - \delta T_1(t_0''') \fallingdotseq t - T_1 - \delta T_1''',$$

with $\delta T_1''' \equiv \delta T_1(t - T_1)$. Thus we get, to the first approximation,

$$J_2 = ne + \frac{ne\alpha_1}{d\omega^2} e^{j\omega t}\Big[2 - j\omega T_1 - (2 + j\omega T_1) e^{-j\omega T_1}\Big]. \tag{20}$$

Thus, by (18) and (20), the total induced current J flowing into G_2 by way of the resonator from G_1 is given by

$$J = J_1 + J_2. \tag{21}$$

The Electronic Admittance in the Gap

In order that the oscillation may occur in this krystron, it is necessary that the negative conductance is produced in the resonator gap.

We can define the electronic admittance in the resonator gap by the following expression:

$$Y = \frac{J}{v_g e^{j\omega t}}, \tag{22}$$

whose real part is the conductance.

For simplicity, we take the case, where $\alpha_2 R = \frac{ev_g}{mD}$ can be neglected against $\alpha_1 = \frac{ev_g}{md}$ because of $d \ll D$. In this case, we get for Y

$$\begin{aligned} Y_1 = \frac{ne^2}{md^2\omega}\Big[&4 - 2j\omega T_1 - (4 + 2j\omega T_1)\, e^{-j\omega T_1} \\ &+ (2 - j\omega T_2)\, e^{-j\omega T_2} + (2 + 2j\omega T_1 - j\omega T_2) e^{-j\omega(2T_1+T_2)} \\ &+ (-4 - 2j\omega T_1 + 2j\omega T_2) e^{-j\omega(T_1+T_2)}\Big]. \end{aligned} \tag{23}$$

We assume ωT_1 to be sufficiently small compared with unity and expand $e^{-j\omega T_1}$ and $e^{-j\omega T_1}$ in powers of $-j\omega T_1$, and then we express (23) in an ascending power series of $-j\omega T_1$.

Then, it will be seen that (23) begins with the second power of $-j\omega T_1$. This corresponds to the factor $1/d^2$, and therefore the approximate expression for Y_1 becomes

$$Y_1 = \frac{ne^2}{mu_0^2}\left[e^{-j\omega T_2} + \frac{1}{2} j\omega T_2\, e^{-j\omega T_2}\right], \tag{24}$$

whose real part is

$$G_1 = \frac{ne^2}{mu_0^2}\left[\cos\omega T_2 + \frac{1}{2}\omega T_2 \sin\omega T_2\right]. \tag{25}$$

The expression (25) of G_1 takes its minima (negative values) in the vicinity of

$$\omega T_2 = 2\pi\left(n + \frac{3}{4}\right), \quad n = 0, 1, 2, \cdots\cdots\cdots. \tag{26}$$

Thus, we can demonstrate the possibility of the oscillation in the

reflex krystron. The relation (26) gives the well-known optimum phase between the bunched current and the gap potential in the reflex klystron.

If we retain the term with the factor $\alpha_2 R$ in the expression of Y, we have the following additional term Y_2 to the expression (23) for Y_1:

$$\begin{aligned} Y_2 = \frac{ne^2}{mDd\omega^2}\Big[& 1 - e^{-j\omega T_2} - j\omega T_2 e^{-j\omega T_2} - e^{-j\omega T_1} \\ & + e^{-j\omega(T_1+T_2)} + j\omega T_2 e^{-j\omega(T_1+T_2)} \\ & - \frac{T_1}{T_2}\left\{(-2 + j\omega T_2)\, e^{-j\omega T_1} + (2 + j\omega T_2)\, e^{-j\omega(T_1+T_2)}\right\} \\ & + \frac{1}{j\omega T_2}\left\{(-2 + j\omega T_2) + (2 + j\omega T_2)\, e^{-j\omega T_2}\right\}(1 - e^{-j\omega T_1})\Big]. \end{aligned} \tag{27}$$

When we expand Y_2 in powers of $-j\omega T_1$, it will be seen that Y_2 begins with the first power of $-j\omega T_1$, corresponding to the factor $1/d$ in this expression and we get approximately

$$Y_2 = \frac{ne^2}{mD\omega u_0}\left[j\{1 - e^{-j\omega T_2} - j\omega T_2 e^{-j\omega T_2}\}\right]. \tag{28}$$

Therefore, in order to justify our neglection of the term with the factor $\alpha_2 R$ against the term with the factor α_1 in Y, we must compare $|\alpha_1(-j\omega T_1)^2|$ with $|\alpha_2 R(-j\omega T_1)|$. This ratio is $\omega T_1 \alpha_1 : \alpha_2 R = \omega T_1 : d/D$.

If ωT_1 is sufficiently larger than d/D, we are justified to adopt (24) as the electronic admittance.

If, however, ωT_1 and d/D are of comparable order of magnitude, (28) cannot be neglected against (24). Then, the electronic admittance is

$$\begin{aligned} Y = Y_1 + Y_2 = \frac{ne^2}{mu_0^2}\Big\{ & \left[e^{-j\omega T_2} + \frac{1}{2} j\omega T_2 e^{-j\omega T_2}\right] \\ & + \kappa\left[j(1 - e^{-j\omega T_2} - j\omega T_2 e^{-j\omega T_2})\right]\Big\}, \end{aligned} \tag{29}$$

with $\kappa = \dfrac{d/D}{\omega T_1}$, and the corresponding conductance is

$$G = \frac{ne^2}{mu_0^2}\left\{\left[\cos\omega T_2 + \frac{1}{2}\omega T_2 \sin\omega T_2\right] + \kappa\left[-\sin\omega T_2 + \omega T_2 \cos\omega T_2\right]\right\}. \tag{30}$$

For the expression (30) of G, we can expect the production of the minimum (negative value) by simple calculation, in the vicinity of $\omega T_2 = \frac{3}{2}\pi$.

For the finite values of ωT_1, we can demonstrate numerically the existence of the minimum, which is negative, of the real part of the function $Y = Y_1 + Y_2$ in the vicinity of $\omega T_2 = \frac{3}{2}\pi$.

REFERENCES

1. I. Takahashi: Über die Dielektrizitätskonstante des Magneto-aktiven ionisierten Gases. This Memoirs, Vol. XXIII, No. 4, (1941).
2. I. Takahashi: On the possibility of Barkhousen-Kurz Oscillation I. This Memoirs, Vol. XXV, No. 1, (1947).
3. H. Hollmann: Ultrakurzwellengeräte mit Laufzeitkompression, ZS. d. H. T. (1941).
4. H. Hollmann: Zur Theorie der Triftröhren. ZS. f. H und E, **56**, (1940).
5. E. U. Condon: Principle of Microwave Radio. Rev. Mod. Phys. Vol. 14, No. 4, (1942).
6. Recknagel : Schwingungsanfachung durch einen Elektronenstrahl im Feld des Plattenkondensators. ZS. f. tech. Phys. Ns. 3, S. 74, (1938).
7. J. C. Slater : Microwave Electronics. Rev. Mod. Phys. Vol. 18, No. 4, Oct. (1946).

Memoirs of the College of Science, University of Kyoto, Series A,
Vol. XXV, Nos. 3 & 4, Article 22, 1949.

On the Molecular Arrangement of Some Organic Films

By

Yoshibumi Fujiki

(Received September 28, 1948)

Abstract

Thin films of paraffin waxes were prepared on metal foils and plates, and their structural changes with temperature were examined by electron diffraction method. It was found that the crystalline state in the basal part of the film was maintained up to a certain definite temperature above its melting point. This temperature increased linearly with increase of the number of carbon atoms in paraffin molecule, but was different from "transition temperature" named by K. Tanaka, at which the regularity of molecular arrangement in the surface layer of the film was completely destroyed. It was also found that molecules in the surface layer of the film were maintained in quasi-crystalline state up to the temperature mentioned above (transition temperature of the second kind). It was inferred that this phenomenon occurred even in the surface layer of the molten paraffin wax in bulk from its cooling curve. Extremely thin film of paraffin wax and films of some other similar compounds were also examined.

Introduction

It was reported by K. Tanaka[1] that the regular molecular arrangement in the surface layer of thin film of a long-chain compound formed on metal surface was maintained up to a definite temperature above its melting point and this phenomenon was reversible with temperature for paraffin, alcohol and others. This temperature was called "transition temperature" of the film by him. There exists a linear relationship between that temperature and the number of methylene groups contained in the molecule for each homologous series. The writer took interests in the internal structure of these films and intended to examine them by transmission method of electron diffraction.

Experiment

Specimens used were five Merck's paraffin waxes whose melting points ranged from 44° C to 74° C. Films of these waxes were prepared on

1. K. Tanaka: This Memoirs, **21** (1938), 85; **23** (1941), 195.

copper foils and plates by dropping benzene solution of a specimen or by smearing the molten wax on them and examined with electron diffraction, one by transmission method and the other by reflection method respectively. These specimens were heated by a small electric furnace in the diffraction apparatus during observations.

Results obtained by reflection method agreed well with Tanaka's previous work. The pattern obtained by transmission method, on the other hand, showed six spots and this corresponded to single crystal of orthorhombic system characteristic to paraffin series. The crystal transformed from orthorhombic to hexagonal system as temperature rose, in agreement with Müller's X-ray examination.[2] This state of hexagonal crystal was maintained up to a certain definite temperature higher than its melting point and at that temperature the spot pattern vanished and there appeared a blured ring, whose Bragg spacing was 4.6 Å which agreed well with the spacing obtained from molten paraffin by X-ray examination.[3] This definite temperature for each specimen is tabulated in Table I together with the transition temperature by reflection method. These temperatures were plotted against the mean number of carbon atoms in the molecule estimated from its melting point for each specimen (Fig. 1). (For convenience the writer will call the transition temperature by reflection method "the first kind" and that by transmission method "the transition temperature of the second kind" hereafter.) It can be seen from the figure that the transition temperature of the second kind also increases linearly with increase of the number of carbon atoms in the molecule, but the rate of increase is not the same as that of the first kind. It is interesting that the spot pattern by transmission method was still maintained above the transition temperature of the first kind for the specimen whose melting point was 74° C. Indeed, the transmission

TABLE 1

Transition temperature of paraffin wax.

Specimen No.	Melting point	Mean number of carbon atoms	Transition temperature	
			The 2nd kind	The 1st kind
1	44° C	22	60~61° C	74~76° C
2	46.5	23	62~64	75~77
3	52	24	66~68	79~80
4	68	31	89~90	89~90
5	74	35	102.5	91~93

2. A. Müller: Proc. Roy. Soc., A, **138** (1932), 514.
3. A. Müller: *ibid.*

pattern obtained for this state showed a blured ring inside the six spots. It is concluded from these facts that the crystalline state of the basal

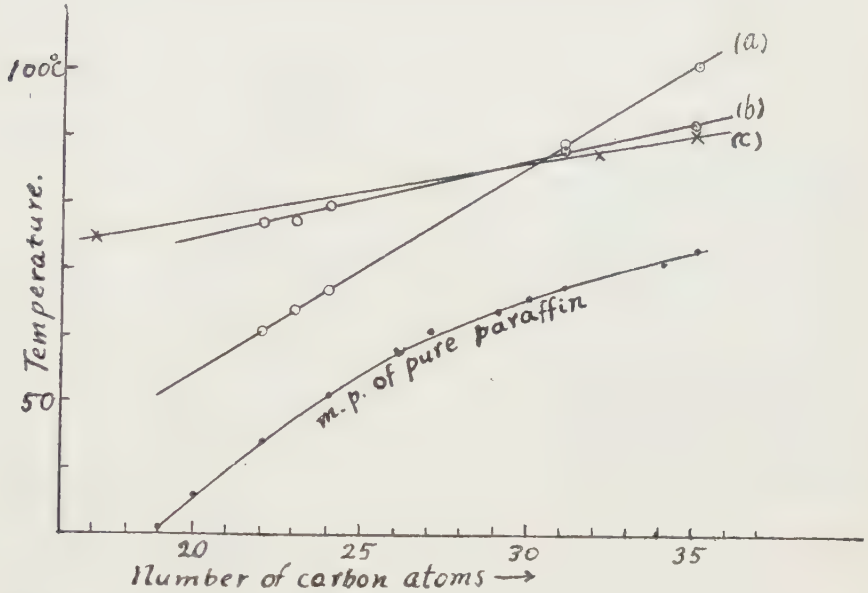

Fig. 1. (a) The transition temperature of the second kind, (b) that of the first kind for paraffin waxes. (c) The transition temperature of the first kind for pure paraffin quoted from K. Tanaka's paper.

part of the film is maintained up to the transition temperature of the second kind. Films formed on silver foils and plates were also examined, but it was found that transition temperatures of both kinds were not different from the corresponding values obtained for films on copper foils and plates.

Anomaly in reflection pattern.

Reflection pattern obtained from comparatively thick film of paraffin wax, whose transition temperature of the second kind was lower than that of the first kind, showed an anomaly as the temperature rose near the transition temperature of the second kind. Layer lines of the second and the third order became broad and blured, and then the line of the second order split up into two lines as temperature rose and approached the transition temperature of the second kind (Plate 1). This state was maintained in the temperature range of 2～3° C, and then the outer one of the double line vanished and the line of the first order became faint as temperature rose. This phenomenon was reversible with temperature.

This pattern was analysed by the usual method (Fig. 2) and it was found that this pattern was the superposition of two "grease patterns," one of which was not affected by refraction, while the other was subjected to the effect of inner potential of about 5 volts. The writer will call the former "C" pattern and the latter "L" pattern for convenience.

"L" pattern agrees well with the one for higher temperatures (Table 2) and it is obvious that this pattern is due to free molecules arranged perpendicularly to the free surface.

TABLE 2. Spacing and inner potential
(for the specimen whose melting point is 44° C)

Temperature	d (Å)	ϕ (volts)
17° C	2.58±0.02	c. a. 1.7~4.8
59 'C'	2.60~2.61	——
'L'	2.52~2.54	4.8~5.1
64	2.53~2.55	5.0~5.5

"C" pattern is rather close to the one for lower temperatures and the side spacings measured for spots on the first order line by Murison's method[4] agree well with those obtained for spot pattern by transmission method at the same temperature (Table 3). Layer lines of "C" pattern often appeared as arcs, especially on heating, which seems to be due to the orientated crystalline state. From these considerations it is concluded that "C" pattern is due to quasi-crystalline state whose c-axis is perpendicular to the surface.

TABLE 3. Side spacings for "C" pattern.

Side spacings measured for spot on the 1st order line.	Spacing & indices obtained by transmission method. (hexagonal system)		Indices estimated
4.16 Å	4.17 Å	(100)	(10 l)
2.40	2.40	(110)	(11 l)

The line of the fourth order of "C" pattern coincided with that of "L" pattern and consequently there exists the discrepancy of about 0.08 Å between the measured value of spacing d, which corresponds to the distance of alternate carbon atoms in a molecule, for "C" pattern and that for "L" pattern (cf. Fig. 2, also Table 2.). It is well known that the normal paraffin takes two crystalline forms[5] and the long spacing,

4. C. A. Murison: Phil. Mag., **17** (1934), 204.
5. A. Müller: Proc. Roy. Soc., A, **127** (1930), 417.

which corresponds to the chain-length of a molecule, increases by 1.25 Å and 1.203 Å per carbon atom for each form respectively. The twice of the difference of these two increments is nearly equal to the discrepancy mentioned above and this fact seems to suggest that there exists some connection between these two crystal forms and the state which produced "C" and "L" patterns.

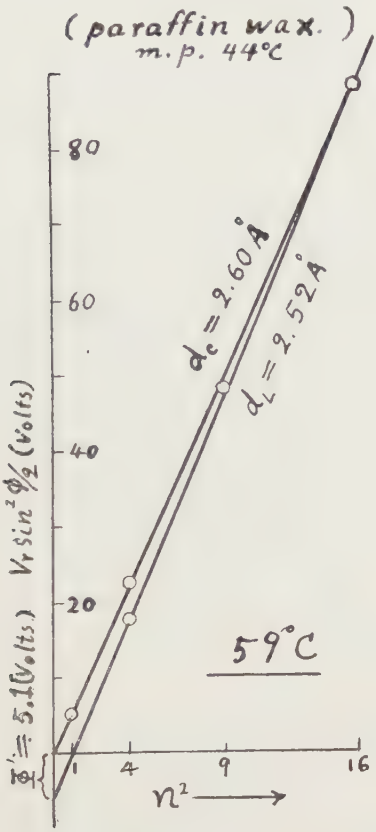

Fig. 2. n, order of reflection, ϕ, angle of reflection, Φ, inner potential, $V_r = V(1 + V \cdot 10^{-6})$, where V is the accelerating potential in volts. d is the spacing calculated from the inclination of straight line.

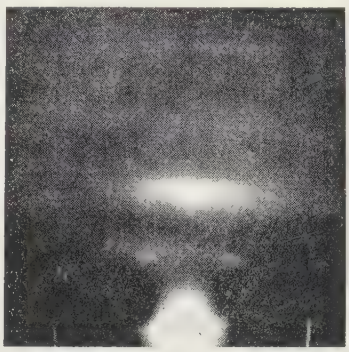

Plate 1.

Setting aside that problem, the writer wishes to interprete the process of transformation of pattern as follows: The quasi-crystalline state in the surface layer of film is maintained above the melting point, and then texture loosening begins, resulting in the unevenness of the surface. This state causes the broadening of layer lines. Then, a part of quasi-crystalline aggregate is decomposed into aggregates of free molecules (but the regularity of molecular arrangement is still maintained). These aggregates compose the flat part of the surface which produces "L" pattern. The remaining aggregate of crystallites produces "C" pattern. On cooling, crystal seeds are formed on the surface of film at the transition temperature of the second kind and they grow larger till quasi-crystalline aggregates cover up the whole surface as the temperature lowered.

The pattern did not show any anomaly when the film was thin enough, and only a temporary broadening of layer lines was observed near that temperature. Perhaps crystal grains formed were small in this case and projections of these crystal grains were not large enough to be free from refraction, on account of the thinness of the film. Specimen whose transition temperature of the second kind was higher than that of the first kind did not show this phenomenon.

Temperature-time curve.

It was expected that some latent heat would be absorbed or released at these transition temperatures, so that the writer intended to examine the cooling curve.

The film of paraffin wax was formed on an aluminium foil (thickness : 0.007 mm, area : $12 \times 12 cm^2$) by smearing molten wax or pouring benzene solution of the specimen on it. This foil was supported horizontally in a bronze box and heated from outside by electric heater. The thermo-couple used was made of manganin and constantan wire whose diameter was 0.1 mm. Temperature was read by the galvanometer in every ten seconds. Temperature-time curve obtained showed small swellings at transition temperatures, but no singularity was seen at the melting point.

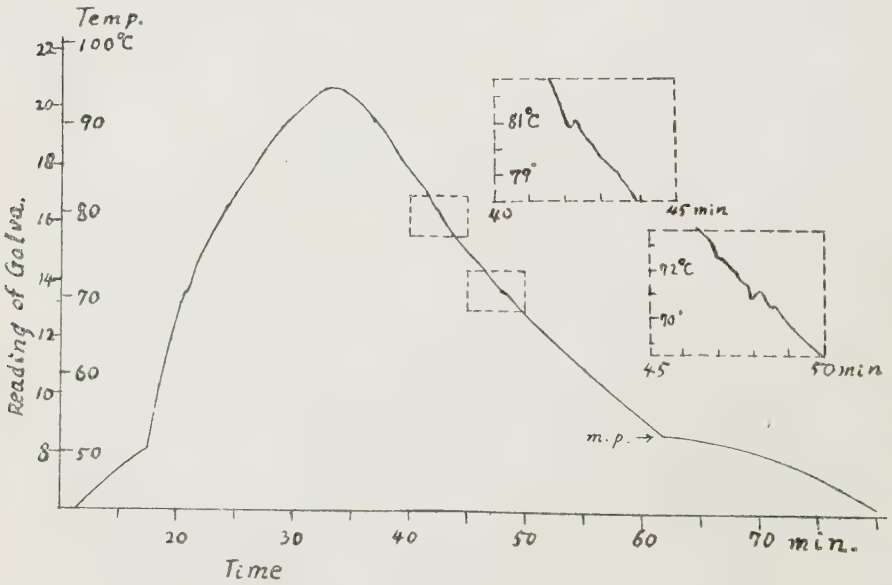

Fig. 3. Temperature-time curve of the surface layer of paraffin wax in bulk. (m. p. 52°C)

Then the same paraffin wax was melted and poured in a shallow pan made of tin-plate about 1 mm. in depth and the thermo-couple was touched lightly on the surface of the specimen. This pan was inserted in the same bronze box and measurement was carried out as before. Curve obtained also showed small swellings at these two transition temperatures (Fig. 3). It indicates that the phenomenon mentioned in the previous paragraph occurred even on the free surface of molten paraffin in bulk. Similar results were obtained with other specimens, but definite results were not obtained for specimens whose melting points were 68° C and 74° C respectively, since their purities were not so high as others.

Extremely thin films and others.

A small flake of paraffin wax was melted on copper plate and wiped off thoroughly with tissue paper while it was still in molten state. Reflection pattern obtained from this specimen, when once heated above its transition temperature and cooled, showed fibre structure whose fibre axis was nearly parallel to the normal of (110) plane and perpendicular to the surface of base metal, and the pattern due to the base metal superposed on it. Origin of this pattern would be as follows: Such film becomes too thin to be able to cover the whole surface of the base metal by evapolation of a part of film during heating process, and the remainder separates into many small groups of crystals whose *c*-axes are parallel to the surface of the base metal.

Films of $(C_{17}H_{35})-\overset{\overset{O}{\|}}{C}-(C_{17}H_{35})$ and $(C_{17}H_{35})-\overset{\overset{OH}{|}}{C}-(C_{17}H_{35})$ were also prepared from their benzene solutions and examined as before. Molecules were arranged with their long-chain axes parallel to the normal of the surface as in the case of paraffin. When once heated and cooled, molecular arrangement was not so regular as before. Tendency to form fibre structure mentioned above was stronger for these substances. Further researches on these substances are now in progress.

In conclusion, the writer wishes to express his sincere thanks to Professor K. Tanaka for his kind guidance.

Memoirs of the College of Science, University of Kyoto, Series A,
Vol. XXV, Nos. 3 & 4, Article 23, 1949.

On the "Precursory Recrystallization" in Copper and Brass Foils prepared by the Mechanical Rolling

By

Hideki Hirata, Masashige Koyama

and

Katsuyuki Yasuda

(Received September 24, 1949)

Abstract

A peculiar phenomenon as may be called a "Precursory Recrystallization," which had been found in our foregoing investigation with iron and nickel pulverized [1] or rolled [2] mechanically, was inferred to occur not only in the transition elements as stated above, but also in most metals undergone by some severe inner strain. To make clear whether such an inference were correct or not, the progress of the structural change by rising the temperature of the copper and brass foils of uniform thickness prepared mechanically by rolling them in various degrees (reduction percentages in thickness amount to 62.70%~99.89% in copper, while 95.00%~99.20% and 93.70% in α and β brass respectively), was examined with X-rays in the present experiment, similarly as in the previous ones.

As the consequence of this X-ray examination, it was confirmed that the usual recrystallization phenomenon in all the copper foils examined, takes place at 100°C~250°C, a temperature somewhat lower than that generally accepted as the recrystallization temperature of copper, almost irrespectively of the duration of annealing (2 min.~5 hr.): i. e., at the temperature above stated, the growth of the micro-crystals forming these foils, which tended to arrange themselves in a fibrous way, each having initially one of its ⟨111⟩ axis parallel to the direction of rolling, was observed to take place in comparatively short time, together with the conversion of the fibrous axis from the aforesaid ⟨111⟩ axis to ⟨100⟩ axis.

Among these copper foils, those corresponding to the reduction percentage 97.31%~99.68% were especially noticed to give rise to the "Precursory Recrystallization" as had previously been found with iron and nickel undergone by a severe mechanical work. By this "Precursory Recrystallization," two fibrous arrangements of the micro-crystals of considerable size were seen to be newly formed. One of these fibrous arrangements consisted of the micro-crystals, each having its ⟨111⟩ axis parallel to the direction of rolling; while in the other, the micro-crystals were so arranged that their common axis of the same indices

1. H. Hirata, H. Fujihira and E. Fujii, Rev. Phys. Chem. Japan, Commemoration Vol., 86, (1946).

2. H. Hirata and M. Yanagisawa, Rep. Inst. Chem. Research, Kyoto Univ., **18**, 94, (1949).

coincided with the normal to the aforesaid direction, in the plane of the surface of the foils. Here, it must be remarked that such a structural change due to the "Precursory Recrystallization" in the foils belonging to this category, was also given rise to by aging these foils at the room temperature for a few days.

The reason why the "Precursory Recrystallization" could hardly be detected in copper foils belonging to the other categories, were found to be explainable by the same consideration, which assumes the existence of two different kinds of the potential barriers of atoms in the metals undergone by a severe mechanical work, as previously reported in connection with iron and nickel. Especially, with regard to these which had been worked more severely than those displaying the "Precursory Recrystallization," it was confirmed that the "Precursory Recrystallization" had already taken place in the midst of the mechanical rolling, by an information deducible from the inner structure of the copper foils inflicted the heating and the rolling procedures alternately, as well from the change of their corrosibility, observed in the present experiment.

Moreover, it must be postscribed that the recrystallization phenomenon could also be detected to take place with α and β brass foils, by which the common axis of the micro-crystals forming a fibrous structure parallel to the direction of rolling, was seen to convert from $\langle 110 \rangle$ axis to $\langle 100 \rangle$ axis of the face-centred and body-centred cubic lattices respectively, in company with the augmentation of each micro-crystal, at a temperature a little higher than that of the copper foils. Nevertheless, within the scope of our examination, the "Precursory Recrystallization" could not be observed to occur with these brass foils.

Introduction

From the results of our foregoing X-ray examination on the structural change due to the annealing of iron and nickel, which had previously been undergone by a severe mechanical work as pulverization or rolling, it was confirmed that the recrystallization in these metals takes place in two distinct steps by heating; i. e., the growth of crystal grains takes place not only at the recrystallization temperature (about 600° C in iron and 700° C in nickel), but at a certain temperature (about 420° C and 470° C in iron and nickel respectively) far lower than the recrystallization temperature.

Such a peculiar phenomenon as may be called a "Precursory Recrystallization" (for the sake of abbreviation, let us denote it by "P. R." hereafter), that occurs at a temperature far lower than the recrystallization temperature, was inferred not to be presented as a characteristic of the transition elements above stated, but by a general property of the most metals containing some potential barriers of atoms considerably lowered due to the mechanical work. To make clear whether the aforesaid inference were correct or not, the writers were induced to repeat essentially the same X-ray examination as before, with copper and brass by the Laue method, utilizing the heterogeneous X-rays emitted from Cu anticathode. In this X-ray examination, the photographic plates were

always placed perpendicularly to the incident beam at a distance of 3 cm. behind the specimen, unless otherwise stated. The results thus obtained will be briefly described below.

Specimens

The specimens used in the present experiment were prepared by rolling electrolytic copper (99.977 % in purity), which had previously been annealed in vacuum at 600° C for 1 hour, in various degrees. Supplementary to these copper foils, some foils of α brass (25.62 % Zn—Cu) and β brass (50.22 % Zn—Cu) prepared by essentially the same procedure were also examined. The detailed conditions under which they were prepared are given in the following Tables 1 and 2 :—

TABLE 1.

Procedures of preparing the Copper Foils

No. of the Specimens	Thickness of the Specimens (in μ.) Before Rolling (d_0)	After Rolling (d)	Reduction % (R) $R=\frac{d_0-d}{d_0}\times 100$	Remark
A	574	204	62.70	
B	1865	50	97.31	On the way of the procedure of rolling the foil was placed between two copper plates for the furtherance of reducing its thickness.
C	ditto	20	98.93	
D	ditto	6～9	99.68～99.52	
E	ditto	2～3	99.89～99.84	
F	ditto	5	99.73	On the way of the procedure of rolling the foil was folded, for the furtherance of reducing its thickness.
G	ditto	2	99.89	

TABLE 2.

Procedures of preparing the Brass Foils

No. of the Specimens	Composition of the Specimens	Thickness of the Specimens (in μ) Before Rolling (d_0)	After Rolling (d)	Reduction % (R) $R=\frac{d_0-d}{d_0}\times 100$	Remark
H	Cu 74.38 %	1000	50	95.00	α Brass
I	Zn 25.62 %	ditto	8～10	99.20～99.00	
J	Cu 49.78 % Zn 50.22 %	800	50	93.70	β Brass

By the way, it must be noted in connection with the thickness of the foils d_0 given in the second columns of Tables 1 and 2, that the values indirectly determined from the weight and the area of the foils, were

always seen to coincide fairly well with those measured directly by means of a varnier caliber (when $d > 50\,\mu$) or Shimazu's minimeter (when $d < 50\,\mu$). This shows us without doubt that all the foils under consideration were of the uniform thickness. Moreover, it should be postscribed that among these specimens here tabulated, Specimens C～G were obtained from Specimen B by the furtherance of the rolling procedure.

Except for Specimen A which was found too thick to give rise to any reliable diffraction pattern of X-rays, each one of the specimens above tabulated was annealed again in vacuum at various temperature (50° C～800° C) for various durations of annealing (2 min.～5 hr.), just before it was illuminated by X-rays, unless otherwise stated. However, to render Specimen A suitable for X-ray examination, the writers were obliged to remove its outer portion by pickling this specimen in dilute nitric acid, after the aforesaid heat-treatment. In addition to the aforesaid specimen, metallic copper deposited by putting a small piece of zinc into a solution of copper sulphate of the concentration 10 %～13 % in weight, was also used as the standard specimen by the way of comparing the effects of the mechanical work.

Experimental Results

Some of the Laue photographs obtained in the present experiment are reproduced in Figs. 1～20, Plate 1 and Figs. 22～26, Plate 2. In each one of these Laue photographs, the corresponding annealing temperatures and durations of annealing of the specimen, are respectively denoted by the abbreviations T and D. To take the Laue photographs here reproduced except for Fig. 20, Plate 1, each specimen was so placed that its foliate surface was perpendicular to the incident X-ray beam, by setting the direction of rolling vertically, while, Fig. 20, Plate 1 was obtained on the photographic plate placed at a distance of 2 cm. behind the specimen, when the direction of rolling was tilted by an angle of 45° from its vertical position towards the incident beam.

Supplementary to Plates 1 and 2, the outlines of the diffraction patterns in some Laue photographs, most of which were not reproduced, were described in Tables 3 and 4 classifying with one another. Here, it must be postscribed that the patterns inserted in Tables 3 and 4, as well as those reproduced in Plates 1 and 2 were only those given rise to by the specimens annealed for 1 hour after the mechanical rolling, unless especially remarked in the brackets. Nevertheless as can be seen from Figs. 7～9 and 11, 12, Plate 1, when the specimens rolled by an equal amount, were annealed at an equal temperature, their structural changes were found to

remain almost unaltered with one another, irrespectively of the duration of annealing. This shows us that the structural changes above stated

TABLE 3. Constituents of Each Diffraction Pattern taken with the Copper Foils.

No. of the Specimens \ Annealing Temp. (in °C)	Room Temp.	50	70	100	120	150	160	200
A	cR cCB				cR cCB	AL cR cCB	dR	dR
B	cR ↑ cSB ⟨111⟩			cR ↑ cSB ⟨111⟩	cB ↑ cCB ⟨111⟩ dCB		dR dCB	
C	ditto		cR ↑ cSB ⟨111⟩	↙↑ dSB ⟨111⟩ cR ↑ cSB ⟨111⟩		↑ cSB ⟨100⟩ ↙↑ dSB ⟨111⟩ dR		
D	ditto	↑ cSB ⟨111⟩ cR ↙↑ dSB ⟨111⟩		↑ cSB ⟨100⟩ ↙↑ dSB ⟨111⟩ ↑ cSB ⟨111⟩ cR		↑ cSB ⟨100⟩ ↙↑ dSB ⟨111⟩ dR		↑ cSB ⟨100⟩ ↙↑ dSB ⟨111⟩ dR
E	ditto	cR cSB ⟨111⟩				cR ↑ cSB ⟨111⟩		
F	ditto			↑ cSB ⟨111⟩ cR	cR ↑ cSB ⟨111⟩ cB		↑ cSB ⟨111⟩ d R cR	
G	ditto			(2 hrs.) ↑ cSB ⟨111⟩ cR	cR ↑ cSB ⟨111⟩		↑ cSB ⟨111⟩ cR	↑ cSB ⟨111⟩ cR

TABLE 3. (continued)

No. of the Specimens \ Annealing Temp. (in °C)	250	300	350	450	500	600	700	800
A								AL
B		dR dCB	dR dCB		dCB dR	dCB AL	dCB AL	dCB AL
C	←↑dSB⟨111⟩ ↑cSB⟨100⟩ dR		←↑dSB⟨111⟩ ↑cSB⟨100⟩ dR	←↑dSB⟨111⟩ ↑cSB⟨100⟩ dR		(5 hr.) ↑cSB⟨100⟩ ←↑dSB⟨111⟩	←↑dSB⟨111⟩ ↑cSB⟨100⟩ AL	←↑dSB⟨111⟩
D	↑cSB⟨100⟩ ←↑dSB⟨111⟩ dR	↑cSB⟨100⟩ ←↑dSB⟨111⟩		←↑dSB⟨111⟩ ↑cSB⟨100⟩		←↑dSB⟨111⟩ ↑cSB⟨100⟩	←↑dSB⟨111⟩ dR ↑cSB⟨100⟩	(5 hr.) ←↑dSB⟨111⟩ ↑cSB⟨100⟩
E	↑cSB⟨100⟩ dR			↑cSB⟨100⟩ dR		↑cSB⟨100⟩ dR		↑cSB⟨100⟩ dR
F	dR ↑cSB⟨100⟩							dR
G		dR ↑cSB⟨111⟩					dR ↑cSB⟨100⟩	

usually comes to the end in a comparatively short time. Consequently, the description in Tables 3 and 4 may be deemed to hold usually good to

all the diffraction patterns taken in the present experiment with copper and brass foils annealed for various durations.

TABLE 4.

Constituents of Each Diffraction Pattern taken with the Brass Foils.

No. of the Specimens \ Annealing Temp. (in °C)	Room Temp.	100	150	200	250	300	400	500
H (α Brass)	↑ cSB ⟨110⟩ cR	↑ cSB ⟨110⟩ cR	cR cSB ?	cR cSB ?	cR	cR	cR	dR
I (α Brass)	cR cWB	cR cWB	cR cWB	cR cWB	cR ↑ cSB ⟨100⟩	↑ cSB ⟨100⟩ dR	↑ cSB ⟨100⟩ dR	↑ cSB ⟨100⟩ dR
J (β Brass)	↑ cSB ⟨110⟩ cR	↑ cSB ⟨110⟩ cR	cCB cR	cCB cR	dR	dR		

P. S. In each block of Tables 3 and 4, the constituents of the diffraction pattern in each Laue photograph are represented in the order of their predominance by the following abbreviations, here the constituents observed before the heat-treatment being underlined. Among these constituents, discontinuous ones consisting of a number of intense spots are designated by the prefix d against c corresponding to the continuous ones.

CB: complex distribution of radiating bands given rise to by an irregular assemblage of several fibrous-like structures; ↑ SB ⟨hkl⟩: a set of radiating bands given rise to by a single fibrous structure corresponding to the rotation of micro-crystals around ⟨hkl⟩ axis parallel to the direction of rolling; ↙↑ SB ⟨hkl⟩: two sets of radiating bands given rise to by two fibrous structures corresponding to the rotations of micro-crystals around the axes parallel and normal to the direction of rolling respectively; WB: intense bands on Debye rings showing the presence of the fibrous nature of weak degree; R: Debye rings; AL: assemblage of a number of small Laue spots.

Discussion of the Experimental Results

1. Copper Foils

Among the experimental results above stated, those represented in Plate 1 and Table 3 lead us to the following considerations with respect to the copper specimens :—

First of all, the rolled copper foils prior to the annealing procedure were found to give rise to the diffraction patterns in the Laue photographs, reproduced in Figs. 1, 3, 6 and 17, Plate 1, as well those inserted in the second column of Table 3. As can be seen in these patterns, those which were produced by the foils of the comparatively small reduction percentage as Specimen A (its reduction percentage R amounts to about 62.70 %), consisted of a set of continuous Debye rings due to the (111) and (200) reflections of the characteristic radiations Cu K_α and Cu K_β from the face-centred cubic lattices of copper crystals ; on these Debye rings, the intense segments attributable to the superposition of the complex congregation of radiating bands also came to appear, showing the presence of an irregular assemblage of several fibrous-like structures. While, in the foils of the larger reduction percentage as Specimens B～G ($R \geqq 97.31$ %), the aforesaid complex congregation of radiating bands was found to fuse together into a set of radiating bands given rise to by a fibrous arrangement of the micro-crystals, each having its $\langle 111 \rangle$ axis parallel to the direction of rolling. Accordingly, the specimens of the copper foils used in the present experiment, to begin with, may be deemed to be composed of the micro-crystals of the diameter 10^{-3}cm.～10^{-4}cm. before they were annealed. It can also be inferred with regard to these specimens prior to the annealing, that the copper foils of the smaller reduction percentage of the order 62.70 %, are composed of an irregular aggregation of the micro-crystals, which arrange themselves quite confusedly, except only those forming several fibrous-like structures ; while, in the foils of the larger reduction percentages than 97.31 %, the micro-crystals are seen to arrange themselves in a definite fibrous way, with one of their $\langle 111 \rangle$ axis parallel to the direction of rolling.

Next, let us reflect upon the structural change of these specimens due to the annealing procedure. Among these specimens, with respect to those undergone by a comparatively slight mechanical work as Specimen A, it can be seen from Figs. 1 and 2, Plate 1 as well as from the second row of Table 3, that the congregation of the radiating bands already mentioned, grew less conspicuous and an irregular assemblage of small spots became newly appreciable, at a temperature of about 150° C.

Furthermore, at about 160° C, the rearrangement of these spots so as to form a set of discontinuous Debye rings was observed, together with the complete extinction of the former radiating bands. But, such a regular distribution of the intense spots sitting in rings was violated again, when the foils were heated at 800° C. Here, it must be remarked parenthetically that a piece of metallic copper deposited from the solution of copper sulphate by the procedure as already mentioned, were seen to give rise to a series of the Laue photographs (not reproduced), which showed that the growth of the newly germinated crystal nuclei begins by heating at about 300° C in such a specimen inferred free from any severe inner strain due to the mechanical works. This shows us that even in Specimen A undergone by a comparatively slight rolling, the temperature at which the growth of the crystal nuclei began to take place, was somewhat lowered by the mechanical work. Thus, Specimen A may be deemed to lose its fibrous-like nature at 150° C∼160° C by the growth of the micro-crystals newly generated, then to display the augmentation of these micro-crystals at about 800° C, up to those of the diameter 10^{-2}cm.

When the reduction percentage of the copper foils was promoted to 97.31 %∼99.68 % as was the case of Specimens B, C and D, a set of radiating bands each consisting of innumerable feathery spots became newly observable accompanied by the old ones, in the diffraction patterns, at an annealing temperature 50° C∼120° C, as can be seen in Fig. 7, Plate 1 and in the third, fourth and fifth rows of Table 3. It goes without saying that the appearance of such coarse radiating bands indicates the segregation of the micro-crystals of a considerable size (10^{-2}cm.∼10^{-3}cm. in diameter), arranged themselves in a fibrous way. The temperature at which these coarse bands begin to appear, was noticed to be far lower than the recrystallization temperature of copper generally accepted (about 200° C), not to mention about that of the deposited copper due to the difference of the solutional pressures as already stated. It was also observed that this temperature was the more lowered the more increased the reduction percentage of the specimen. Especially, from Specimen D of the largest reduction percentage among the specimens belonging to this category, the aforesaid coarse radiating bands were noticed to be produced, when it was kept even at the room temperature for a few days. Thus, the appearance of such radiating bands may be conceived to be due to the "P. R." in copper, similar to those previously detected with iron and nickel.

If we inspect the diffraction patterns in which the coarse radiating bands above stated are visible as in Figs. 4, 5, 7, 13, 16, Plate 1, and as some

of those inserted in the third, fourth and fifth rows of Table 3, it can be remarked that the angular distribution of these bands coming to appear from Specimen B undergone by a comparatively slight mechanical work, is rather confused; while, the bands taken with Specimens C and D rolled more severely than the above, are found to be distributed symmetrically to the direction of rolling. This fact shows us that when the copper foils are heated at a low temperature, the micro-crystals separate out without any remarkable influence of their orientation effect, in the specimen of the comparatively small reduction percentage of the order 97.31 %; but in the specimens of the somewhat larger reduction percentages of the order 98.93 %～99.68 %, they tend to arrange themselves in a fibrous way. Further, the fibrous nature beared by the specimens of the somewhat larger reduction percentage above stated as Specimens C and D, was conceived from the diffraction patterns containing the coarse radiating bands of a regular distribution as shown in Fig. 7, Plate 1, to consist of two fibrous arrangements of the micro-crystals newly formed. One of these fibrous arrangements was made of the micro-crystals with their ⟨111⟩ axis parallel to the direction of rolling, while in the other, the micro-crystals being so arranged that their common axis ⟨111⟩ coincided with the normal to the aforesaid direction in the plane of the surface of foils. It can also be seen in Figs. 10, 12 and 15, Plate 1, together with the fourth and fifth rows of Table 3, that four radiating bands distributed symmetrically to the direction of rolling come to appear from Specimens C and D at a temperature about 100° C ～150° C, besides those given rise to by the " P. R." already mentioned. Such radiating bands were detected too, even with Specimen B, by the annealing at a temperature 160° C, though they are faint and rather confused (cf. Fig. 4, Plate 1). By rising the annealing temperature, these radiating bands were seen generally to grow the more conspicuous at the outset, then to tend fainter and fainter, until they became sometimes indetectable at 800° C especially in such a specimen as Specimen C (cf. the fourth row, Table 3). The annealing temperature at which the aforesaid bands came to appear most markedly, was confirmed also to vary according to the degree of the mechanical work: i. e., this temperature was observed to rise with the increase of the reduction percentage of the specimen, as to attain 700° C in Specimen C (cf. Fig. 11, Plate 1 and the fourth row of Table 3), when the mechanical work inflicted upon the specimen was comparatively small, but it lowered by the further increase of the reduction percentage. In addition to those above stated, these continuous bands were inferred from Figs. 10, 12 and 15, Plate 1,

to be given rise to by a fibrous arrangement of micro-crystals of the diameter 10^{-3}cm.$\sim 10^{-4}$cm., each having its $\langle 100 \rangle$ axis parallel to the direction of rolling.

To make clear the cause of such a structural change above stated, let us refer to the Laue photographs taken in the present experiment with the specimens belonging to the same category as Specimens C and D, which were reannealed immediately after the procedure of the annealing, at a certain temperature lower than that of the succeeded reannealing. According to this reference, the inner structures of the specimens indicated by these Laue photographs, were seen to remain nearly the same as those caused by the simple annealing at the reannealing temperature (say 600° C$\sim$800° C in the case of Specimen C) without preannealing, provided that the preannealing temperature was not so high (say 70° C$\sim$100° C in Specimen C) as to give rise to the aforesaid continuous band. On the contrary, if the preannealing temperature were high enough to produce these bands (say 350° C in Specimen C), the inner structures of the specimens were confirmed almost unaltered, as is clear by comparing Figs. 13 and 14, Plate 1, with those of the same specimens simply annealed only once at that preannealing temperature, irrespectively of the occurrence of the reannealing procedure. Thus, the aforesaid fibrous structure having $\langle 100 \rangle$ axis of the micro-crystals in common being tolerably stable, it may be deemed to arise from the usual recrystallization.

Previously, it has been inferred that the common axes of the fibrous structures produced by the " P. R." were two $\langle 111 \rangle$ axes intersecting perpendicularly with each other ; while, that corresponding to the usual recrystallization was deemed to be $\langle 100 \rangle$ axis of the micro-crystals. To decide whether the above inference were correct or not, the writers tried to take a Laue photograph with Specimen C, which had been annealed at 800°C for 1 hour to give rise to the precursory as well as the usual recrystallizations, by tilting by an angle of 45° the direction of rolling from its vertical position towards the incident X-ray beam, as already stated. The Laue photograph thus obtained was reproduced in Fig. 20, Plate 1. In the annexed figure, Fig. 21, the theoretical positions of the radiating bands due to the " P. R." and the usual recrystallization calculated following to the

Fig. 21.

aforesaid inference by the aid of Nishikawa's formula,[3] are represented respectively by the dotted and full lines: while, the shaded part of the same figure is the copy of the diffraction pattern in the original plate[4] of Fig. 20, Plate 1. As may be seen from Fig. 21, the agreement between the calculated curves and the observed ones is satisfactory. Accordingly, it must be concluded that our foregoing inference is correct.

The facts which have hitherto been stated in connection with Specimens C and D, show us that in some district of the copper foils rolled at the reduction percentage 97.31 %～99.68 % the "P. R." takes place by heating these foils at a temperature (the room temperature～120° C) far lower than the usual recrystallization temperature. By this "P. R." the superposition of two fibrous structures are newly generated besides the former one due to the foregoing mechanical work, each one of these fibrous structures given rise to by the "P. R." being confirmed to be composed of the micro-crystals of the diamater 10^{-2}cm.～10^{-3}cm., so arranged that their common axes of the indices ⟨111⟩ are situated parallel and perpendicular respectively to the direction of rolling.

Moreover, in the other district of these foils which has not been inflicted the "P. R.", the usual recrystallization also occurs at a temperature somewhat lower than the recrystallization temperature generally accepted. By this recrystallization, the tendency of the growth of the micro-crystals as well as that of the conversion of the fibrous axis from the ⟨111⟩ axis to the ⟨100⟩ axis, can be detected.

Lastly, let us advance our considerations to the cases of Specimens E, F and G, which had been inflicted a mechanical work so severe as to correspond to the reduction percentage over 99.73 %. Among these specimens, Specimen E was prepared by the same procedure as those of preparing the others hitherto been mentioned; while Specimens F and G were rolled by a somewhat different way as denoted in the remark of Table 1. It was noticed, as may be seen from Figs. 7～19, Plate 1 as well as the diffraction patterns recorded in the rows that follow the sixth row of Table 3, that any one of these specimens did not give rise to the coarse radiating band even after the procedure of the annealing: furthermore, such an indication of the occurrence of the "P. R." could not be detected, even when these specimens were kept in the room temperature for several days. Merely, it was found that when Specimens E, F and G were annealed at a temperature 250° C, the diffraction patterns taken

3. S. Nishikawa and S. Ono: Proc. Tokyo Math. Phys. Soc., **11**, 131, (1913).

4. It is to be noticed that the diffraction patterns reproduced in Plates 1 and 2 are interchanged from right to left as compared with those of the original plates.

with them always indicated the occurrence of the recrystallization : i. e., these diffraction patterns were in some cases seen to contain a set of discontinuous Debye rings consisting of a number of small intense spots, as had previously been observed with Specimen B, while in the other cases, the patterns were made of by a set of radiating bands disclosing the presence of a fibrous structure in which the micro-crystals rotated around their common axis ⟨100⟩ parallel to the direction of rolling, as had been the cases of Specimens C and D. Thus, Specimens E, F and G must be looked upon not to present the "P. R." in spite of the far more severe mechanical work inflicted on them. Such a peculiar fact may be inferred probably to be due to the occurrence of the " P. R." early in the very midst of the procedure of rolling.

To make clear the above inference more decisively, the writers repeated X-ray examination essentially the same as before with a copper foil undergone by the heat and mechanical treatments alternately. Speaking the more precisely in connection with the procedure of the heat and the mechanical treatments above mentioned, a copper foils as Specimen C, which had preliminarily been rolled by an amount somewhat smaller than those in the cases of Specimens E, F and G, was annealed at a temperature high enough to give rise to the " P. R." (e. g., at 250° C in the case of Specimen C), then rolled again until the total amount of its reduction percentage from the beginning amounts to 99.73 %, before the progress of its structural change by heating was examined with X-rays. As the consequence of this X-ray examination, the aforesaid progress indicated by the Laue photograph, was seen essentially unaltered from those traced with Specimens E, F and G. This fact is in good accordance with our foregoing inference.

By way of the further confirmation of the above inference, the writers examined the corrosibility of Specimens A, C and E kept at the room temperature for several days, by pickling them into a dilute nitric acid of the concentration 10 %. It is expected in this case, that if the " P. R." had not taken place either in the midst or in the afterwards of the procedure of mechanical rolling, the aforesaid corrosibility should have increased with the increase of the reduction percentage of the specimens.[5] But, contrary to the above expectation, this corrosibility was found to decrease in the order of Specimens A, C and E, with the increase of their reduction percentages. This shows us that not to mention about Specimen C but even in Specimen E, the activation energy of the atoms

5. E. g., D. Uno, H. Hirata and K. Niimi, J. Metallog. Soc. Japan, **6**, 372, (1942).

had been decreased by "P. R." Our foregoing inference being thus confirmed again, we may conclude without doubt that the "P. R." took place in Specimens E, F and G in the midst of the mechanical rolling.

II. Brass Foils

As has already been mentioned, the specimens of the brass foils used in the present experiment belonged to the categories of α and β brass, which are generally known to form the face-centred cubic and the body-centred cubic lattices respectively. The results of X-ray examination carried out with regard to the structural change of these specimens due to the procedure of the annealing, were represented in Plate 2 together with in Table 4.

According to these results, the diffraction patterns taken with the foils of α brass prior to the annealing procedure (cf. Fig. 22, Plate 2 and the second column of Table 4), were seen to consist of a set of the radiating bands due to the fibrous arrangement of micro-crystals of the diameter 10^{-3}cm.$\sim 10^{-4}$cm., having $\langle 110 \rangle$ axis of each face-centred cubic lattices parallel to the direction of rolling, when the reduction percentage of the specimen was of the order 95.00 % as in Specimen H; while, the specimen corresponding to the reduction percentage of the order 99.00 %$\sim$99.20 %, as Specimen I, did not display any fibrous nature all the more, but gave rise to a number of continuous Debye rings (not reproduced). The fibrous structure of Specimen H was observed to begin to be gradually violated at a temperature 100° C$\sim$150° C, henceforth the violation of this fibrous structure being continued, until it was replaced by an assemblage of the comparatively larger micro-crystals of the diameter 10^{-2}cm.$\sim 10^{-3}$cm. at 500° C, due to the recrystallization, which gave rise to numerous small intense spots on the Laue photograph. One part of these spots distributed themselves on the Debye rings showing an irregular assemblage of the micro-crystals; while, the others were seen to form a set of discontinuous radiating bands corresponding to the fibrous structure made of the micro-crystals, each having its $\langle 100 \rangle$ axis parallel to the direction of rolling. With regard to Specimen I, the Debye rings and the radiating bands made of numerous intense spots in the Laue photographs (cf. Figs. 23 and 24, Plate 2, together with the third row of Table 4), which represented the occurrence of the recrystallization, were found to appear at a temperature about 250° C, the rise of the annealing temperature merely causing the augmentation of each spot.

Next, in connection with the foils of β brass, our examination was

restricted only to Specimen J corresponding to the reduction percentage 93.70 %. The Laue photographs taken with this specimen prior to the annealing procedure, were found to consist of a set of the Debye rings together with the radiating bands (cf. Fig 25, Plate 2 and the fourth column of Table 4). Thus, Specimen J may be looked upon as to be made of by a fibrous structure having ⟨110⟩ axis of each body-centred cubic lattices parallel to the direction of rolling, which was buried into an irregular assemblage of the micro-crystals of the diameter 10^{-3}cm. $\sim 10^{-4}$cm. Still, the diffraction patterns in these Laue photographs altered by an annealing at 250° C, as can be seen in the fourth row of Table 4, to those consisting of a set of Debye rings formed by a number of intense spots. This shows us that the micro-crystals in the specimen grew up by the recrystallization due to an annealing at 250° C, to those of the diameter 10^{-2}cm.$\sim 10^{-3}$cm., rearranging themselves without any regularity.

Anyhow, it must be remarked that with the foils of α and β brass undergone a severe mechanical works, the recrystallization was observed to take place at a temperature a little higher than that of the copper foils prepared by a similar procedure. Neverthless, within the scope of our examination, the " P. R." could not be observed to occur with these brass foils.

Conclusion

The arguments which have hitherto been advanced with respect to the progress of the structural change of the rolled foils of copper and brass due to the procedure of the annealing, lead us to the following conclusions :—

First of all, the copper foils prior to the annealing were found to consist of the micro-crystals of the diameter 10^{-3}cm.$\sim 10^{-4}$cm., which aggregated without any regularity except for those forming the fibrous-like structure. These foils can be classified into three classes, by the difference of the progress of the structural change due to the annealing ; the reduction percentages of the foils belonging to each one of these three classes were estimated to be the orders 62.70 %, 97.31 %$\sim$99.68 % and 99.73 %$\sim$99.89 % respectively.

Among these above classified, the foils belonging to the first class, which correspond to the reduction percentage of the order 62.70 %, are composed of the complex congregation of several fibrous-like structures buried into an irregular aggregation of the micro-crystals. These foils do not exhibit the " P. R." by heating. But, the growth of the micro-

crystals in these foils due to the recrystallization, begins at 150° C～160° C, a temperature somewhat lower than that generally accepted as the recrystallization temperature of copper. This shows us that the effects of the mechanical work upon the inner structure of the foils belonging to the first class, is not so severe as to produce the remarkable lowering of some potential barriers of the atoms forming these foils, as has already been stated in the previous reports.[1, 2]

The foils belonging to the second class, which have been rolled mechanically so as their reduction percentage amounts to 99.31 %～99.68 %, are made of the micro-crystals arranged themselves in a fibrous way, having their ⟨111⟩ axis parallel to the direction of rolling, except for those irregularly aggregating, prior to the annealing procedure. These foils are distinguished for the "P. R." displayed by them, when they are annealed. The temperature at which the aforesaid "P. R." begins to take place, is varied from 120° C to the room temperature, according to the conditions. By this "P. R.", two fibrous arrangements of the micro-crystals of considerable size, each having the axis of the indices ⟨111⟩ in common. One of these fibrous arrangements has its common axis of the same indices coinciding with the normal to the aforesaid direction, in the plane of the surface of the foils. Anyhow, the occurrence of the "P. R." indicates that the mechanical work given to the copper foils belonging to the second class is severe enough to give rise to the remarkable of some potential barriers of atoms in these foils, as has previously been seen with iron and nickel inferred to bear a considerable amount of the inner strain due to the mechanical works of the pulverization or the rolling.

The usual recrystallization begins to take place in the foils belonging to the second class, by heating at a temperature of 100° C～150° C, which is seen generally to be lowered with the increase of the reduction percentage of these foils. By this recrystallization, the growth of the micro-crystals up to those of the diameter 10^{-2}cm.～10^{-3}cm., as well as the conversion of the fibrous axis from the axis of the indices ⟨111⟩ to that of ⟨100⟩, situated parallel to the direction of rolling, can be detected.

Lastly, the copper foils belonging to the third class, which have been rolled so severely as to correspond to the reduction percentage over 99.73 %, are seen prior to the procedure of the annealing to be essentially the same inner structure as those belonging to the second class. It is remarked that any indication of the occurrence of the "P. R." in these foils cannot be detected, notwithstanding the severe mechanical work inflicted on them. Merely the usual recrystallization is observed to take

place in these foils at a temperature about 250° C. Such a peculiarity of the foils belonging to the third class, can be attributed to the occurrence of the " P. R." early in the very midst of the procedure of rolling.

Next, the foils of α and β brass are confirmed also to be made of the micro-crystals of the diameter 10^{-3}cm.$\sim 10^{-4}$cm. prior to the procedure of the annealing. These micro-crystals aggregate without any regularity, except that some of them arranged themselves in a fibrous way, as those in the foils of α and β brass corresponding to the reduction percentages of the orders 95.00 % and 93.70 % respectively. This fibrous nature does not necessarily increase with the increase of the reduction percentage of the foils.

The axis of fibre is found to coincide with $\langle 110 \rangle$ axis of either face-centred or body-centred cubic lattices of α and β brass. In the former case, the recrystallization phenomenon takes place by the annealing at a temperature 500° C, which gives rise to a new fibrous structure with $\langle 100 \rangle$ axis situated parallel to the common direction as in the copper foils. But, the recrystallization temperature above stated is lowered with the increase of the reduction percentage, until it becomes to 250° C in the foils of α brass corresponding to the reduction percentage of 99.00 %$\sim$99.20 %. While, in the latter case, the foils of β brass recrystallize at a temperature of 250° C. Nevertheless it must be remarked that the " P. R." was seen to occur neither in α nor in β brass, within the scope of our examination.

In conclusion, the writers wish to express their best thanks to Dr. M. Sumitomo of the Sumitomo Metal Industrial Co., who supplied them with various samples of brass used in this experiment. Their thanks are also due to the Department of Education for the Scientific Research Expenditure defrayed in the present research.

PLATE 1. Laue Photographs of Copper Foils.

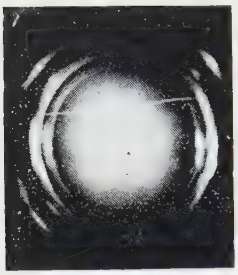

Fig. 1. Specimen A
(before annealing)

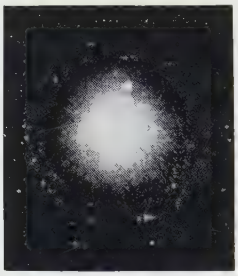

Fig. 2. Specimen A
(T=160° C)

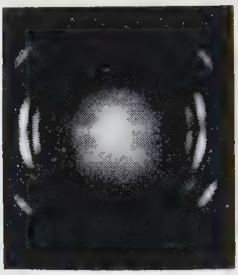

Fig. 3. Specimen B
(before annealing)

Fig. 4. Specimen B
(T=160° C)

Fig. 5. Specimen B
(T=800° C)

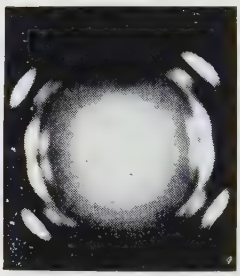

Fig. 6. Specimen C
(before annealing)

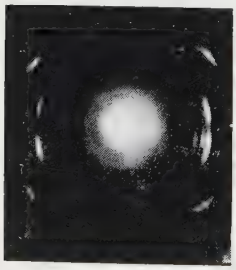

Fig. 7. Specimen C
(T=100° C)

Fig. 8. Specimen C
(T=100° C, D=5 min.)

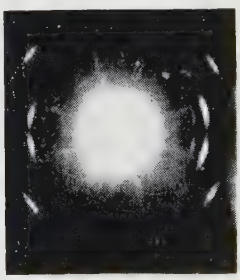

Fig. 9. Specimen C
(T=100° C, D=30 min.)

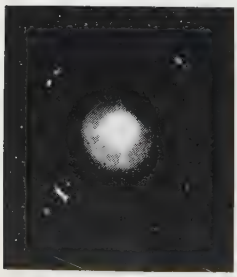

Fig. 10. Specimen C
(T=150° C)

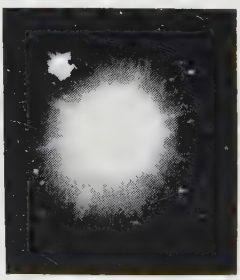

Fig. 11. Specimen C
(T=700° C)

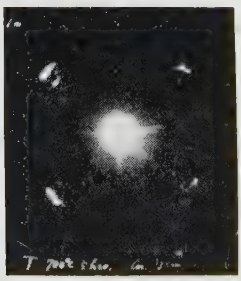

Fig. 12. Specimen C
(T=700° C, D=5 hr.)

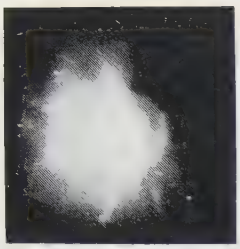

Fig. 13. Specimen C
(T=800° C)

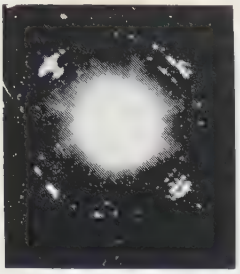

Fig. 14. Specimen C
(T=350° C, D=1 hr.
reannealed at
T=800° C, D=1 hr.)

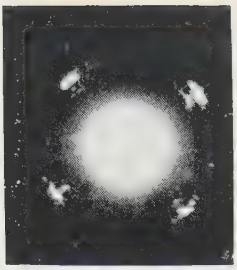

Fig. 15. Specimen D
(T=150° C)

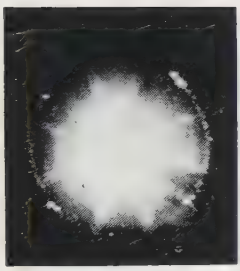

Fig. 16. Specimen D
(T=700° C)

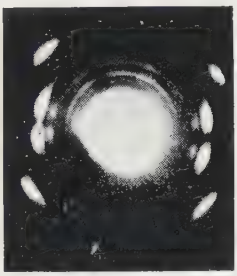

Fig. 17. Specimen E
(before annealing)

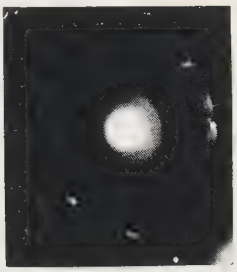

Fig. 18. Specimen E
(T=150° C)

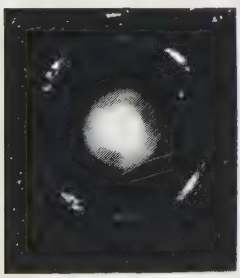

Fig. 19. Specimen E
(T=800° C)

Fig. 20. Specimen C
(T=800° C
obliquely illuminated)

PLATE 2. Laue Photographs of Brass Foils.

Fig. 22. Specimen H (before annealing)

Fig. 23. Specimen H (T=400° C)

Fig. 24. Specimen H (T=500° C)

Fig. 25. Specimen J (before annealing)

Fig. 26. Specimen J (T=250° C)

Memoirs of the College of Science, University of Kyoto, Series A,
Vol. XXV, Nos. 3 & 4, Article 24, 1949.

Thermal Conductivities of Single- and Polycrystalline Bismuth*

By

Shigeka Nishioka

(Received September 7, 1949)

Abstract

Thermal conductivities of single- and polycrystalline bismuth were measured by using specimens in the form of a cube. The values found at 14° C were as follows:—

The thermal conductivity of polycrystal: 0.01914 cal./cm. sec. deg.
The thermal conductivity of single crystal parallel to the trigonal axis: 0.01269 cal./cm. sec. deg.
The thermal conductivity of single crystal perpendicular to the trigonal axis: 0.02252 cal./cm. sec. deg.

Linder's theory for the relation between the thermal conductivities of single- and polycrystalline bismuth was verified by applying the above values.

Measurements were also carried out on several specimens in the form of rectangular plates of single crystal, of which the orientation of the trigonal axis with respect to the normal to the plate ranges from 0° to 89°. The results showed that the Voigt-Thomson's relation is satisfied fully for thermal conductivities of bismuth.

Introduction

A number of investigators[1–4] have measured the thermal conductivities of single- and polycrystalline bismuth by using specimens in the form of a plate or a cylinder. The relation between the thermal conductivities were studied by Kaye and Roberts[3] and by Linder.[5] Two entirely different formulae were given by them:—

$$\text{Kaye and Roberts}: \quad \frac{1}{k} = \frac{1}{3}\left(\frac{1}{k_{\parallel}} + \frac{2}{k_{\perp}}\right),$$

$$\text{Linder}: \quad k = \frac{1}{3}(k_{\parallel} + 2k_{\perp}),$$

* Communicated by Professor K. Tanaka.

1. Jaeger and Diegelhorst, Wiss. Abh. d. Phys.-tech. Reich., **3**, 369 (1906).
2. E. Giebe, Ber. d. deutsch. phys. Gesell. **5**, 60 (1903).
3. G. W. C. Kaye and J. K. Roberts, Proc. Roy. Soc. London, **104**, 98 (1923).
4. G. W. C. Kaye and W. F. Higgins, Phil. Mag., **8**, 1056 (1929).
5. E. G. Linder, Phys. Rev., **39**, 554 (1927).

where k is the thermal conductivity of polycrystal, and $k_\perp$ and $k_\parallel$ are two principal thermal conductivities of single crystal respectively.

The objects of the present work are (1) to measure the thermal conductivities of polycrystalline and single crystal bismuth by using the identical method, (2) to ascertain the previously reported values and the formulae of the relation between the thermal conductivities and (3) to check the Voigt-Thomson's law[6] for the thermal conductivity. The method applied was one of a guard-tube type. The specimen used was in a form of a cube or a plate.

Preparation of specimens

Merch pure bismuth was employed in this experiment. Three kinds of specimens were prepared: (1) specimens of polycrystal in the cubic form, of which the length of one edge being about 0.93 cm, (2) specimens of single crystal in the cubic forms of which the length of the edge being about 0.93 cm and one plane being perpendicular to the trigonal axis of crystallization, (3) specimens of single crystal in the form of rectangular plate, 2 mm in thickness and 0.93 cm in width and length, of which the orientation of the trigonal axis with respect to the normal to the plane ranges from 0° to 89°. The method of growing the single crystal was one used ordinarily[7].

Apparatus and experimental procedre

The apparatus was consisted essentially of the following parts (Fig. 1): a specimen S, a heating block B_1, a cooling block B_2 and water jackets G_1, G_2, H_1 and H_2. Heat supplied by a heater coil C_5 wound round B_1 was transmitted to B_1, next to the specimen S and finally to the cooling block B_2 which was soldered to the upper surface of the water jacket G_1. B_1 and B_2 were in the form of a rectangular parallelepiped with the same sectional area 0.94 cm × 0.94 cm and 1.5 cm, 0.4 cm in height respectively. The doublewalled water jacket H_2 and the water jacket H_1 served to prevent the heat loss from the surface of B_1 by controlling the temperature of water circulating through them. Between H_2 and G_2 was inserted a hollow wooden block D with the same section as H_2. By controlling the temperature of water circulating through H_2 and G_2, and the power supplied to the heater coil C_5, the same temperature gradients could be established in S and in D. The tem-

6. W. Voigt, Lehrbuch der Kristallphysik.
7. S. Ito, This Memoirs, A, XII, 97 (1924).

peratures of B_1, G_2 and H_2 were measured by platinum thermometers C_1, C_2, C_3 and C_4 respectively. C_1, C_2, C_3, C_4 and C_5 were 35 cm in length and 0.10mm in diameter. The middle part 33 cm of the wires C_5 and C_4 were wound round B_1, and C_2 around B_2 in the same way, and the both ending 1 cm of them were used as leads, the ends of which were soldered to copper leads in turn. The load W which is not described in Fig. 1, pressed B_1 through the support M, H_1 and a hollowed wooden block A successively. The space enclosed by B_1, H_2 and H_1 was filled with caolin powder. H_1 and H_2 were surrounded by a cotton wool to prevent heat loss.

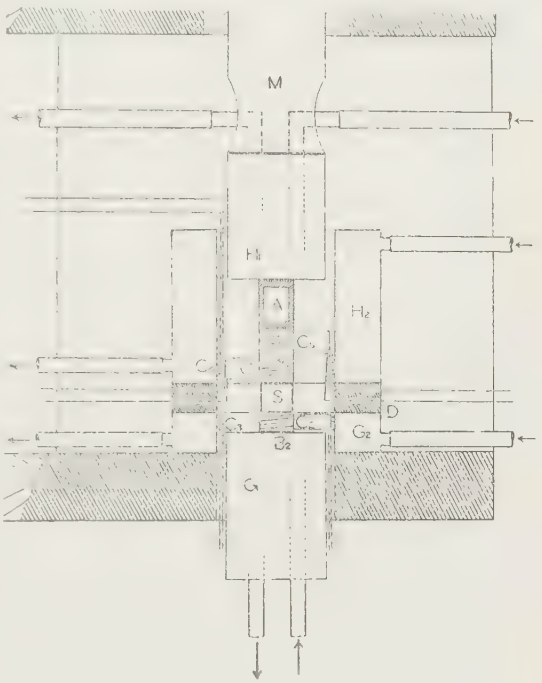

Fig. 1. Diagram of apparatus.

The specimen S was coated at upper and lower surfaces with glyceline and was inserted between B_1 and B_2. The water was flowed through H_1, H_2, G_1 and G_2. When the steady state was reached, the temperatures of C_1, C_2, C_3 and C_4 were measured. Then the heater coil C_5 was supplied with power from batteries. The temperatures of the water flowing through H_1, H_2 and G_2 were controlled so that the temperatures of H_1 and H_2 became equal to that of B_1, and the temperature of G_2 to that of B_2, and the same temperature gradient were established in the specimen S as in the hollow disk D. When the steady state was reached, the temperatures of C_1 and C_2 were measured. In order to calculate the resistance of the coil of the portion wound round the copper block, the resistance of the lead must be subtracted. This was done by using compensating wires as usual.[8] The temperature drop in the specimen was calculated by applying the first correction as described in the following paragraph to the temperature difference between C_1 and

8. For example, Handbuch d. Experimental Physik, VIII, 1 Teil, p. 62.

C_2. The intensity of the electric current through C_5 was measured with a standard resistance and a potentiometer. The power conducted through the specimen was calculated by applying the second and third corrections as described in the following paragraph to the power supplied to the heater coil C_5.

Corrections

(1) *Temperature correction.* In order to obtain the temperature drop in the specimen, the sum of the temperature difference between C_1 and the upper surface of S, and that between the lower surface of S and C_2, must be subtracted from the temperature difference between C_1 and C_2. The value of this correction was estimated by the experiment of measuring the thermal conductivity as usual with a silver specimen. By subtracting the temperature drop in the silver specimen which can be calculated from the power conducted through it and the thermal conductivity of silver, from the temperature difference between C_1 and C_2, the value of the correction was determined against the power conducted through the specimen. The results were as follows: the temperature drop which must be corrected was nearly proportional to the power conducted through the specimen, and was 2.16° C per cal/sec.

(2) *Power correction.* When the copper block B_1 was heated with an electric current through C_5, the heat Q_2 produced in the platinum leads will enter B_1 also, besides the heat Q_1 which was produced in the portion of the coil C_5 wound round B_1. For the purpose of measuring the ratio Q_2/Q_1 an experiment of measuring the thermal conductivity of bismuth was carried out, using the same arrangement of the apparatus as usual, except for a difference that a copper plate B_3 was inserted between B_1 and A. Platinum wires which are similar to the platinum leads of C_5, were soldered at their ends to a point P on B_3 and to the ends of copper leads as is evident from the diagram in Fig. 2.

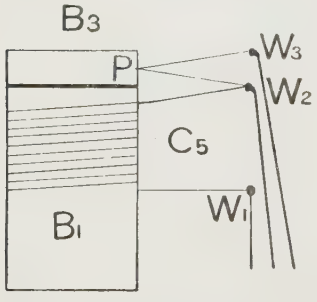

Fig. 2. B_3, copper block with same sectional area as B_1 and 1 mm in height; W_1, W_2 and W_3, junctions of platinum leads with copper leads.

Supposing that, to an electric current through $W_1 C_5 W_2$ corresponds a temperature difference T' between C_1 and C_2, and also that, to the electric current of the same intensity through $W_2 P W_3$ corresponds a temperature

difference T'' between C_1 and C_2, we have

$$\begin{matrix} Q_1 + Q_2 \\ Q_1 + 2Q_2 \end{matrix} = \begin{matrix} T' \\ T'' \end{matrix}.$$

Therefore

$$\frac{Q_2}{Q_1} = \frac{T'' - T'}{2T' - T''}.$$

The results of the measurements were as follows:—

$$\frac{Q_2}{Q_1} = 0.0298.$$

(3) *Power correction.* In order to prevent the heat loss from the surfaces of B_1 and S, the temperature of B_1 was made equal to those of H_1 and H_2. Despite of doing so, however, a portion of heat was still lost. This is attributed to the complex distribution of temperatures in the space between S_2 and H_2 owing to the leads laid in it. The heat loss was measured experimentally. Caolin powder was filled in place of the bismuth specimen. And then the experiment of measuring the thermal conductivety was carried out as usual. The power which was conducted through the caolin powder filled in the space between B_1 and B_2 was able to be calculated from the temperature difference between C_1 and C_2, and the thermal conductivity of caolin powder which was measured by another experiment. The results were as follows: the heat loss was nearly proportional to the temperature difference between C_1 and C_2, and was 0.00163 cal./sec. per 1° C of the temperature difference between C_1 and C_2 at 14° C.

Thermal conductivity of caolin powder

The thermal conductivity of caolin powder against its density was measured with a method similar to that used by Seeman.[9] The results are given in Table 1.

TABLE 1. Thermal conductivity of caolin powder against the density at 14° C.

Density (gm/cm³)	0.407	0.625	0.685	0.744
Thermal conductivity (cal./cm. sec. deg.)	0.000144	0.000272	0.000313	0.000325

9. H. E. Seeman, Phys. Rev., **29**, 616 (1927)

Results

(1) *Experiments using the cubic specimen.* The experimental values of temperatures and heat quantities in detail are shown in Table 2, taking the measurements on the specimen No. 1 as an example. The lengths of its edge are 0.9114 cm, and the directions along these edges are denoted by X, Y and Z respectively, X being parallel to the trigonal axis of the crystallization.

TABLE 2. Results using specimen No. 1

Direction	T_1	T_2	ΔT	T	$Q'\left(\frac{\text{cal}}{\text{sec}}\right)$	$\Delta Q_1\left(\frac{\text{cal}}{\text{sec}}\right)$	$\Delta Q_2\left(\frac{\text{cal}}{\text{sec}}\right)$	$Q\left(\frac{\text{cal}}{\text{sec}}\right)$	$k\left(\frac{\text{cal}}{\text{cm.sec.deg}}\right)$
X	0.099	2.879	0.070	2.710	0.03224	0.00096	0.00046	0.03264	0.01268
	0.228	2.002	0.046	1.729	0.02046	0.00061	0.00029	0.02078	0.01265
	0.179	2.843	0.067	2.597	0.03092	0.00092	0.00042	0.03142	0.01274
	0.101	1.929	0.046	1.782	0.02094	0.00062	0.00029	0.02127	0.01259
								Mean	0.01265
Y	0.036	1.122	0.045	1.041	0.02052	0.00061	0.00017	0.02096	0.02217
	0.062	1.757	0.071	1.624	0.03232	0.00095	0.00026	0.03302	0.02239
	0.296	1.399	0.046	1.058	0.02097	0.00061	0.00017	0.02121	0.02208
	0.108	1.743	0.069	1.566	0.03122	0.00093	0.00025	0.03190	0.02244
								Mean	0.02227
Z	0.099	1.173	0.045	1.029	0.02050	0.00061	0.00017	0.02094	0.02224
	0.126	1.792	0.070	1.596	0.03204	0.00096	0.00026	0.03274	0.02242
	0.232	1.864	0.069	1.563	0.03145	0.00094	0.00025	0.03214	0.02244
	0.108	1.187	0.046	1.033	0.02084	0.00062	0.00017	0.02129	0.02253
								Mean	0.02241

T_1 and T_2, temperatures of C_1 and C_2 respectively; ΔT, correction with respect to temperature drop; T, temperature drop in the specimen; Q', power supplied to the heater coil; ΔQ_1, correction of power with respect to the platinum lead; ΔQ_2, loss of power; Q, power conducted through the specimen; k, thermal conductivity.

The results obtained on the specimens of the single crystal No. 1, No. 2 and the polycrystal No. 3, No. 4 are summarized in Table 3. In this table, $k'_{\perp}$ and $k''_{\perp}$ are the thermal conductivities in directions perpendicular to each other. k', k'' and k''' are those of the polycrystal in the directions parallel to each edges of the specimens.

TABLE 3. Thermal conductivities of bismuth at 14° C.

Specimen	Thermal conductivity	
Single crystal No. 1	$k_{\parallel} = 0.01265$ $k_{\perp}' = 0.02227$ $k_{\perp}'' = 0.02241$	Mean $k_{\parallel} = 0.01269$ Mean $k_{\perp} = 0.02252$
Single crystal No. 2	$k_{\parallel} = 0.01273$ $k_{\perp}' = 0.02258$ $k_{\perp}'' = 0.02281$	
Polycrystal No. 3	$k' = 0.02101$ $k'' = 0.01973$ $k''' = 0.01621$	Mean $k = 0.01914$
Polycrystal No. 4	$k' = 0.01984$ $k'' = 0.02077$ $k''' = 0.01728$	

The values of k', k'' and k''' differ considerably from one another, which is attributed to the anisotropy of the specimen of polycrystal bismuth.

In order to discuss the validity of Linder's formula, the writer has calculated the thermal conductivity k of polycrystalline bismuth by putting the above values $k_{\parallel} = 0.01269$ and $k_{\perp} = 0.02252$ into the said formula. This gives

$$k = \frac{1}{2}(2 \times 0.02252 + 0.01269) = 0.01924 .$$

Thus, it is found that the value of k calculated by Linder's formula is nearly equal to that obtained experimentally for the polycrystalline bismuth.

The writer's values are compared with those obtained by other authors in Tables 4 and 5.

TABLE 4. Thermal conductivity of polycrystalline bismuth.

Author	Temperature	k
Jaeger and Diegelhorst[1]	18° C	0.0193
Giebe[2]	18° C	0.0192
Nishioka	14° C	0.0191

TABLE 5. Thermal conductivities of single crystal bismuth.

Author	Temperature	$k_{\parallel}$	$k_{\perp}$	$k_{\perp}/k_{\parallel}$
Kaye and Roberts[3]	18° C	0.0159	0.0221	1.39
Kaye and Higgins[4]	27° C	0.0129	0.0223	1.73
Nishioka	14° C	0.0127	0.0225	1.77

Table 5 shows that the writer's value for the polycrystal agree well with those obtained by other authors. The value of $k_{\parallel}$ obtained by Kaye and Higgins is distinctly lower than that obtained by Kaye and Roberts, while the values of $k_{\perp}$ agree well with each other. Kaye and Higgins explained this disagreement by the presence of fissures parallel to the principal cleavage plane. As the writer's experiment gave a low value like that of Kaye and Higgins, he examined the inner parts of the specimen if there were any fissures. But he looked out nothing.

(2) *Experiments using plate-shaped specimens.* The experimental procedure were similar to the case of using the cubic specimen. The results are given in Table 6 and shown graphically in Fig. 3, where θ is the orientation of the trigonal axis with respect to the normal to the plane of the specimen and k is the thermal conductivity. The value of the thermal conductivity k for $\theta = 89^\circ$ in Table 6 is about 4 % lower than $k_{\perp}$ in Table 3, while the value of k for $\theta = 0^\circ$ in Table 6 agrees well with $k_{\parallel}$ in Table 3. This is perhaps due to the fact that the temperature drops in glyceline films become larger as compared to that in the specimen by using a thin specimen, especially when the substance under test is of good conductivity, and consequently the error may be enlarged. However, the results are still capable of showing that the relation between the orientation and the thermal conductivity is linear, as this verifies the validity of Voigt-Thomson's law.

TABLE 6.

θ	$\sin^2\theta$	k
0°	0	0.0126
14.7	0.064	0.0133
27.2	0.209	0.0142
50.7	0.599	0.0177
67.9	0.859	0.0203
74.3	0.927	0.0210
89.0	0.900	0.0217

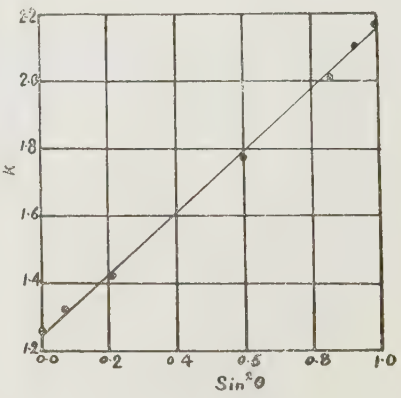

Fig. 3.

Memoirs of the College of Science, University of Kyoto, Series A,
Vol. XXV, Nos. 3 & 4, Article 25, 1949.

A Decade Scaling Circuit*

By

Ryutaro Ishiwari and **Kazunori Yuasa**

(Received November 29, 1949)

I. Introduction

The principle of duo-scalers has become universally applied to construct scale-of-eight, scale-of-sixteen etc. in the experiments of high speed counting by linear amplifiers or Geiger-Müller counters. In busy works, however, a system of decade scaling circuit is earnestly desired, since it is more convenient for rapid summation and interpolation. The writers have designed and constructed a new decade scaling circuit of very simple construction but of extremely steady use. It is a modification of a circuit system of vacuum-tube scale-of-sixteen, and easily restored to its basic circuit by necessities.

II. Basic Circuit

Any type of the circuit used for the scale-of-sixteen may be modified into the decade scaling circuit. It was found, however, that a circuit devised by Higinbotham[1] seemed to be exclusively suitable for the purpose. While, in his circuit, Higinbotham used twin-triodes 6SN7-GT's or 6SL7-GT's, which are not easily obtainable in our country, we used more popular tube UY-76's. The diagram of the circuit is shown in Fig. 1. The amplitude discriminator which selects pulses and sharpens and equalises them was so modified as to fit for our purpose.

III. Description of Circuit

As it is shown in Fig. 1. the valves V_1, V_2, V_3,$\cdots\cdots V_{12}$ constitute themselves the original scale-of-sixteen. The diagrams in Fig. 2 (a) show the potential changes of the anode plates of V_3, V_6, V_9, V_{12} and V_{15} in their working state respectively.

* Under the same title the writers read a paper at the annual meeting of the Physical Society of Japan held at University of Kyoto, 21st May, 1948.

1. W. A. Higinbotham, J. Gallager and M. Sands. Rev. Sci. Instr., **18** (1947), 706.

These patterns are easily observed on a screen of a cathode-ray oscilloscope by applying regular signals of an adequate frequency to the input of the circuit.

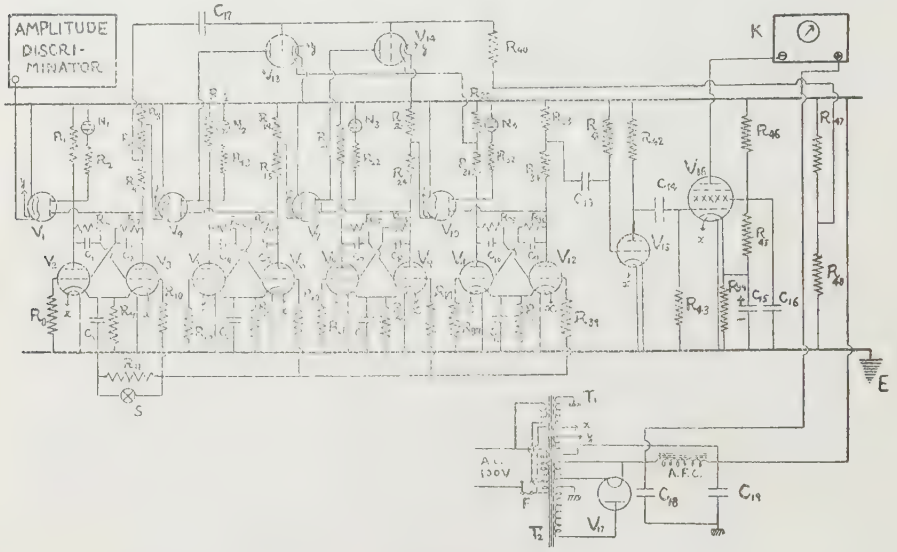

Fig. 1.

1) V···Vacuum tubes

1, 4, 7, 10	Kt—6H 6A
2, 3, 5, 6, 8, 9, 11, 12, 13, 14, 15	UY—76
16	UZ—42
17	KX—12F

2) R·····Resistances

1, 12, 21	40 K
2, 13, 22, 32, 43	1 Meg
3, 5, 14, 23, 33, 45	10 K
4, 9, 19, 28, 30, 31, 33, 46	20 K
6, 7, 16. 17, 25, 26, 35, 36	400 K
11, 40	100 K
8, 10, 18, 20, 27, 29, 37, 39, 42	200 K
15, 24, 34	30 K
41	2 Meg
47	25 K
48	60 K

3) C·····Capacitances

1, 2, 4, 5, 7, 8, 10, 11	50 pf
3, 6, 9, 12	0.01 μf
13	0.05 μf
14	0.005 μf
15	10 μf 50 V
16	2 μf 1000 V
17	100 pf
18	8 μf 1000 V
19	6 μf 1000 V

4) AFC···Audiofrequency choke
30 H 40 mA

5) T···Power transformer
1 ··· Primary 100 or 110 V 60~
Secondary 6.3 V 4A
2 ··· Primary 100 or 110 V 60~
Secondary 6.3 V 2A
5 V 1A
300 V 50mA

6) S···Push button switch
(normally closed)

7) K···Mechanical counter
RIKEN-type (readjusted) working current 10 mA, resolving time 1/60 sec.

Now, in order to convert the scale-of-sixteen into the scale-of-ten, we adopt the most straightforward and simplest method. It is to insert a circuit system C_{17}, V_{13} and V_{14} parallel to the main, so that the ninth

signal plays a role of the fifteenth in the original circuit system. The potential of the cathodes of the triodes V_{13} and V_{14} are so adjusted that they may take about 210 V when V_{11} is conductive, while they are maintained at 290 V when it is nonconductive. As the potential of their anodes are 120 V or 280 V according as the tubes V_5 and V_8 are in the conducting state or not, so the relative potentials of their anodes against their cathodes are maintained negative so long as V_{11} is nonconductive. It follows that the inserted parallel circuit has no influence upon the basic circuit during it counts from the first to the seventh kick. In the eighth stage, however, V_{11} becomes conductive and the potential of the cathodes of V_{13} and V_{14} so drop that the potential of the plates of V_{13} and V_{14} becomes positive against those of the cathodes. But their grids are so properly biased as they conduct no current in this state.

(a) SCALE-OF-16

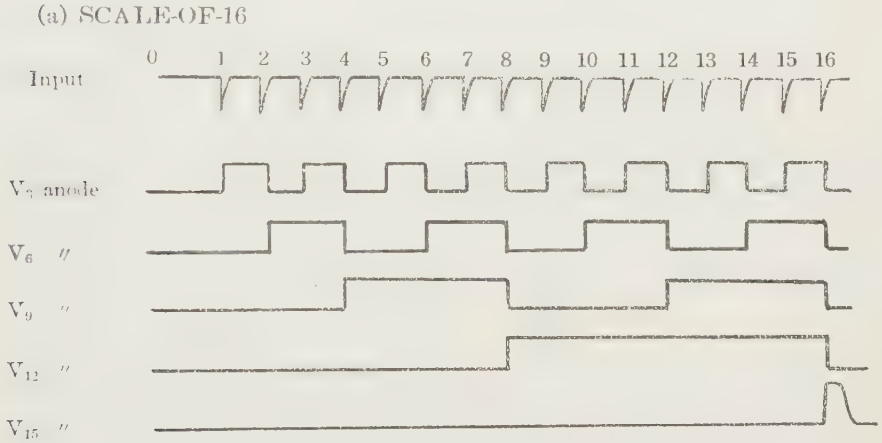

Fig. 2. (a)

Now, then, consider a positive signal is given to the circuit in this stage by the transition of the first pair. They at once rob currents from the plates of V_5 and V_8, resulting in the interchange of the states between the second and the third pairs, and the circuit recovers to its original state by the next, i. e. the tenth signal. The aspects of the conditions of V_{13} and V_{14} are shown in Fig. 2 (b).

IV. Construction

The amplitude discriminator and the scaling circuit is mounted on a 30 × 28 × 5 (cm) chassis. There are no need of electric shieldings for vacuum tubes. The vacuum tubes are used without any precautious

(b) SCALE-OF-10

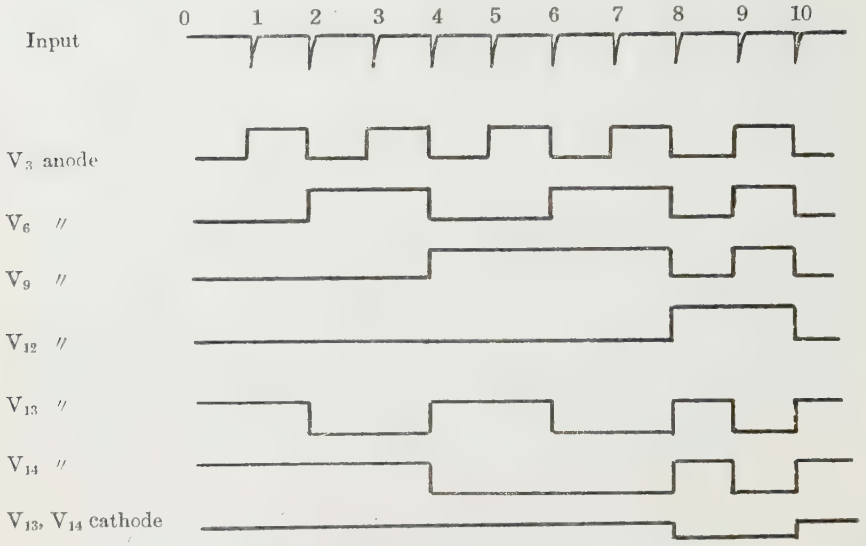

Fig. 2. (b)

selection. The only precaution is that the input circuit should be arranged apart from the register. The allowance of the values of registances marked on Fig. 1 is fairly large. The set is found to be easily handled and works reliably even though no special care is taken.

V. Test

To test the function of the circuit, we applied the sine-wavefrom a standard low-frequency oscillator (capable of generating oscillations ranging from 50 c.p.s. to 50,000 c.p.s.) and observed the oscillogram on the screen of the Braun tube. It was observed that it operated with success at frequenciesup to 50,000 c.p.s. No attempt has been made so far to determine the upper limit of the number of the reliable count, since the resolving time of this circuit is considered to be satisfactorily small for our present purpose.

The function of the aparatus was found to be satisfactorily reliable when the circuit was used in combination with the neutron-counter and linear amplifier system, and no need of readjustment has yet occurred.

In conclusion the writers wish to express their heartfelt thanks to Prof. Dr. B. Arakatsu and Prof. Dr. K. Kimura for their kind guidance and valuable suggestions throughout this work.

Memoirs of the College of Science, University of Kyoto, Series A,
Vol. XXV, Nos. 3 & 4, Article 26, 1949.

Residual Stress in Iron Alloys Variously Heat-Treated

By

Keizo Iwase and **Tadao Sano**

(Received April 20, 1949)

I. Introduction

Concerning the stress restored in alloys variously heat-treated, a number of interesting papers have been hitherto published[1]. The present writers have carried out a series of similar experiments on some iron alloys and steels, and the results which are somewhat different from those previously published, are briefly described in the present paper.

II. Experimental Procedure

In the present experiments, a small prismatic specimen ($4 \times 9 \times 100 mm^3$) prepared from 3 kg of forged ingot, was chiefly used to eliminate the mass effect as much as possible. Measurement of the stress restored in the specimen after heat-treatment was performed by Prof. T. Nishihara's etching method[2]; as shown in Fig. 1, two needles were attached to both ends of the specimen and the apartures of these needles at their upper and lower points were measured with a comparator with 1/100mm precision after each removal of 0.1mm of the specimen in its thickness by etching off one side of the surface of $9 \times 100 mm^2$ with an adequate reagent. The thickness was measured by means of a micrometer with 1/100mm precision. The stress which had been restored in each removed part of the specimen is calculated as follows.

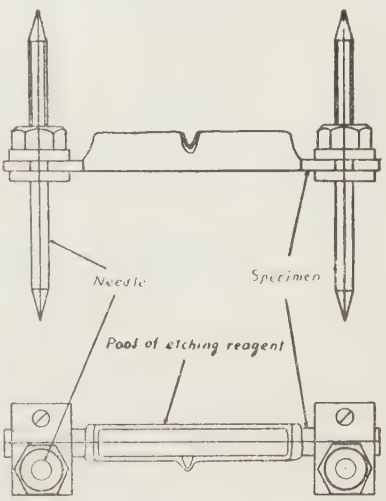

Fig. 1.

1. H. Bühler: Archiv. f. Eisenhüttenwes., **6** (1932) 247, 277, 283, 413; **7** (1933) 315, 359.
   T. Kawaguchi: Jap. Soc. f. Met., **8** (1944) 578; **9** (1945) 20.
   T. Sugeno: J. Iron & Steel Inst. Jap., **30** (1944) 19, 52.
2. T. Nishihara & S. Tahira: Trans. Jap. Soc. Mech. Eng., **14**, No. 49, (1948) 2.

The radius of curvature ρ can be obtained from the readings of the apartures of the needles by the formula:

$$\rho = \frac{(l_1 + l_2)}{2\Delta} g \,, \text{ with } \Delta = (P - Q) - (P_0 - Q_0) \,,$$

where l_1, l_2: lengths of the two needles,
g: length of the part to be etched (50 mm in this case),
P_0, P: apartures between the upper points of the needles before and after etching respectively,
Q_0, Q: apartures between the lower points of the needles before and after etching respectively.

Then the bending moment M_n is calculated from ρ above obtained as follows:

$$M_n = \frac{E}{P} \cdot \frac{a}{12} (2b - n\,\Delta h) \,,$$

where a: width of the specimen (9 mm in this case),
$2b$: thickness of the specimen (4 mm in this case),
Δh: depth removed at one time (0.1 mm in this case),
M_n: bending moment after n times removal of Δh,
E: Young's modulus.

The stress σ_n restored in n-th removed part is connected with the bending moment as follows:

$$M_n = a\left\{\sigma_n + \frac{\sum_{n=1}^{n} \sigma_{n-1}\Delta h}{2b - (n-1)\Delta h}\right\} \int_{2b - n\Delta h}^{2b} \left(\frac{2b - n\Delta h}{2} - t\right) dt$$

Therefore

$$\begin{aligned} M_n = -a\Bigg[& \sigma_1 \frac{2b + (n-1)\Delta h}{2} \Delta h \\ & + \left(\sigma_2 + \frac{\sigma_1}{2b - \Delta h}\Delta h\right) \frac{2b + (n-3)}{2} \Delta h + \cdots\cdots\cdots \\ & + \left\{\sigma_m + \frac{\sigma_1 + \sigma_2 + \cdots + \sigma_{m-1}}{2b - (m-1)\Delta h} \Delta h\right\} \frac{2b + \{n - (2m-1)\}\Delta h}{2} \Delta h \\ & + \left\{\sigma_n + \frac{\sigma_1 + \sigma_2 + \cdots + \sigma_{n-1}}{2b - (n-1)\Delta h} \Delta h\right\} \times \frac{2b - (n-1)\Delta h}{2} \Delta h \Bigg] \,, \end{aligned}$$

where t: thickness of the remaining part of the specimen after n-th removal of its surface.

Thus the mean value of the longitudinal stress which had been restored in each removed part of the specimen is obtained and may be plotted against the thickness of the specimen and thus the stress distribution curve is obtained.

Some iron alloys were used as specimens, which undergo no change of phase during the heat-treatment, in order to know the nature of the merely cooling stress. The effects of the cooling rate and of the plasticity of the alloy have been studied in this series of experiments. In the next place, some iron-nickel alloys as well as steels were used as specimens in order to know the effects of the phase change upon the residual stress. There are found many interesting papers about the residual stress in the case of iron nickel alloys[3], but to the present writers it seems very difficult to analyse the results without solving the nature of the irreversibility of the $\alpha-\gamma$ transformation in this alloy, about which a thorough study has been recently made in the senior writer's laboratory in Sendai[4].

Accordingly, the explanation of the results obtained are made very clear as will be seen later.

When steels are heat-treated, various structures are obtained according to the conditions, and hence in the present study the stress restored in steels variously heat-treated was measured and finally in those of the specimens carbulized or decarbulized.

III. Results

(1) α or γ phase iron alloys undergoing no phase change during cooling: Some Fe–V and Fe–Cr alloys were used as α alloys and 36 % Ni–Fe alloys as γ. The specimens were cooled from 300～1200° C by different cooling rates, and the elastic stress restored in the specimen was measured. Figs. 2 and 3 show some of the results obtained for example. In the case of furnace cooling (5° C per min.), no stress remained in all cases, but when the cooling is accelerated, the stress appeared. The stress distribution curves (half of them are drawn) shown in these figures are simple in their type, no minimum point being found on them. The stress is highest on the surface and is compressive and gradually decreases towards the interior of the specimen and at last it changes into tension. The highest tensional stress in the interior is always less than the compressive one on the surface. As the cooling velocity or the temperature from which the specimen is cooled increases

3. H. Bühler: Archiv. f. Eisenhüttenwes., **6** (1932), 283.
4. K. Iwase & S. Takeuchi: Jap. Soc. f. Met., **6** (1942), 361.

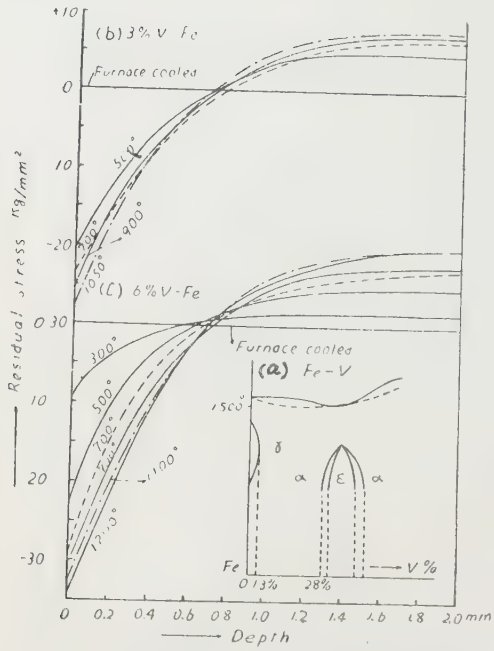

Fig. 2. Stress-depth curves of Fe–V alloys quenched from various temperatures.

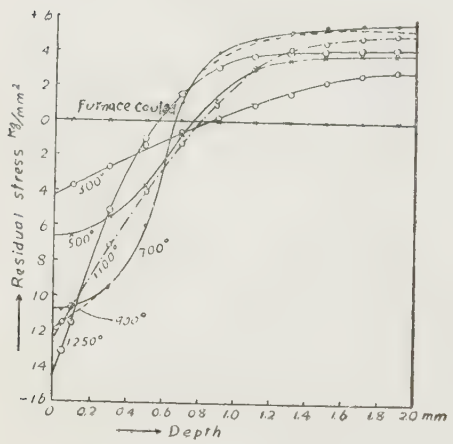

Fig. 3. 36 % Ni-Fe.

the stress becomes greater and when these cooling conditions are the same, the stress becomes greater as the strength of the alloy increases (The alpha alloy is stronger than the gamma alloy and 6 % V-alloy than the 3 % one). As the size of the specimen in the present study is very small, the residual stress is not so great.

(2) γ phase iron alloys undergoing the lattice transformation during cooling: In the foregoing section, the stress restored in the specimen was merely the cooling stress. In the present section, the quenching or the transformation stress will be explained. For this purpose 3～ca. 30 % Ni alloys have been used as specimens. According to the result of the investigation recently made by one of the writers[4], in these alloys, as the rate of diffusion is very feeble, the ordinary A_3 transformation hardly takes place and in place of it the lattice transformation commences on passing the curve GA on cooling and GB on heating without any change of the composition (in Fig. 4). This lattice change continues for a certain range of temperature and is completed only by passing through this range. This temperature interval of the lattice transformation increases as the Ni content in the alloy increases. It has been also ascertained that the furnace cooling is sufficient to prevent the diffusion in these alloys whose Ni content

are not less than ca. 5 %, and that it results only in the lattice transformation.

According to the results of investigations found in literature, the residual stress of the quenched Fe–Ni alloy is compressive on the surface and the expansion caused by the transformation acts as additive to the cooling stress which had been restored in the specimen before the transformation, and the stress distribution curve have a minimum or maximum point in general. These results seem to the present writers to be attributed to the mass effect of the specimen so large as $\phi(50\sim70) \times 350\,\mathrm{mm}^3$. As the lattice change above said is accompanied by a remarkable expansion, the transformation stress may be thought as tensional on the surface of the specimen, because the merely cooling stress was compressive as shown in the preceding section. The results obtained by the present writers have justified this view as the following sections show.

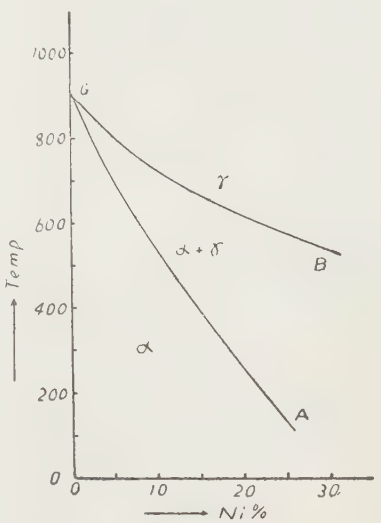

Fig. 4. γ–α of Fe–Ni alloys equilibrium.

(a) 29.8—31.5 % Ni–Fe alloys.

In the first place, it has been intended to make clear the effect of the lattice transformation upon the residual thermal stress of the alloy. For this purpose 29.8 % Ni alloy was used as a specimen, because it remains in the gamma state at the room temperature when it is cooled from a higher temperature as shown in Fig. 4. By cooling the alloy in the liquid air it transforms into alpha completely. Therefore, the alloy was cooled in the furnace on the one hand and quenched in ice water on the other, and the cooling stress has been measured respectively

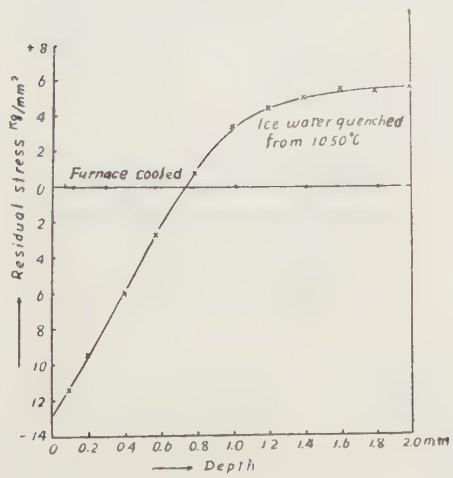

Fig. 5. 29.8 % Ni–Fe.

with the result that scarcely no stress remained in the furnace cooled specimen while not small amount of the stress (Fig. 5) remained in the quenched specimen. By cooling these two sorts of specimens, similarly heat-treated as before, to the liquid air temperature with various speeds, the lattice change from gamma into alpha was completed. The stress restored in these specimens has been measured at the room temperature. As shown in Fig. 6, the distribution curves in these cases are also simple and are near to each other regardless of their heat-treatments. The stress on the surface are tensional in all cases, the quicker cooling by the liquid air temperature resulting in slightly greater stress though the cooling rate prior to the lattice change had little effect upon the residual stress. Thus the large cooling stress of the quenched specimen, which existed before the lattice change, seems to have been released by the lattice change. As this fact is very important it was confirmed with the specimen containing 31.5 % Ni as shown in Fig. 7. This fact as well as the fact that the stress on the surface is tensional do not coincide with the results obtained by previous investigators probably bebecause the mass effect predominates in the cases on very large specimens.

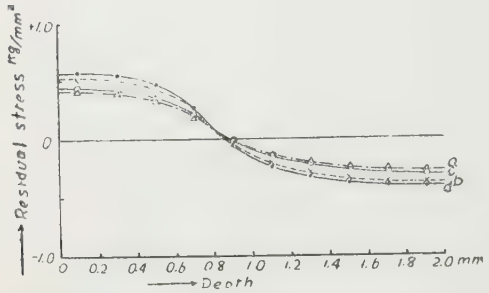

Fig. 6. a. △ Slow cooled till −185° from 23° C after slow cooled in furnace.
b. × Quenched into −185° from 23° C after slow cooled in furnace.
c. ○ Slow cooled till −185° from 23° C after ice water quenching.
d. ● Quenched into −185° from 23° C after ice water quenching.

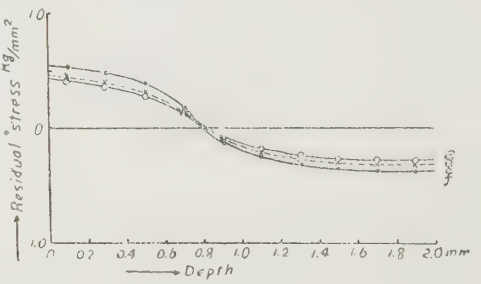

Fig. 7. e. ○ Slow cooled till −185° from 23° C after ice water quenching.
f. ● Quenched into −185° from 23° C after ice water quenching.
g. × Quenched into −185° from 23° C after slow cooled in furnace.

As the lattice transformation is a kind of recrystallization, if it happens on the surface layer of the specimen, the cooling stress existing within that layer may be released by the transformation and the stress existing within the remaining part of the specimen will be influenced

thereby and the distribution curve of that part will be somewhat altered while the free expansion followed by the transformation may be restricted by the rigidity of the remaining part and thus also the distribution curv of that part may be again altered. In this meaning the transformation stress may be additive to the cooling stress which existed beforehand. If the size of the specimen is small, the time lag of the occurrence of the transformation in the centre as compared to that on the surface is very small and as the cooling stress is small, and so all the cooling stress which existed beforehand in the whole specimen may be released by the lattice change as the results shown in Figs. 6 and 7 represent.

(b) The effect of the transformation velocity.

As shown in the preceding section, the cooling stress becomes greater as the cooling velocity increases. The transformation stress also becomes greater as the velocity with which the transformation proceeds in the specimen from the surface into the interior increases as the obtained results in Fig. 8 show. The specimen in this case contains 23% Ni and the lattice change commences at about 160～170° C and is completed before the temperature reaches 0° C. In this figure the curves *a* and *c* show that the cooling stress existed before the transformation is released, and so the restored stress shown in these four curves may be taken as they represent the transformation stress not influenced by the cooling stress which existed beforehand.

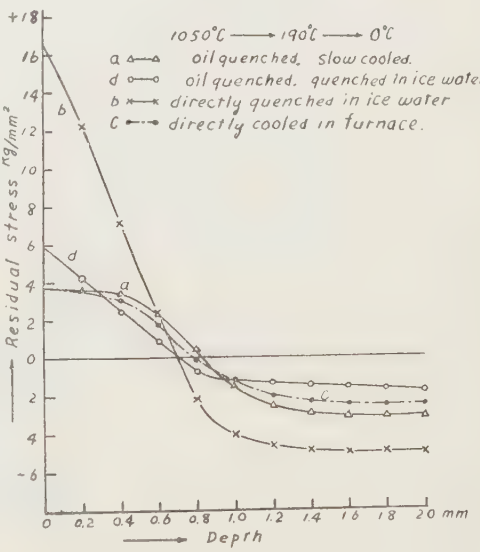

Fig. 8. 23% Ni-Fe.

(c) The restored stress in the α phase specimen containing Ni in various percentage.

As the Ni content of the alloy increased, the transformation point gradually decreased as shown in Fig. 4, and so when these alloys are quenched from 1050° C to room temperature or so, the plasticity of the alloy at the temperature of the transformation as well as the interval

of the temperature after the transformation, through which the alloy is quickly cooled, decrease. These facts may naturally influence the stress restored in the quenched specimen. The specimens containing 3～25 % Ni have been quenched in ice water or furnace cooled (5° C per min.) from 1050° C and the stress restored in them as well as their hardness have been measured and the results obtained are shown in Figs. 9 and 10, the tensional stress and the Vickers hardness on the surface respectively are represented in the figures. On the curves drawn in these

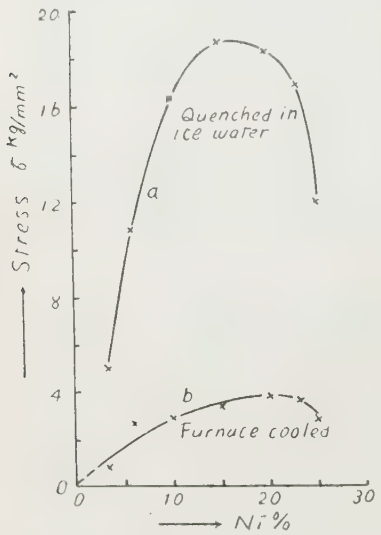

Fig. 9.

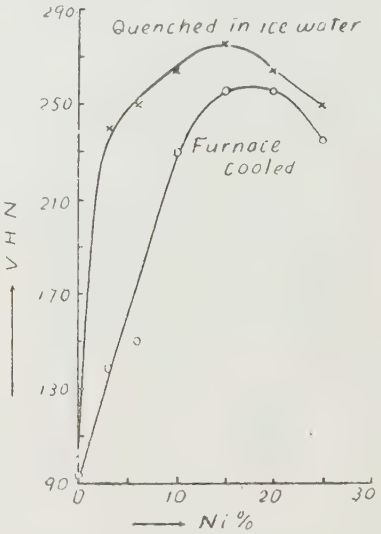

Fig. 10.

figures, the maximum points are found and those on the stress curves move to the left or right as the quenching medium is changed as shown in Fig. 11. The decrease of the plasticity of the alloy at the temperature

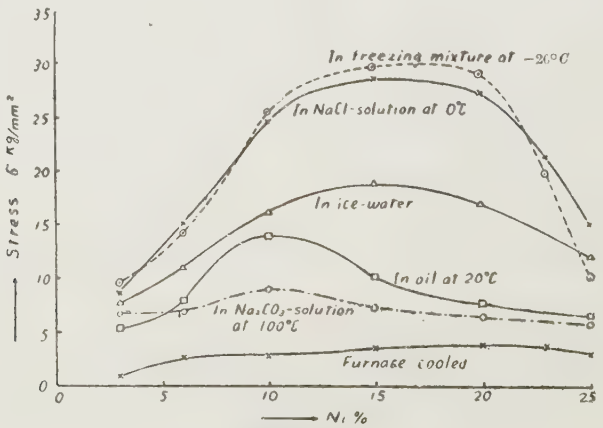

Fig. 11.

of the transformation, as the Ni content of the alloy increased, may cause the increase of the residual stress while the increase of the temperature range of the transformation, as the Ni content of the alloy increased, may cause the decrease of the stress, and the quicker cooling may weaken the effect of the increase of the range. The existence of the range of the temperature of the lattice transformation may result in the occurrence of the transformation at the same time in the different parts of the specimen whose temperatures are different and this may diminish the stress. It is to be noticed that the hardness curve of the furnace cooled alloys is closely situated to that of the quenched ones as shown in Fig. 10 while the two corresponding stress curves are remarkably different as shown in Fig. 9.

In all of these specimens, no trace of the gamma phase remained at the room temperature, being completely transformed into alpha phase. The influence of the existence of the gamma phase in the partly transformed specimen has been studied in the next experiments.

(d) The restored stress in the specimen partly transformed.

The lattice transformation point of the 29.8 % Ni alloy is below the room temperature and the alloy is completely transformed into alpha by immersing it in liquid air, and so when this alloy is cooled to some points between these temperatures, the alloy may consist of alpha and gamma phases, varying the amount of each phases according to the immersed temperature. The residual stress on the surface of the alloy in these specimens are as shown in Fig. 12, in which a maximum point is also found on the curve. Also in this figure it is shown that the hardness curve and the stress curve have aspects different from each other.

The stress distribution curve of such specimen shows a minimum as shown in Fig. 13, which is quite different from the cases treated in the foregoing sections. It seems to the present writers that the existence of the minimum point may be closely related to the heterogeneity of the structure of the alloy thus treated.

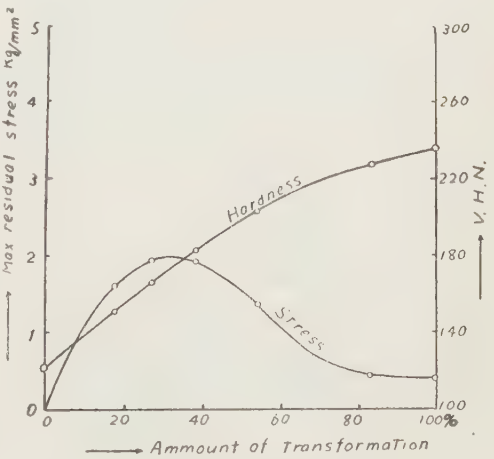

Fig. 12. 29.8 % Ni-Fe.

In the followings the stress restored in the specimen having a non-uniform structure has been measured to see whether the stress distribution curve is simple or not.

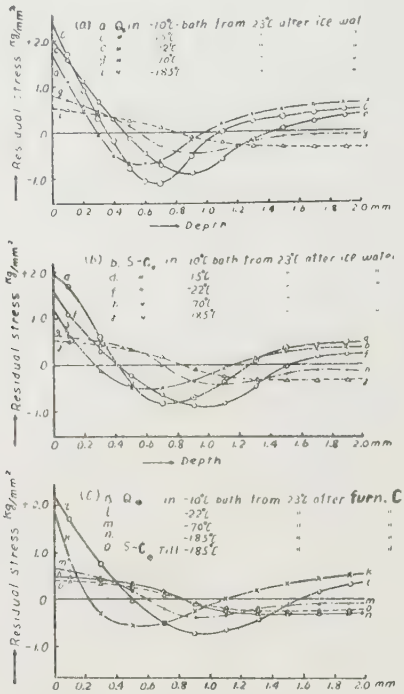

Fig. 13. Stress-depth curves of 29.8 % Ni–Fe.

(3) Residual stress in steels variously heat-treated.

(a) Residual stress in steels quenched or furnace cooled.

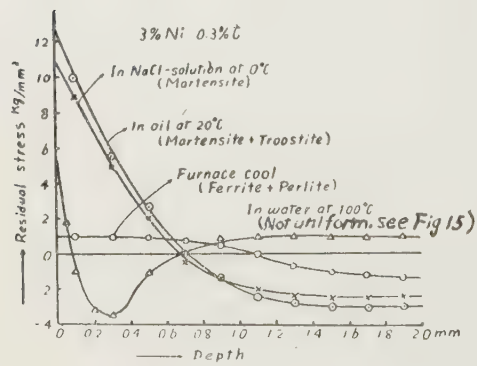

Fig. 14.

The steel containing 3 % Ni and 0.3 % C has been variously heat-treated (quenched from 950° C) and the structure obtained was observed and the restored stress was measured. Fig. 14 shows the results obtained. The structures of the specimens were uniform throughout their section except that of the specimen quenched in water at 100° C, though they

are single phased or two phased. While that of the specimen quenched in water at 100° C was not uniform and was troostic in its periphery or external part and sorbitic in the central part, ferrite being mixed in both parts, and the stress distribution curve showed a minimum point only in this specimen. In the other three curves no minimum point is found and the stress is greater as the cooling rate is increased. From the result above explained it seems that the minimum point on the distribution curve is closely related to the non-uniform structures of the specimen which is also proved by the upper curve shown in Fig. 15.

The similar minimum point on the distribution curve was also obtained when the structure of the specimen was made non-uniform by the carburization or the decarburization as the following lines show.

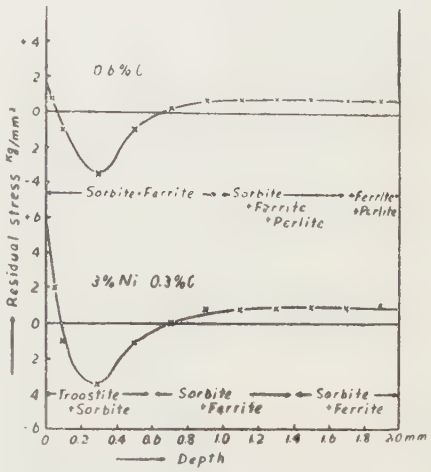

Fig. 15. Residual stress and structure of steel quenched in water from 950° C to 100° C.

(b) In the case of carburized and decarburized steels, furnace cooled or quenched.

The specimens containing 3 % Ni and 0.1 % C were carburized at their two surfaces corresponding to $9 \times 100\,\text{mm}^2$ under various conditions, and the carbon content depth curves obtained being shown in Fig. 16–(a). The carbon content and consequently the structure of such specimen is heterogeneous throughout its section and such heterogeneity of the structure has caused the occurrence of the minimum point on the stress distribution curve of each specimen slowly cooled or quenched, as shown in Figs. 16 and 17. The minimum point is near the point of the eutectoid carbon content in the case of slow cooling and moves to the right in the case of quenching. It is to be noticed that the distribution curves of the quenched specimens are far steeper than those of the slow cooled. In the quenched specimens the structures are all martensitic (thought he carbon content of the specimen is not uniform in its section) and in this meaning their structures are not heterogeneous,

but the temperatures at which the Ar″ change takes place are different in every points along the depth of the specimen, and this fact may be taken as the cause of the occurrence of the minimum point.

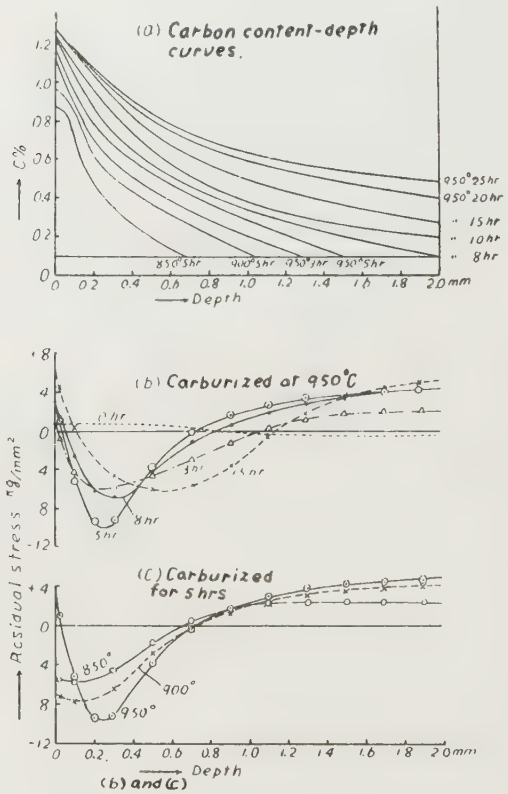

Fig. 16.

Similar sesults have been obtained in the case of the decarburization with the steel containing 1.3 % C as shown in Fig. 18. It is well-known fact that when the steel is decarburized on account of its bad treatment, such steel is apt to bring quenching cracks and this is conceivable from the result shown in Fig. 18.

When a large specimen is heat-treated, the structure will become heterogeneous owing to the mass effect and the occurrence of the minimum point on the distribution curve may move to the left or right by its cooling conditions.

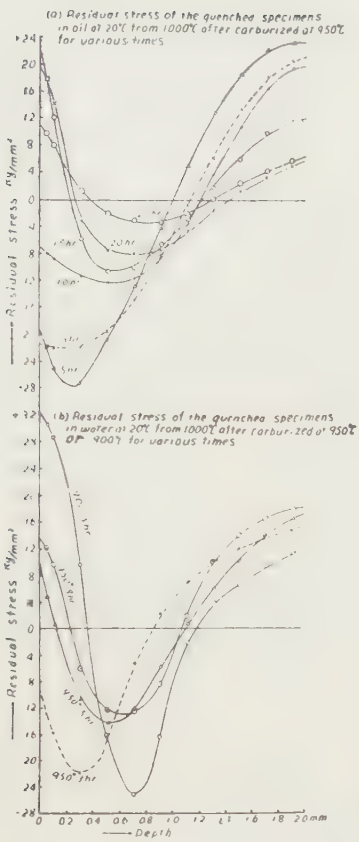
(a) Residual stress of the quenched specimens in oil at 20°C from 1000°C after carburized at 950°C for various times
Residual stress kg/mm²
(b) Residual stress of the quenched specimens in water at 20°C from 1000°C after carburized at 950°C or 400°C for various times
Depth

Fig. 17.

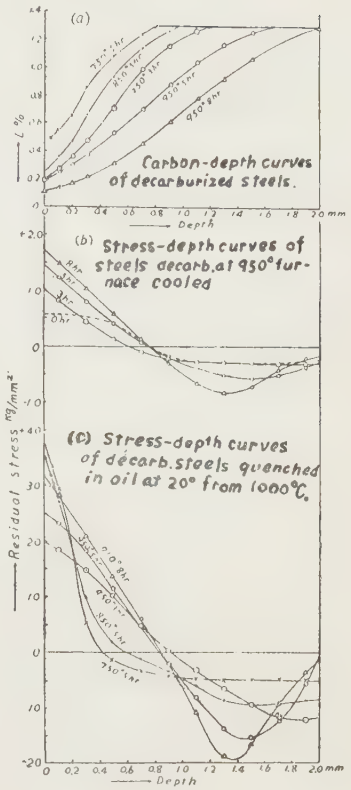
(a)
Carbon-depth curves of decarburized steels.
Depth
(b) Stress-depth curves of steels decarb. at 950° furnace cooled
(c) Stress-depth curves of decarb. steels quenched in oil at 20° from 1000°C.
Residual stress kg/mm²
Depth

Fig. 18.

(c) In the case of the stepped quenching and of the austempering.

The steel containing 3 % Ni and 0.5 % C can be quenched in lead bath at the temperature between 450° and 750° C from 950° C with no change of the phase and so this steel was quenched in the lead bath at these temperatures and then quickly in oil or salt solution at 20° C and the stress restored in the specimen was measured with the results as shown in Fig. 19. The curves in this figure show that the stepped quenching should be done in lead bath having the tem-

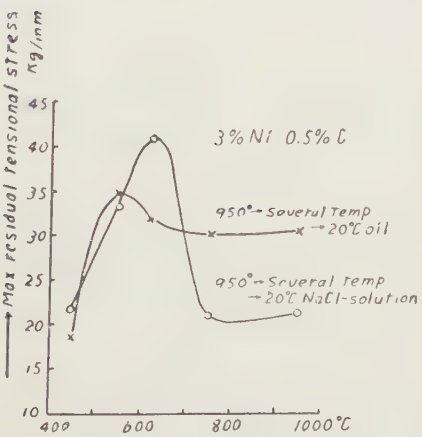

Fig. 19

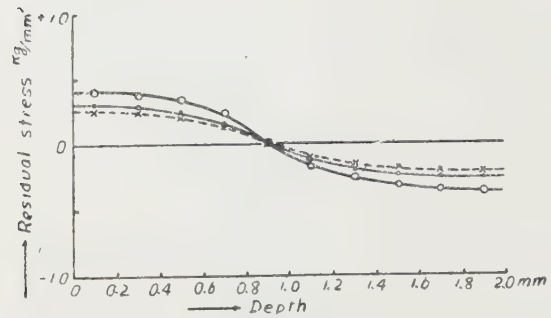

Fig. 20. Residual stress of 0.6 % C after austempering treatment.
× Air cooling after holding 20′ at 700° C Pb-bath (Ferrite+Pearlite)
● Air cooling after holding 12″ at 620° C Pb-bath (Sorbite)
○ Air cooling after holding 7″ at 480° C Pb-bath (Troostite)

perature lower than that corresponding to the maximum point in these curves in order to avoid the greater stress. In the austempering treatment only a very faint stress is restored in the specimen as the result shown in Fig. 20 represents.

(d) In the case of tempering of steel and of the aging of alloys.

By the tempering of the quenched steels the stress is decreased as the tempering temperature is elevated as shown in Fig. 21. In this treatment the separation of the cementite takes place and this may diminish the stress while the heating process may also act similarly. In order to make clear the two effects above explained, ageable silver alloy containing 6.3 % Cu and non-ageable silver alloy containing 6 % Mg have been quenched from 770° C and aged at various temperatures and the stress restored in them were measured. The result obtained is shown in Fig. 22–a, in which the compressive stress on the surface is plotted against the aging time. The precipitation of the copper rich phase has lowered the stress in the alloys.

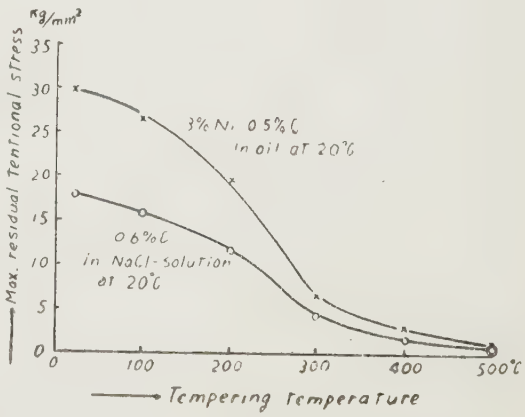

Fig. 21.

The curves in Fig. 22–b represent the results obtained by aging aluminium —4 % copper alloy quenched from 500° C. The aging at 20° C for 24 hrs. does not substancially diminish the stress while that

at 150° C increases the stress at first and then decreases just as the hardness of the alloy increases (Fig. 23). The aging at 150° C for 24 hrs., it is said, in the separation of so-called θ'-$CuAl_2$ phase and after this period the θ-$CuAl_2$ phase appears, but this appearance of the θ'-$CuAl_2$ phase has no effect upon the stress curve and the stress decreases steadily from about 2～3 hrs. tempering which is quite different in the case of the change of the hardness. This relation is also seen at 200° C aging. From these results it may be supposed that the stress decreases when the atomic group is formed within the mother solution even if it is not separated from the solution. It is very interesting to compare this with the hardness curves in Fig. 23.

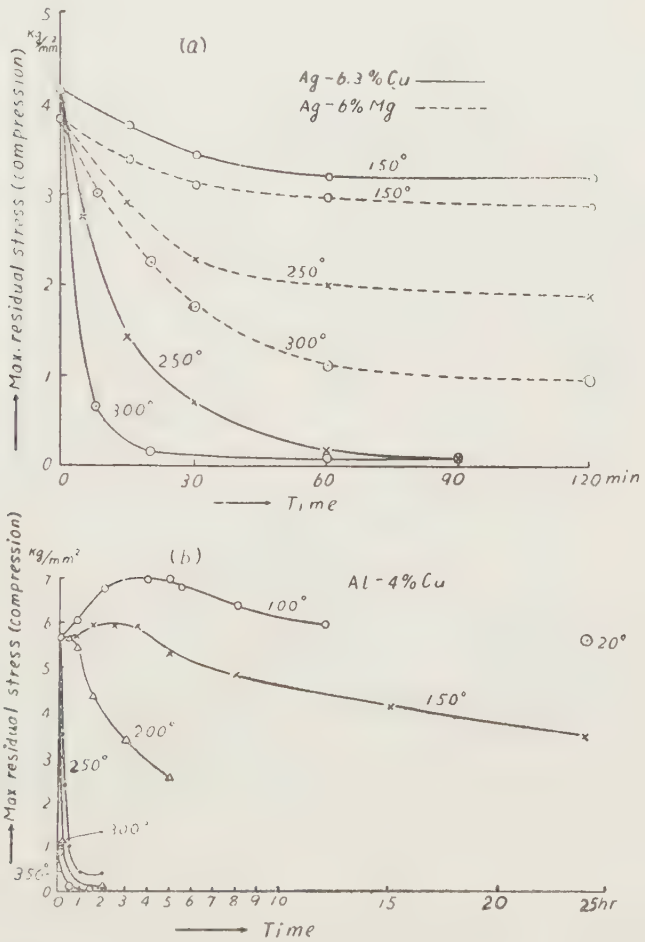

Fig. 22. Relation between maximum residual stress and aging.

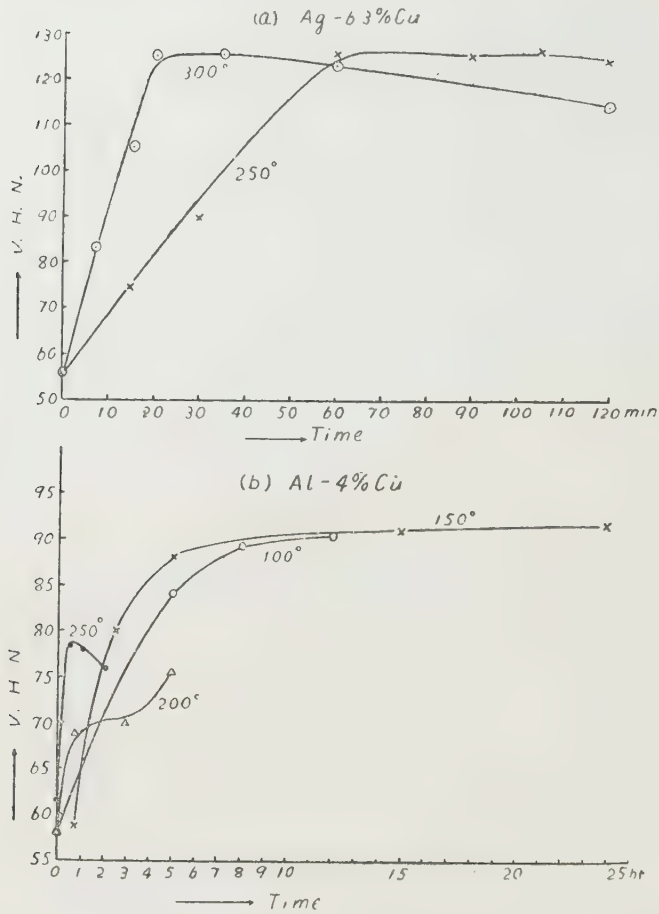

Fig. 23. Age-hardening at various temperatures.

IV. Summary

The cooling as well as transformation stress have been measured with some Fe–Ni and other Fe alloys and some steels using small specimens, and some new facts have been obtained, among which the release with the transformation of the cooling stress, which had been restored in the specimen beforehand, may be applicable in practice.

Memoirs of the College of Science, University of Kyoto, Series A,
Vol. XXV, Nos. 3 & 4, Article 27, 1949.

A Type of Geiger-Müller Counter suitable for the Measurement of High Energy Gamma-Rays

By

Masateru SONODA

(Received December 15, 1949)

Introduction

The Geiger-Müller tube counter is widely used in the nuclear experiments for measuring β-particles, γ-quanta and cosmic rays. The properties and the counting mechanism for the counter have been investigated by many workers,[1-13] but are not yet decidedly known. It is, however, a most important problem to construct a stable counter which can reliably be used for a long time. In order to obtain such a counter, it is necessary to pay careful attentions to every constituent part of the counter, especially to the insulation and the state of the internal electric field. Thus we could construct a very stable counter which had a wide plateau, gave no spurious counts and could be reliably operated for a long time. This counter could satisfactorily be used for the γ-rays of comparatively low energies.

On the other hand, we have investigated for these several years the properties and the various effects of the high energy γ-quanta such as emitted by the (Li–p) or (F–p) reactions.[34-37] It became necessary to construct a reliable counter which has a high efficiency for these high energy γ-quanta and does not response to the scattered or secondary rays produced by the surrounding materials. A type of Geiger-Müller counter of comparatively thick wall of lead was found to be suitable for our purpose. Then the counting efficiency was calculated theoretically for various energies of γ-quanta, since the values are essentially useful for the determination of the absolute cross sections of various photo-nuclear reactions.

Construction

A brass counter, mainly used for measuring the γ-rays of lower energies, is shown in Fig. 1. A brass tube of 2 mm in thickness,

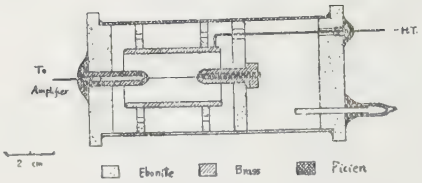

Fig. 1.

having the inner diameter of 2 cm and the length of 4 cm is mounted by the ebonite insulators in an outer cylinder of 1 mm in thickness, the diameter and the length of which are 4.4 cm and 10 cm respectively. The small wire of tungsten or piano wire is stretched along the axis of the inner tube. The outer cylinder is grounded and is used to shield the counter from the outer electric disturbances. Furthermore, since the surface leakage along the ebonite insulators from the inner tube on which the negative high voltage is applied is always earthed by this outer cylinder, it cannot give rise to any spurious pulse on the central wire which is connected in usual manner to the grid of the first valve of the amplifier. After several tests, the diameter of the central wire from 0.2 mm to 0.1 mm was found to be suitable for our counter. Since, however, the larger diameter gives the pretty wider range of plateau, we choose usually 0.2 mm diameter. The wire is supported at both ends by the poles of about 6 mm diameter which jet out 1 cm into the inner tube. In the counter of ordinary type the central wire is merely stretched along the axis of the tube, and therefore the electric field in the counter is distorted at the ends of the tube, resulting in the spoiling of the counter properties. In our counter, such a disadvantage is avoided. The effective length of the counter may be thought to be practically equal to the length between the tops of the poles and nearly 2 cm in our case. The central wire is tied at the one end to a small spiral spring of steel wire set inside the pole and can always be stretched tight, so that the length of the wire is constant throughout the experiment of a long time. The ebonite plugs which support the central poles are not directly fitted to the inner tube. If the insulator plugs are directly contacted in usual manner with the counter wall on which the negative high voltage is applied, the surface charge built up on the insulator may influence the field inside the counter and distort its uniformity. To avoid such disadvantages we adopted the type described above. The ebonite insulators supporting the inner tube must have fairly large surface to minimize the leakage along the surface, since this leakage may cause the spurious counts by the electric induction.

A hole at the end of the pipe through which argon gas and alcohol vapor are filled, is situated on the side of the pipe to avoid the cor-

ruption of the insulation of the ebonite surface by the impairment due to the impinging of the stream of alcohol vapor on the surface.

On the practical mounting of the counter, various attentions must be carefully payed. The tungsten wire must be cleaned adequately with benzine and heated in Bunsen flame to remove the undesirably contaminated matter on its surface. The wire is then inspected by a microscope. The inner surface of the counter tube was carefully treated with metal polishing powder and afterwards cleaned with benzine and distilled water untill there were no irregular scars and traces of grease. The ebonite surface was also carefully prepared and a very high surface resistance was obtained.

The counter thus constructed had the very good characteristics and gave no spurious counts due to bad insulation of the materials used and external electric disturbances. It was found excellent for the measurement of the γ-quanta of comparatively low energies.

In dealing, however, with the high energy γ-quanta such as emitted by (Li–p) or (F–p) reactions, the secondary electrons emitted from the outer shield cylinder and the surrounding materials are able to penetrate through the counter wall and enter into the effective space of the counter and give rise to additive counts. It is therefore very difficult to obtain the absolute intensity of the γ-ray with such a counter. A more reliable counter must be constructed for the measurement of the γ-rays of such high energy region.

The lead counter of comparatively thick wall was found to be suitable for our purpose. The one used in the experiments with 17.6 MeV γ-ray from (Li–p) reaction, was shown in Fig. 2. The construction is almost the same as the brass counter described above. The outer shield cylinder is made of aluminium of 1 mm thickness to minimize the absorption of the γ-ray to be measured. The counting part is a lead tube of 6.5 mm thickness whose inner diameter and length are 2 cm and 4 cm respectively. The reason of selecting lead of 6.5 mm thickness is that the lead wall of this thickness can just prevent those electrons of 17 MeV or less from entering into the effective space which may be emitted from the surrounding materials by this 17 MeV γ-ray. The counts are all due to the secondary electrons emitted from the lead wall and there-

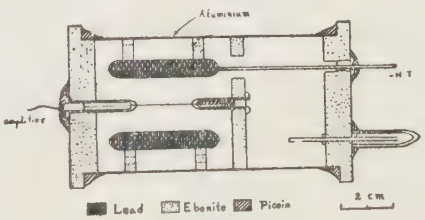

Fig. 2.

fore the counting efficiency of the counter can theoretically be calculated. Further this thickness is nearly equal to the maximum range of the secondary electrons produced by the 17 MeV γ-ray and so the efficiency is possibly high for these γ-ray quanta.

As is shown in the later paragraph, the counter is found to be reliably used for the experiments of determining the absolute number of high energy γ-ray quanta emitted from a γ-ray source.

Amplifier Circuit

The amplifier used by us is shown in Fig. 3. It is an ordinary resistance capacity coupling circuit of 2 stages, but many filter condensers are effectively used to prevent the electrical disturbances from entering into the valves. The central wire of the counter is connected to the control grid of the first valve UZ 77, 6C6 or 6SJ7 through the minute condenser of about 20 pF. The high resistance, through which the central wire is grounded is of the order of $10^8 \sim 10^9$ ohms.

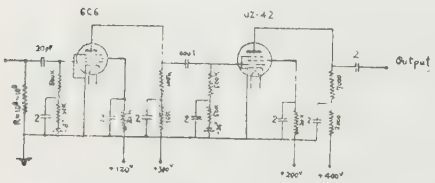

Fig. 3.

This high resistance was carefully prepared in the following manner. A fine silk thread was immersed in the alcoholic suspension of colloidal carbon for about two days, wound on a pyrex tube of about 6 mm diameter after having been dried and covered with bee wax. The resistance thus prepared was found to be very stable and scarcely affected by the atmospheric conditions, if it had been perfectly dried.

Each of the stages of the amplifier was mounted separately in the iron box of 1 cm thick and thus the electrical disturbances from the neighbouring electrical devices could be perfectly eliminated which may cause the spurious counts. This precaution is necessary for the counter to be used in the high tension laboratory.

The output from the power valve was supplied to the scale-of-16 counting system with a mechanical recorder. It was found that the counter system could be reliably operated up to the number of the kicks of about 8000 per minute.

Gas Mixture

Many workers[4,9-18] studied the gas filled in the counter. A. Trost[1] succeeded to diminish considerably the duration of pulse and improve

the characteristics of the counter by using the mixture of the vapor of an organic substance and a rare gas. It is found also in our laboratory that the good characteristics with a wide flat plateau is obtained if argon gas is mixed with the vapor of ethylalcohol. Such a counter can be used for a long time without any failure.

Before the filling up of the gas mixture, the counter must be evacuated continuously for more than fifty hours and the vapors or gases must be perfectly removed which may be absorbed in the counter materials. If this treatment is not perfect, the characteristics of the counter is not good and the life time is very short.

The argon gas and the vapor of ethylalcohol to be filled was dehydrated in the drying vessel containing the phosphorus pentoxide and calcium oxide, respectively, for 2 days at least and thus the moisture was perfectly removed.

After many tests it was found that the best characteristics was obtained when the mixture of 90% argon and 10% ethylalcohol was used. The slight change of this ratio or of the total pressure, however, does not seem to affect appreciably the properties of the counter except for the displacement of the characteristic curve as a whole.

Characteristic Curve

The characteristic curve of the so-called self quenching counter described above has been investigated by many workes.[1,4,19] The results obtained in our laboratory are also consistent with those of the other authors. They are shown in the following.

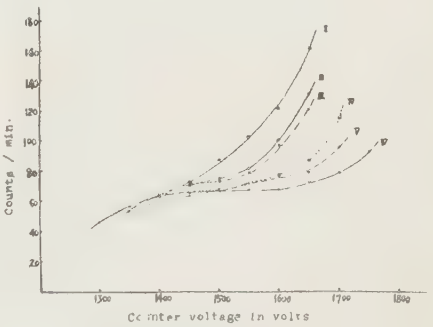

Fig. 4.

I R= 0.1 MΩ
II R= 1 MΩ
III R= 10 MΩ
IV R= 50 MΩ
V R=100 MΩ
VI R=370 MΩ
(Ar 9 cmHg+Alcohol 1 cmHg)

Fig. 4 shows the characteristic curve of the lead counter for several values of the high resistance R through which the central wire of the counter is grounded. As is shown, the length of the plateau is short for smaller values of R and becomes wider for larger R. It can be seen from the figure that R must be greater than 100 MΩ at least.

In the practical use, the measurments are made in the wide range of counting rate and therefore it must be ascertained whether the counter has a good characteristics at each counting rate. This was shown in Fig. 5, in which the characteristic curves were taken for several counting rate by changing the distance between the counter and the 1 mg Radium source. The radium source was filtered 13.6 mm lead and placed at the distances of 45, 90, 180 and 253 cm respectively. It is seen that the counter has a good characteristic curve independent of the counting rate.

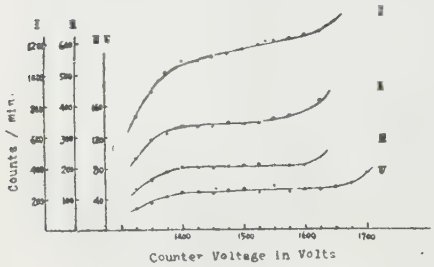

Fig. 5.

Ar 9 cmHg+Alcohol 1 cmHg
$R=23\times10^8\,\Omega$
1 mg Ra (filtered with 13.9 mm Pb) was placed at
I 45 cm II 90 cm III 180 cm IV 253 cm

Figs. 6 and 7 show the change of the counter properties with the gas pressure in the counter. The relative efficiency for Radium γ-rays and the length of the plateau are plotted against the total pressure of the gas when the vapor pressure of alcohol is kept at 1 cm Hg. The relative efficiency is smaller for the lower pressure. It increases gradually at first with the pressure and then remains constant at the pressure greater than about 10 cmHg. The length of the plateau is also small at first and it increases almost linearly with the pressure. The threshold voltage also increases linearly with the pressure.

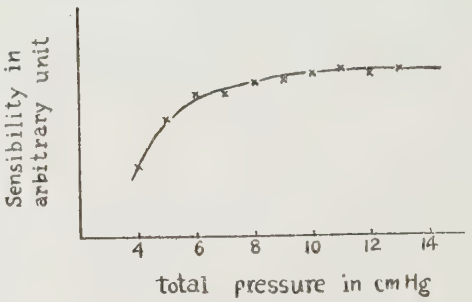

Fig. 6.

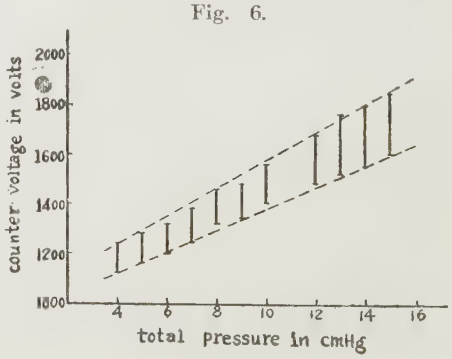

Fig. 7.

From the above results, it is concluded that our counter has the satisfactorily good characteristics and can be reliably used when the total pressure of the gas is about 10 cmHg$\sim$15 cmHg (90 % Ar + 10 % alcohol) and R is greater than

100 MΩ.

Efficiency of Counter

In order to obtain the absolute number of the incident γ-quanta from the measurement with counter, it is always necessary to determine the efficiency of the counter. A few workers[20-27,38] studied this problem for the γ-rays of comparatively low energies up to about $5\,mc^2$ and some results were obtained for the brass or aluminium counter. There is, however, no reliable knowledge for the high energy γ-rays such as emitted by the (Li–p) or (F–p) reactions. The author has tried to calculate theoretically the efficiency of the above-mentioned lead counter for the high energy γ-rays, since the experimental determination belongs to a very difficult thing in the present state of matter.* The calculation was made at first for the rectangular counter with the same thickness of wall as the cylindrical one for the sake of simplicity and afterwards the correction due to the oblique incidence was considered.

According to the quantum mechanical calculation,[29,30] the great majority of electrons are expected to be emitted in the forward direction in the processes of the pair creation and the Compton effect by such high energy γ-rays. Then the efficiency $\eta_a(h\nu,\ t)$ of the rectangular counter of the thickness t for the γ-quantum of energy $h\nu$ may be given by the following expression : **

$$\eta_a(h\nu,\ t)=\int \exp[-\tau(t-x)]dx\int[\sigma_c(h\nu,\ E)p(E,\ x) + \{2\sigma_p(h\nu,\ E)p(E,\ x)-\sigma_p(h\nu,\ E)p(E,\ x)p(h\nu-E,\ x)\}]dE,$$

where τ is the absorption coefficient of the γ-quantum considered,

x is the distance from the inner surface of wall where the secondary electron is produced,

$\sigma_c(h\nu,\ E)$ and $\sigma_p(h\nu,\ E)$ are the probability for the production of secondary electron of energy E by the incident γ-quantum of energy $h\nu$ by the Compton effect and the pair

* The author made a preliminary calculation of the efficiency of the thick walled lead counter described above, disregarding the effects of the multiple scattering and the radiation loss of the secondary electrons for the sake of simplicity.[28]

** A preliminary report of this calculation was given at the meeting of the Institute for Chemical Research, Kyoto University, November 1949. (Rep. Inst. Chem. Res. Kyoto Univ. **20** in press) The details of the calculation will be published soon. (Journ. Phys. Soc. Japan)

creation process respectively,

and $p(E, x)$ is the probability with which the electron of energy E can penetrate through the thickness x of the wall.

The probabilities for the production of the secondary electron σ_e and σ_p can be given by the ordinary theory of quantum mechanics. To calculate the penetration probability $p(E, x)$, we must consider the effects of the multiple scattering and the radiation loss of the secondary electrons.

Fowler and others[31] studied the effect of the multiple scattering of electron in aluminium by the method developed by W. Bothe.[32] We have made a similar calculation for the case of the lead counter.

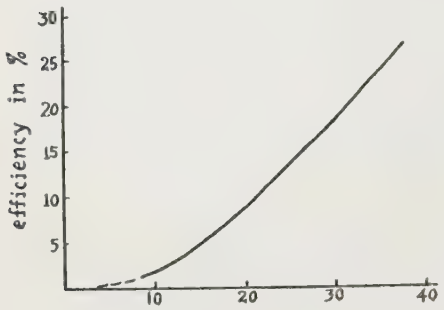

Fig. 8.

As to the radiation effect, the theory of the cosmic ray shower[33] has been applied, since the similar multiplication process is supposed to occur when a secondary electron of high energy penetrates through the wall of the counter.

The final results after making the correction due to the cylindrical shape, are listed in Table 1 and shown in Fig. 8.

TABLE 1. The Efficiency of the Cylindrical Counter (inner diameter : 2 cm)

Wall thickness in cm	Energy of γ-ray quantum in mc^2				
	12	20	25	30	34
0.20	3.7%	9.7%	13.6%	16.0%	17.4%
0.30	3.5	10.4	15.2	19.1	21.8
0.40	3.4	10.2	15.0	19.8	23.5
0.50	3.2	9.7	14.4	19.6	23.7
6.60	3.1	9.0	13.8	18.8	23.2
0.65	3.0	8.7	13.5	18.3	22.3

In conclusion, the author wishes to express his cordial thanks to Prof. B. Arakatsu, Prof. K. Kimura and other members of our laboratory for helpful suggestions on experiments and to Prof. M. Kobayasi for valuable discussions on theoretical calculations.

References

(1) A. Trost: ZS. f. Phys. **105** (1937), 399.
(2) C. G. Montgomery and D. D. Montgomery; Phys. Rev. **57** (1940), 1030.
(3) H. G. Steven: Phys. Rev. **59** (1941), 765; **61** (1942), 38.
(4) O. Minagawa: Proc. Imp. Acad. Tokyo, **18** (1942), 460, 468, 644; **19** (1943), 19,246,377; **20** (1943), 77, 288, 291.
(5) C. H. Collie and D. Roaf: Proc. Phys. Soc. **52** (1940), 186.
(6) R. D. Present: Phys. Rev. **72** (1947), 243.
(7) S. H. Liebson: Phys. Rev. **72** (1947), 602.
(8) H. Kumagai and others: Journ. Phys. Soc. Japan, **4** (1949), 39, 44, 48.
(9) H. Geiger and W. Müller: Phys. Zeits. **29** (1928), 859; **30** (1928), 489.
L. F. Curtiss: Bur. Stand. Journ. Res. **4** (1930), 601; **5** (1930), 115.
(10) W. Schultz: ZS. f. Phys. **78** (1932), 99.
(11) C. Bosen: Ann. d. Phys. **19** (1934), 65.
(12) C. L. Haines: R. S. I. **7** (1936), 411.
(13) O. S. Duffendack, H. Lifschutz and M. M. Slawsky: Phys. Rev. **52** (1937), 1231.
(14) S. C. Brown: Phys. Rev. **58** (1940), 1121.
(15) I. S. Allm and L. W. Alvarez: R. S. I. **6** (1935), 329.
(16) J. A. Bearden and C. L. Haines: Phys. Rev. **40** (1932), 1048.
(17) A. S. Keston: R. S. I. **14** (1943), 293.
(18) S. H. Liebson: Phys. Rev. **72** (1947), 181.
(19) H. Aoki and others: Proc. Phys.-Math. Soc. Japan, **22** (1940), 746; **23** (1941), 861.
(20) H. J. v. Baeyer: ZS. f. Phys. **95** (1935), 429.
(21) G. F. v. Droste: ZS. f. Phys. **100** (1936), 529.
(22) G. J. Sizoo and H. Willemsen: Physica **5** (1936), 105.
(23) F. Norling: Phys. Rev. **58** (1940), 277.
(24) J. v. Dunworth: R. S. I. **11** (1940), 107.
(25) I. Nonaka: Proc. Phys.-Math. Soc. Japan, **25** (1943), 227.
(26) K. Buchmann: Phys. Zeits. **38** (1937), 817.
(27) H. Yukawa and S. Sakata: Sci. Pap. Phys-Chem. Res. **31** (1937), 187.
(28) M. Sonoda: Journ. Phys. Soc. Japan, **5** (1950), 53.
(29) See, for example, W. Heitler: Quantum Theory of Radiation (1936).
(30) H. Bethe: Proc. Cambr. Phil. Soc. **30** (1934), 524.
(31) W. A. Fowler, C. C. Lauritsen and T. Lauritsen: Rev. Mod. Phys. **20** (1948), 258.
(32) W. Bothe: Handbuch der Physik XX II/2 (1933).
(33) See, for example, B. Rossi and K. Greisen: Rev. Mod. Phys. **13** (1941), 240.
(34) B. Arakatsu and others: Proc. Phys.-Math. Soc. Japan, **23** (1941), 440.
(35) B. Arakatsu and others: ibid. **23** (1941), 633,
(36) B. Arakatsu and others: ibid. **25** (1943), 173.
(37) B. Arakatsu and others: Journ. Phys. Soc. Japan, **1** (1943). 24.
(38) A. Roberts, J. R. Downing and M. Deutsch: Phys. Rev. **60** (1941), 544.

Institute of Physics,
University of Kyoto.

Memoirs of the College of Science, University of Kyoto, Series A,
Vol. XXV, Nos. 3 & 4, Article 28, 1949.

On the Proportional Counter

By

Masateru SONODA

(Received December 15, 1949)

Introduction

When the cylindrical counter ordinarily used is operated under the threshold of the Geiger-Müller region, there is a certain range of voltage in which the charge accumulated on the central wire is proportional to the primary ionization. This is called the proportional counter and can discriminate the nature of the incident particles by the amount of ionization. It has recently been used widely because of its various advantages.

I. α-Proportional Counter

The cylindrical proportional counter was investigated by several workers,[1] but it had a serious disadvantage that the amplification factor is very sensitive to the small change of the applied voltage.[2] It was, however, found by Korff and Rose[3] that the amplification factor became a slowly changing function of the applied voltage when the comparatively large amount of methane or other complex gas was used and the proportional counter could be successfully used if the applied voltage was sufficiently stable.

This counter has the following advantages:

(1) It has a small pulse-width and accordingly a better resolving time than the ionization chamber of an ordinary Wynn-Williams type owing to its higher applied voltage.

(2) In the proportional counter, a certain amplification is performed in the counter itself and therefore the pulse height on the collector is greater than in the Wynn-Williams ionization chamber. Accordingly the large counter can be used without making the pulse height too small by its large capacity which is very convenient for the observation of very rare events.

(3) Furthermore, the amplifier can be simplified and that of four stage is sufficient.

We have investigated for these several years the various photo-nuclear effects by the γ-rays from the (Li–p) or (F–p) reactions.[4] In these cases, the very rare events must be counted under the intense γ-ray background. The large proportional counter was found suitable for such investigations and so its properties were investigated.

Construction

The details of the counter are shown in Fig. 1. The counter wall W is made of aluminium of 1 mm in thickness and has the inner diameter of 6.25 cm and the length of 26 cm. The collector C is a tungsten wire of 0.15 mm in diameter and is supported at both ends by the cupper poles P of 3 mm in diameter which jet out about 3 cm into the inner tube. S is an outer aluminium cylinder of 10 cm in diameter which is grounded to shield the counter from the outer electrical disturbances. There is the guard ring G between the central wire and the counter wall on which the negative high tension is applied so that the surface leakage from the counter wall may always be earthed not so as to reach the collecting wire. The other constituent parts are similar to those of the Geiger-Müller counter.

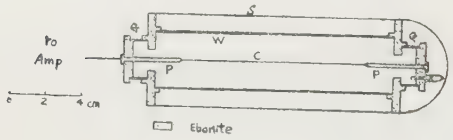

Fig. 1.

Amplifier Circuit

The amplifier adopted is a four stage resistance capacity coupling type and is shown in Fig. 2. It is a simplified form of the linear amplifier used with the ionization chamber.[5] The central wire of the counter is connected directly to the control grid of the first valve 6C6 or 6SJ7, which is earthed through a high resistance of the order of $10^8 \sim 10^9$ ohms and a small bias cell. The second and third valves are also 6C6 or 6SJ7 and the fourth one is a power valve UZ 42 or 6F6.

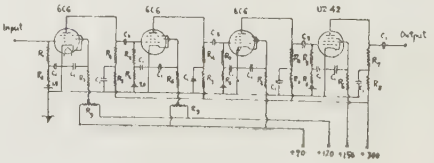

Fig. 2.

$R_2 = 10^6\ \Omega$ $R_8 = 1\ \mathrm{K}\Omega$
$R_3 = 20\ \mathrm{K}\Omega$ $R_9 = 10\ \mathrm{K}\Omega$
$R_4 = 250\ \mathrm{K}\Omega$ Potentiometer
$R_5 = 500\ \mathrm{K}\Omega$ $C_1 = 2\ \mu\mathrm{F}$
$R_6 = 50\ \mathrm{K}\Omega$ $C_2 = 0.0001\ \mu\mathrm{F}$
$R_7 = 7\ \mathrm{K}\Omega$ $C_3 = 0.001\ \mu\mathrm{F}$

The amplification factor is controlled by the slight change of the screen grid potential of the first or second valve. It is desirable to

control both potentials complementarily in order to avoid the unwanted disturbances of linearity.

Each stage of the amplifier is mounted in a separated iron case in order to eliminate the electric disturbances. The linearity of the amplifier was tested by the pulse of known voltage from a pulse generator.

The high voltage supply of an ordinary Gingrich type[6] was used which was capable of giving a very stable voltage up to 5000 volts.

Characteristic Curve

According to Rose and Korff,[3] it is necessary to adsorb the photo-quanta and suppress the photoelectric effect in the counter by filling it up with a certain amount of complex gas such as methane, in order to obtain a reliable proportional counter. We have adopted the mixture of methane and argon gas and investigated its counting properties for different mixing ratios and various values of total pressure under an intense γ-ray background.

As an α-ray source, we used a piece of pitchblende or active deposit from Tn placed at a given distance from the counter. The α-particles were introduced into the counter through a thin aluminium window of 2 mg/cm^2 in thickness. The intense γ-ray background was produced by a 5.4 mg Radium in a lead case of 6 mm in thickness placed at a distance of 7.1 cm from the center of the counter. The number of the incident γ-ray quanta was estimated to be of the order of 4×10^7 per sec.

A typical characteristic curve was shown in Fig. 3 a for the case of Ar 2 cm Hg + CH_4 19.8 cm Hg. It is seen from the figure that the counting rate increases rather rapidly at first and then the rise becomes gradual in some region of applied voltage.* In this region, the rate of rise is about 15～20 % and therefore the counter can be practically used,

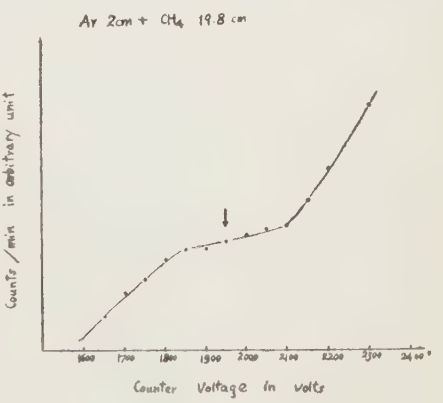

Fig. 3 a.

* This region can be called "plateau" as in the case of the Geiger-Müller counter, although it is not so flat as that of the latter case.

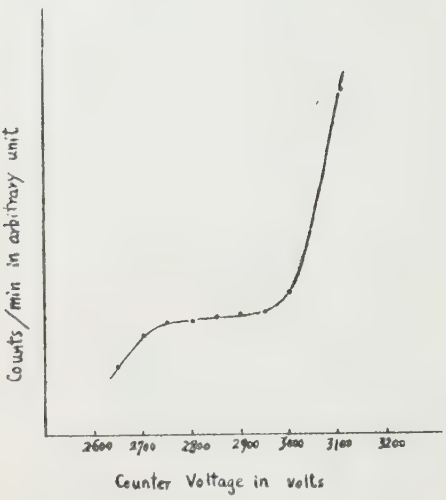

Fig. 3 b.

contrary, the amount of methane must be greater than a certain lower limit (about 2 cmHg).

These are shown in Figs. 4 and 5. Fig. 4 gives the relation between the plateau and the total pressure when the partial pressure of argon is maintained at 2 and 0 cmHg (no argon) respectively. Fig. 5 shows the plateau against the mixing ratio of both components at the total pressure of 10 and 7 cmHg. The γ-point is indicated as the cross and the dotted line in both figures. As is seen, the γ-point falls on the region of plateau for a high pressure and therefore the relatively smaller pressure is preferable to detect α-particles or protons under such intense γ-ray background.

if the high tension supply is sufficiently stable. The arrow indicates the voltage at which the counter begins to become sensitive to the pile-up of the γ-ray quanta. We will call this point the γ-point hereafter.

The plateau is displaced as a whole to the higher voltage for the greater value of the total pressure. Argon is not always necessary. It seems, however, that the plateau region becomes wider and the operating voltage decreases when a small amount of argon is added. On the

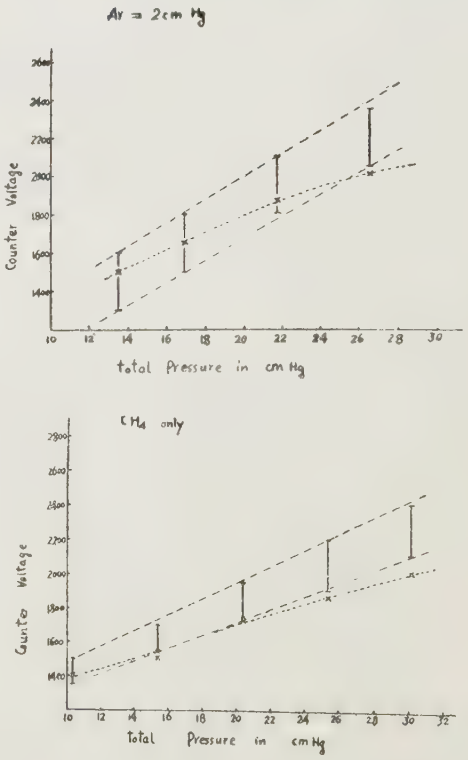

Fig. 4.

The methane gas can be replaced by the vapor of alcohol. Although similar characteristic curves are obtained in this case, alcohol vapor is not so convenient as methane gas, since its vapor pressure is very sensitive to the room temperature.

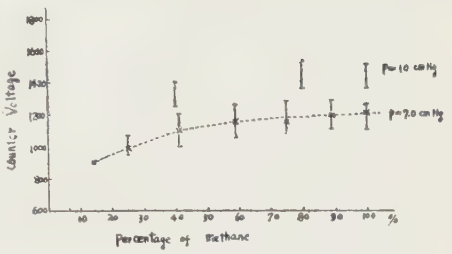

Fig. 5.

II. α–Proportional Counter of Flow Type

Recently J. A. Simpson[7] devised the α-proportional counter which operated at the atmospheric pressure, the methane gas having been flowed through the counter from the commercial bomb at the atmospheric pressure. Since it has no need of evacuation, it is convenient especially when the counter wall must be coated with various samples.

The properties of this counter were also investigated by us. The construction of the counter was similar to the one shown in Fig. 1, except that the gas inlet and outlet were provided in this case, through which the methane gas flowed into and out from the counter. The diameter of the central wire is smaller and namely 0.1 mm in order to diminish the operating voltage. The method of operation will be described in detail in the next section.

The characteristic curve is shown in Fig. 3 b. The rate of rise in the plateau is smaller than in the case of the ordinary type.

III. β–Proportional Counter of Flow Type

We have applied Simpson's method to the β-proportional counter and obtained the satisfactory results. This β-ray proportional counter of flow type has the various advantages. Since it has no need of evacuation, it can be used immediately after putting together. The window can be made extremely thin or, if necessary, can be removed entirely and the sample to be measured can be directly put on the aperture of the counter. Thus we can measure the β-particles of very low energies. The counter of this type will be very convenient for the tracer of low energy β-activity such as C^{14} or S^{35}.*

* The energies of β-rays are 0.15 and 0.16 MeV respectively.

Construction

The details of the counter are shown in Fig. 6. It is an end window type. A brass tube of 2 mm in thickness, 2 cm in diameter and 4 cm in length, is mounted by an ebonite insulator in an outer cylinder. The outer cylinder is 4.4 cm in diameter and 6 cm long, and is grounded in order to prevent the electrical disturbances from imposing on the central wire. The central wire used is so fine that we can diminish the operating voltage as possible and namely 0.075 mm in diameter. It is supported at one end by a small brass pole of about 3 mm in diameter which is put 1 cm into the inner tube. A small glass ball of about 0.5 mm in diameter was attached to the other end of the central wire to eliminate sparking and situated 3 mm beneath the end plane of inner tube to minimize the end effect of the electric field. This value was experimentally determined after several tests. The window is a thin collodion foil of 0.18 mg/cm^2 * and 3.5 cm in diameter, and 3 mm apart from the end plane of the inner cylinder.

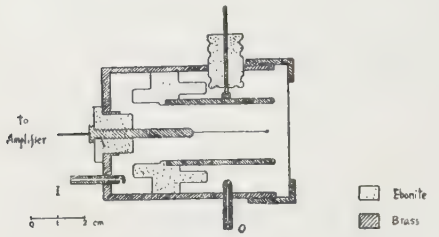

Fig. 6.

The ebonite insulator which supports the inner tube and the one through which the high tension lead is connected to the counter tube must have the large surfaces as possible in order to minimize the leakage. I and O are the gas inlet and the gas outlet respectively. The holes through which the gas flows into and out from the counter are situated on the sides of the inlet and outlet pipes to avoid the probable impairment of the ebonite surface caused by the direct impact of the stream of gases. Careful attentions were payed to every constituent part as described in the previous paper on the γ-ray counter.

Operation and Characteristics

The manner of operation is schematically shown in Fig. 7. The methane gas flows into the counter through the inlet I and out from the outlet O. F is a glass bottle filled with vacuum pump oil at the height of about 2 cm through which the methane gas is bubbled and serves as a simple flow meter which indicates the flow rate of the gas.

* This thickness corresponds to the β-ray energy of 7.6 KeV.

S is the same bottle as F, but contains more amount of oil, namely at the high of about 10 cm. C_1, C_2, C_3 and C_4 are the cocks. In the state of operation, all the cocks are opened and the methane flows through the counter and the flow meter. The bubbles are seen in the flow meter F but not in the bottle S, because the higher pressure is necessary to bubble through S. If the pressure of the methane gas rises suddenly by an accident, the gas will flow through S and the thin foil of the window will be protected from breaking. Namely, S is a simple safety valve. In the actual operation, the amount of oil in S and F must suitably be adjusted, taking account of the strength of the foil.

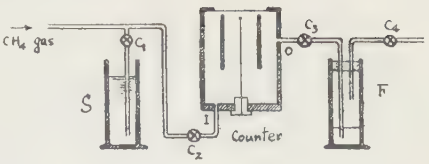

Fig. 7.

Before operating, the counter must be cleaned for about one hour by flowing methane gas so rapidly that the air in the counter may be prefectly removed. We see that the threshold voltage decreases gradually after the beginning of the flow and finally it becomes to a constant value. Then, during the operation the flow is diminished to a rate of 20 or 30 bubbles per minute through a hole of 1 mm in diameter.

The characteristic curve obtained is shown in Fig. 8, when 1 mg Radium source within a 6 mm lead shield was placed at the distance of 107 cm from the counter. It is not affected by the atmospheric conditions such as the pressure or the temperature. The curve rises at first more rapidly and then the rise becomes gradual in the voltage range from 3600 to 3800 volts in our case. In this range the rate of rise is about 15% and therefore the counter can be practically useful if the high voltage supply is sufficiently stable. The natural background is about 11.4/min at the middle of the plateau. The amplifier is the same as that shown in Fig. 2.

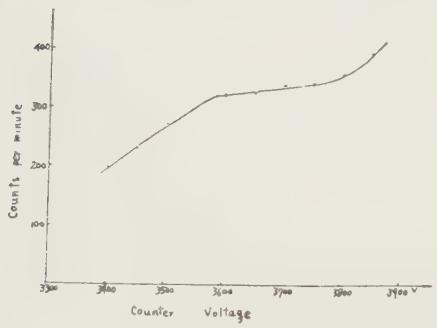

Fig. 8.

Finally, the author wishes to express his cordial thanks to Prof. B. Arakatsu and Prof. K. Kimura for their valuable discussions during this work.

References

(1) For example, G. Brubaker and E. Pollard: R. S. I. **8** (1937), 254.
(2) S. A. Korff: Rev. Mod. Phys. **11** (1939), 211.
(3) S. A. Korff and M. E. Rose: Phys. Rev. **59** (1941), 850.
(4) B. Arakatsu and others: Proc. Phys.-Math. Soc. Japan, **23** (1941), 440, 633; **25** (1943), 173; Journ. Phys. Soc. Japan, **1** (1946), 24.
S. Shimizu and J. Muto: Memo. Coll. Sci. Kyoto Imp. Univ. **25**, No. 2, Art. 11 (1949).
(5) K. Kimura and Y. Uemura: Memo. Coll. Sci. Kyoto Imp. Univ. **23** (1940), 1.
(6) N. S. Gingrich: R. S. I. **7** (1936), 207.
(7) J. A. Simpson, Jr.: R. S. I. **18** (1947), 884.

Institute of Physics,
University of Kyoto

Memoirs of the College of Science, University of Kyoto, Series A,
Vol.XXV, Nos. 3 & 4, Article 29, 1949.

Photo-induced Reaction $Cu^{63}(\gamma, n)Cu^{62}$ produced by the Gamma-Rays of Lithium bombarded with High Speed Protons*

By

Sakae Shimizu

(Received December 15, 1949)

Abstract

We observed $Cu^{63}(\gamma, n)Cu^{62}$ reaction produced by the gamma-rays emitted from lithium bombarded with 460 Kev protons, and a fairly accurate value of the cross section for this reaction was determined by the measurements of the induced positron activities produced in copper samples against the total number of irradiated gamma-ray quanta. In order to eliminate the effect of self-absorption of positrons of Cu^{62} in the samples, the ratio of activities of samples to those of a monitor sample was plotted as a function of thickness of samples. From this curve we could extrapolate a value which is not suffering from the effect of self-absorption. Total number of gamma-ray quanta concerned was measured with a Geiger-Mueller counter of thick lead wall, of which counting efficiency was computed theoretically. After measurements of the decay constant of Cu^{62} and of various factors concerning the geometrical arrangement and analysis of the experimental data, the cross section of $Cu^{63}(\gamma, n)Cu^{62}$ for 17.6 Mev $h\nu$ was obtained as $7.7_5 \times 10^{-26}\,cm^2 \pm 15\,\%$, which, however, was increased then to $8.5 \times 10^{-26}\,cm^2 \pm 15\,\%$ by taking into account the fact that the lithium gamma-rays have a line at 14.8 Mev besides a line at 17.6 Mev. The discussions on the value obtained by other workers are also given.

I. Introduction

Since 1937, studies of photo-neutron effect of 17 Mev and 12 Mev gamma-rays on heavier elements have been made by several investigators[1].

* Preliminary report was read at the 4th annual meeting of the Physical Society of Japan at University of Tokyo (April 27, 1949).

1. W. Bothe and W. Gentner, Zeits. f. Physik **106** (1937), 236; **112** (1939), 45; W. Y. Chang, M. Goldhaber, and R. Sagane, Nature **139** (1937), 962; P. R. Carlson and J. E. Henderson, Phys. Rev. **58** (1940), 193; O. Huber, O. Lienhard, P. Scherrer, and H. Wäffler, Phys. Rev. **60** (1941), 910; Helv. Phys. Acta **15** (1942), 312; **16** (1943), 33; **18** (1945), 221; O. Huber, O. Lienhard, and H. Wäffler, Helv. Phys. Acta **16** (1943), 226; **17** (1944), 195.

With another type of photo-nuclear reactions[2] the said effects have been carefully studied by us in these ten years. We have been able to confirm the occurrence of (γ, n) reaction produced by 17 Mev gamma-rays which results in the induced activities in some irradiated samples, while, in spite of careful experiments, we could not ascertain the occurrence of this reaction with 6.1 Mev gamma-rays of F (p, γ). The latter fact may be expected from the knowledge that the average binding energy of a neutron in middle-weight nuclei is generally about 8 Mev and more. In the meanwhile, the researchers in Zürich[3] observed the photo-disintegration of (γ, p) type of several elements with the irradiation of 17 Mev gamma-rays. On the other hand, in the United States of America the production of high energy X-rays by betatrons and synchrotrons was achieved and several types of photo-induced nuclear reactions were observed[4]. Baldwin and Koch[5] measured the thresholds of (γ, n) reactions by using the high voltage X-rays from the 20 Mev betatron. Perlman and Friedlander[6] used the X-rays from the 100 Mev betatron and the 80 Mev synchrotron to induce (γ, n), (γ, p), $(\gamma, 2n)$ and $(\gamma, 2p)$ reactions of several nuclei and determined the relative yields for a number of these reactions. Baldwin and Klaiber[7] measured the yield curves for the reactions $C^{12}(\gamma, n)C^{11}$ and $Cu^{63}(\gamma, n)Cu^{62}$ with X-rays up to 100 Mev and found that the relative cross section has a maximum at about 22 Mev for Cu^{63} and 30 Mev for C^{12} while it decreases to negligible value at high quantum energies. Recently, McElhinney *et al.*[8] have estimated approximate cross sections of tantalum and copper for the X-rays from the 22 Mev betatron. In those experiments, however, knowledges of the spectral distribution of the intensity in X-radia-

2. B. Arakatsu, Y. Uemura, M. Sonoda, S. Shimizu, K. Kimura, and K. Muraoka, Proc. Phys.-Math. Soc., Japan **23** (1941), 440; B. Arakatsu, M. Sonoda, Y. Uemura, and S. Shimizu, Proc. Phys.-Math. Soc., Japan **23** (1941), 633; B. Arakatsu, M. Sonoda, Y. Uemura, S. Shimizu, and K. Kimura, Proc. Phys.-Math. Soc., Japan **25** (1943), 173; B. Arakatsu, S. Shimizu, T. Hanatani, and J. Muto, Journ. Phys. Soc., Japan **1** (1946), 24.

3. O. Huber, O. Lienhard, P. Scherrer, and H. Wäffler, Helv. Phys. Acta **16** (1943), 431; **17** (1944), 139; O. Hirzel and H. Wäffler, Ibid. **19** (1946), 214; **20** (1947), 373.

4. G. C. Baldwin and G. S. Klaiber, Phys. Rev. **70** (1946), 259 & 586; **71** (1947), 3; **73** (1948), 1156; J. L. Lawson and M. L. Perlman, **74** (1948), 1190; D. L. Mock, R. C. Waddel, L. W. Fagg, and R. A. Tobin, Phys. Rev. **74** (1948), 1536; M. L. Perlman, Phys. Rev. **75** (1949), 988.

5. G. C. Baldwin and H. W. Koch, Phys. Rev. **67** (1945), 1.

6. M. L. Perlman and G. Friedlander, Phys. Rev. **74** (1948), 442.

7. G. C. Baldwin and G. S. Klaiber, Phys. Rev. **73** (1948), 1156.

8. J. McElhinney, A. O. Hanson, R. A. Becker, R. B. Duffield, and B. C. Diven, Phys. Rev. **75** (1949), 542.

tion from the targets of the betatron or the synchrotron, though it is theoretically predicted, are yet insufficient to make the accurate determination of the absolute cross sections for the photo-disintegration reactions induced by these high voltage X-rays. For the theoretical interest, therefore, it is preferable to make an accurate experiment with monochromatic gamma-rays. Since the (γ, n) reaction of copper for high energy gamma-rays is comparatively strong and the measurements of (γ, n) yield values of various other nuclei have generally been done by taking the value of $Cu^{63}(\gamma, n)\, Cu^{62}$ yield as standard, the measurement of the absolute cross section of this reaction is particularly important. Notwithstanding, there are very few experiments with monochromatic radiation. In 1937, the rough measurement on the cross section of $Cu^{63}(\gamma, n)\, Cu^{62}$ reaction for gamma-rays of $Li(p, \gamma)$ was made by Bothe and Gentner,[9] while a measurement has recently been made by Wäffler and Hirzel[10] with the same gamma-rays and a value about three times as large as that of Bothe and Gentner has been obtained.

In the present experiment the absolute cross section of $Cu^{63}(\gamma, n)\, Cu^{62}$ reaction for the 17.6 Mev gamma-rays of $Li(p, \gamma)$ reaction has been determined experimentally as carefully as possible, and we have obtained the result that $\sigma_{Cu(17)} = 8.5 \times 10^{-26} cm^2 \pm 15\ \%$.

II. Apparatus

For the production of 17.6 Mev gamma-rays we used a high voltage machine of Cockcroft-Walton type equipped in our laboratory. The proton beam of about 460 Kev was directed on the target of thin metallic lithium placed on the bottom of a thin brass tube of 0.2 mm thickness. It was focused to a spot of about 1.5 mm in diameter.

As it is well experienced in our laboratory, the number of gamma-ray quanta was counted by a specially constructed Geiger-Mueller counter with a lead wall of 6.5 mm thickness, the inside diameter and the effective length of which are 2 cm and 2 cm respectively. It was filled with argon of 9 cm Hg mixed with ethyl alcohol of 1 cm Hg. The lead wall of 6.5 mm thickness is able to prevent those electrons from entering into the counter which may be expelled from the surrounding materials exposed to the gamma-rays of $Li(p, \gamma)$. The counting efficiency of this lead counter for 17.6 Mev quantum, ε_{ff}, was computed theoretically by

9. W. Bothe and W. Gentner, Zeits. f. Physik **106** (1937), 236.
10. H. Wäffler and O. Hirzel, Helv. Phys. Acta **21** (1948), 200.

M. Sonoda[11] by taking into account the knowledges of Compton effect, electron-pair creation and the effect of multiple scattering and bremsstrahlung of the secondary electrons in the counter wall etc. His result is

$$\varepsilon_{ff} = 0.21_7 \quad \text{for the gamma-ray quantum of 17.6 Mev.}$$

Since in the present stage of our knowledges the rigorous determination of the counting efficiency by accurate experiments is yet difficult, the above theoretical value was presumably used in the computation for determination of the absolute number of gamma-ray quanta concerned. The pulses from the lead counter, after amplification, were counted by a system of scale-of-ten devised by R. Ishiwari and K. Yuasa.[12] In actual measurements the lead counter was placed at a point 29.4 cm apart from the Li-target and was usually shielded by a lead cylinder of 1.05 cm thickness. The practical absorption coefficient of this lead cylinder covering the counter was measured as μ_γ (Pb cylinder) $= 0.53\ \text{cm}^{-1}$. By adopting the above figures of ε_{ff} and μ_γ the actual readings of the counter were corrected in computating the absolute number of gamma-ray quanta concerned; namely, from the net counts, n_γ, the absolute number of gamma-ray quanta emitted from the Li-target, N_γ, is given by the formula:

$$N_\gamma \frac{\omega}{4\pi} \varepsilon_{ff} \exp(-\mu_\gamma x) = n_\gamma , \qquad (1)$$

where ω is the solid angle subtended by the effective space of the counter at the target, and x is the thickness of wall of the lead cylinder covering the counter. In the present geometry ω is given by $2 \times 3.3/29.4^2$ steradians and $x = 1.05$ cm.

The samples irradiated were a number of copper (c. p. grade) circular discs. The diameter of all the discs was precisely equal to 22.8 mm, while the thickness was varied from $40.8_1\ \text{mg/cm}^2$ to $1761.9_8\ \text{mg/cm}^2$ as listed in Table I. The effect of irregularity of activation due to the fluctuation of emission of irradiating gamma-rays was corrected by the usage of copper activation monitors of 40 mm in diameter and $801.3_2\ \text{mg/cm}^2$ in thickness.

For the measurement of positron activities induced in these copper samples two Geiger-Mueller counters of end-window type were constructed, of which structural details are shown in Fig. 1. The inside

11. M. Sonoda, Journ. Phys. Soc., Japan, now in press.
12. R. Ishiwari and K. Yuasa, Mem. Coll. Sci. Univ. of Kyoto **25** (1950), 155.

TABLE I. Thickness of copper samples.

Sample No.	Thickness in mg/cm²	
1	40.8_1	
2	54.9_4	
3	82.9_4	
4	120.9_6	
5	271.5_3	diameter = 22.8 mm.
6	523.5_1	
7	858.6_5	
8	1369.9_9	
9	1761.9_8	
Monitor sample	801.3_2	diameter = 40.0 mm.

diameter is 34 mm and the interval between the effective space of the counter and the mica window of 26 mm in diameter is about 6 mm. Each counter was filled with argon of 9 cm Hg mixed ethyl alcohol of 1 cm Hg. One was used for the measurements of activities of samples and the other was used for those of monitors. These two counters have the same dimensions except that the thickness of mica window of the sample counter is 3.7_9 mg/cm² while that of the monitor counter is 6.1_3 mg/cm². Pulses of each counter, after amplification, were fed to a scale-of-four recording circuit of Higinbotham type[13] with a mechanical recorder respectively. Counting measurements with these beta-counters were carefully corrected for counter sensitivity, for geometrical conditions of the arrangement of samples and for absorption in a mica window as described in the following section.

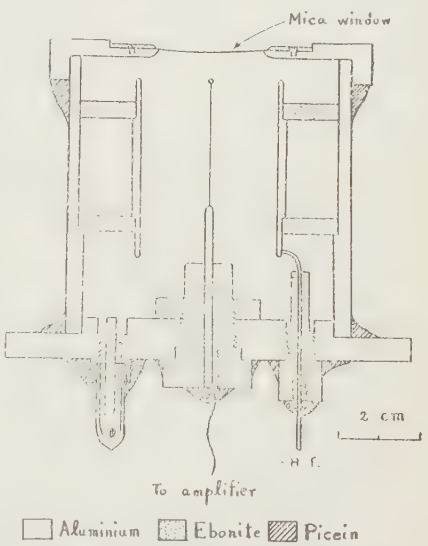

Fig. 1. Beta-ray Geiger-Mueller counter of end-window type.

13. W. A. Higinbotham, J. Gallager, and M. Sands, Rev. Sci. Inst. **18** (1947), 706.

III. Experimental Procedures

A set of sample and monitor, which were fitted closely each other, was mounted, as is shown in Fig. 2, on a plastic circular plate and placed in a definite orientation in the standard geometrical condition of irradiation. The upper surface of a monitor was directly fitted under the bottom of the target tube in such a manner as the axis of proton beam passed through the centers of both monitor and sample.

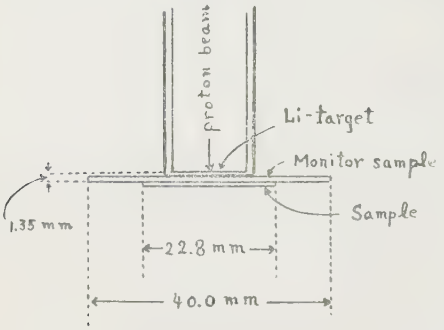

Fig. 2. Standard geometry of irradiation of samples.

The lower surface of the monitor, which was faced immediately to the upper surface of the sample, was laid 1.3$_5$ mm apart from the point regarded as the gamma-ray source on the Li-target. After the irradiation for several minutes both sample and monitor were transferred to the definite positions respectively, where the lower surface of monitor was faced to the mica window of the monitor counter separating 2.0 mm while the upper surface of the sample was faced to the window of the sample counter separating 1.7 mm. During the lapse of one minute, after the end of irradiation, the mentioned measurement condition was realized for each run of experiments by using the device having the delicately adjustable screws. In this standard geometry, the counting measurements of induced activities produced respectively in sample and monitor were begun simultaneously at just one minute after the end of irradiation and were continued for the following 10 minutes. Such measurements for each of samples of different thickness were carried out.

The results obtained are plotted in Fig. 3, in which N_s/N_m is given in a dotted curve and $N_s/N_m \cdot w_s$ in a solid curve as a function of thickness of samples respectively, where net counts of the sample counter and those of the monitor counter are denoted by N_s and N_m respectively. The thickness of samples is presented in this case by weight per unit area, w_s, in g/cm^2. We see that the dotted curve tends to saturation as the thickness of samples becomes larger. The aspect may be expected from the fact that the induced beta-rays have the definite maximum energy of about 2.6 Mev corresponding to about 1.4 mm range in copper. The solid curve shows the variation of the value which is proportional

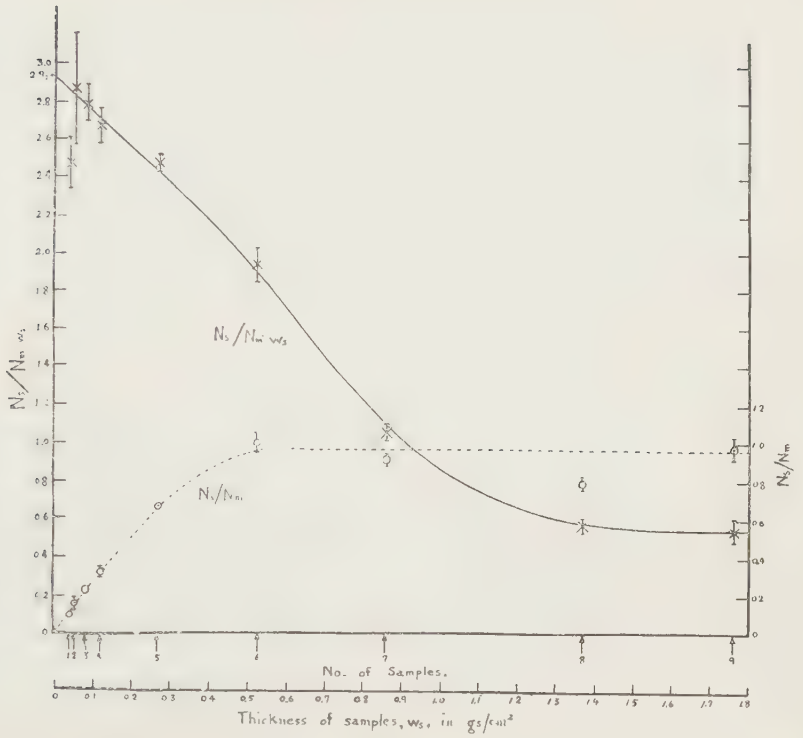

Fig. 3. The ratio of net counts of the sample counter, N_s, to those of the monitor counter, N_m, as a function of the thickness of samples, w_s.

to the apparent activities produced in unit thickness of samples. This curve was extrapolated to zero thickness by taking the weight of measurements into account. By this procedure we obtained a limiting value $\lim_{w_s \to 0} (N_s/N_m \cdot w_s) = 2.9_2$, which is obviously be taken as the value without suffering from the effect of self-absorption of positrons in the samples. However, in order to obtain the absolute number of Cu^{62} produced in a sample, it must be necessary, furthermore, to make the correction for the absorption of beta-rays in a mica window of the counter and that for the effects of the radiative position of the sample and the counter. We need, now, to know how many percent of beta-rays emitted from the surface of a sample may be counted by the sample counter.

By assuming the simple exponential law, the absorption coefficient of mica for positrons of Cu^{62}, μ_β, was determined by inserting a series of thin mica sheets between the sample and the counter, and we have found that $\mu_\beta = 0.0123\,(\mathrm{mg/cm^2})^{-1}$. The correction factor for the absorption in a mica window of the sample counter was obtained as: $C_\beta = 1.04_7$.

Since the geometrical correction was one of the most important factors for the calculation of the cross section, we determined this value carefully by laborious experiments. As a first step we observed the variation of counts against the varying distance between sample and mica window. It was found that the logarithm of counts decreases linearly with the distance. After a series of separate experiments done on this line we arrived at the conclusion that the geometrical correction, C_g, is 2.1 ± 0.1. And hence the total number of positrons emitted from the whole surface of the sample, N_β, is given by

$$N_\beta = 2C_g C_\beta N, \qquad (2)$$

where N is the net counts of the counter.

The mean life, τ, or decay constant, λ, of Cu^{62}, which is inevitably necessary for calculation of the cross section, was determined by the counting data obtained throughout the course of the present experiment by applying the rigorous theoretical treatment of Peierls.[14] The result obtained was $\tau = 15.2_1 \pm 0.4$ min. or $\lambda = 1/\tau = 0.0657 \pm 0.0017$ min^{-1}.

In practice, moreover, we ascertained that the effect of annihilation radiation of positrons upon the counting data was almost negligibly small by observing that the counts due to activities of the sample were reduced to natural counts of the counter when about 3 mm thick copper plate was inserted between the counter and the sample.

During the experiment the number of grmma-ray quanta was measured for the time interval of each half minute continuing 8 minutes necessitated for the irradiation.

IV. Calculation of Reaction Cross Section

When the irradiation of gamma-rays is made in the geometry shown in Fig. 4, in which a disc sample of radius r_0 and thickness δ is placed apart a from the gamma-ray point source, $(a < r_0)$, the number of active nuclei, dA, produced in an infinitesimal time interval, $(t, t + dt)$, can be written in a form:

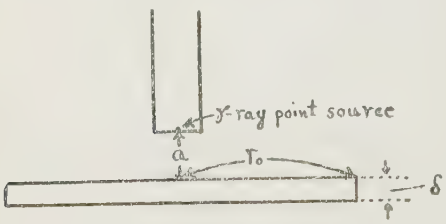

Fig. 4. A geometry of irradiation: a circular disc sample is placed closely under the gamma-ray point source.

$$dA = \sigma m N_\gamma \left[\frac{1}{4} \int_a^{a+\delta} \log\left(\frac{a^2 + r_0^2}{a^2} \right) da \right] dt, \qquad (3)$$

14. R. Peierls, Proc. Roy. Soc., A, **149** (1935), 467.

where

σ = reaction cross section for $Cu^{63}(\gamma, n)$ Cu^{62},
m = number of Cu^{63} atoms per cc in copper sample,
N_γ = total number of 17.6 Mev quanta emitted from the Li-target per unit time.

If the irradiation continues for T minutes with constant intensity, the number of active nuclei produced, A, is given by

$$\begin{aligned} A &= \int_{t=0}^{T} \exp\Big[-\lambda(T-t)\Big] dA \\ &= \int_0^T \sigma m N_\gamma \Big[\frac{1}{4}\int_a^{a+\delta} \log\Big(\frac{a^2+r_0^2}{a^2}\Big) da\Big] \exp\Big[-\lambda(T-t)\Big] dt \\ &= \frac{\sigma m N_\gamma}{4\lambda}\Big[\int_a^{a+\delta} \log\Big(\frac{a^2+r_0^2}{a^2}\Big) da\Big]\Big[1-\exp(-\lambda T)\Big], \end{aligned} \tag{4}$$

where λ is the decay constant of Cu^{62} in min^{-1}. Since, in practice, as described in the preceding section, the sample was irradiated during 8 minutes and for each half minute of which gamma-ray counts were recorded, the number of Cu^{62} atoms existed at the time when the measurement of activities was commenced—one minute after the end of irradiation—can be given by

$$\begin{aligned} A_0 = \frac{\sigma m}{4\lambda}\Big[\int_a^{a+\delta} \log\Big(\frac{a^2+r_0^2}{a^2}\Big) da\Big]\Big[1-\exp(-0.5\lambda)\Big] \\ \times \sum_{i=1}^{16} 2N_{\gamma_i} \exp\Big[-\lambda(9-0.5i)\Big], \end{aligned} \tag{5}$$

where N_{γ_i}'s are the total number of gamma-ray quanta emitted from the target during each half minute interval in 8 minutes of the irradiation. Since, according to Eq. (1), the net counts of the gamma-ray counter, n_{γ_i}, are related with N_{γ_i} as

$$N_{\gamma_i} \frac{\omega}{4\pi} \varepsilon_{ff} \exp(-\mu_\gamma x) = n_{\gamma_i}, \tag{6}$$

and the number of Cu^{62} atoms that disintegrate in the following 10 minutes, A_d, can be expressed by, using Eqs. (5) and (6),

$$\begin{aligned} A_d &= A_0\Big[1-\exp(-10\lambda)\Big] \\ &= \frac{\sigma m \pi}{\omega\, \varepsilon_{ff}\, \lambda \exp(-\mu_\gamma x)}\Big[\int_a^{a+\delta} \log\Big(\frac{a^2+r_0^2}{a^2}\Big) da\Big] \times \end{aligned}$$

$$\times \left[1 - \exp(-0.5\lambda)\right]\left[1 - \exp(-10\lambda)\right]$$

$$\times \sum_{i=1}^{16} 2n_{\gamma_i} \exp\left[-\lambda(9 - 0.5i)\right]. \qquad (7)$$

Now, the observed counts for sample, N_s, and those for monitor sample N_m, are given by, according to Eqs. (2) and (7),

$$\left.\begin{aligned} N_s &= \left[\frac{A_a K}{2C_g C_\beta}\right]_s = \left[\frac{K\int_a^{a+\delta} \log\left(\frac{a^2 + r_0^2}{a^2}\right)da}{2C_g C_\beta}\right]_s \times P, \\ N_m &= \left[\frac{A_a K}{2C_g C_\beta}\right]_m = \left[\frac{K\int_a^{a+\delta} \log\left(\frac{a^2 + r_0^2}{a^2}\right)da}{2C_g C_\beta}\right]_m \times P, \end{aligned}\right\} \qquad (8)$$

where K is the correction factor for self-absorption and, referring to Eq. (7), a common factor, P, is given by

$$P = \frac{\sigma m \pi}{\omega\, \varepsilon_{ff}\, \lambda \exp(-\mu_\gamma x)}\left[1 - \exp(-0.5\lambda)\right]$$

$$\times \left[1 - \exp(-10\lambda)\right] \sum_{i=1}^{16} 2n_{\gamma_i} \exp\left[-\lambda(9 - 0.5i)\right]. \qquad (9)$$

And the suffixes s and m mean that the notations contained in each bracket are concerned in the sample and the monitor respectively. From the expressions (8) we obtain

$$\frac{N_s}{N_m w_s} = \frac{N_s}{N_m \rho\, \delta_s} = \frac{P}{N_m \rho\, \delta_s}\left[\frac{K\int_a^{a+\delta} \log\left(\frac{a^2 + r_0^2}{a^2}\right)da}{2C_g C_\beta}\right]_s, \qquad (10)$$

where ρ is density of the sample.

Now, when $w_s \to 0$ or $\delta_s \to 0$,

$$\left.\begin{aligned} &K_s \to 1, \\ &\left[\frac{1}{\delta}\int_a^{a+\delta} \log\left(\frac{a^2 + r_0^2}{a^2}\right)da\right]_s \to \left[\log\left(\frac{a^2 + r_0^2}{a^2}\right)\right]_s. \end{aligned}\right\}$$

Applying these relations to Eq. (10) we obtain at once

$$Q \equiv \lim_{w_s \to 0} \frac{N_s}{N_m w_s} = \lim_{\delta s \to 0} \frac{N_s}{N_m \rho\, \delta_s} = \frac{P}{N_m \rho}\left[\frac{\log\left(\frac{a^2 + r_0^2}{a^2}\right)}{2C_g C_\beta}\right]_s. \qquad (11)$$

The value of Q is obtained experimentally as described in the preceding section.

Using Eqs. (9) and (11) we get the final expression of σ:

$$\sigma = \frac{2 N_m \rho [C_g]_s [C_\beta]_s Q \omega \varepsilon_{ff} \lambda \exp(-\mu_\gamma x)}{m\pi \left[\log\left(\frac{a^2 + r_0^2}{a^2}\right)\right]_s \left[1 - \exp(-0.5\lambda)\right]\left[1 - \exp(-10\lambda)\right]} \times \frac{1}{\sum_{i=1}^{16} 2 n_{\gamma i} \exp\left[-\lambda(9 - 0.5i)\right]}. \tag{12}$$

It is to be noticed that this expression contains no counting data concerning the samples but those of the monitor used simultaneously with the samples. Thereby we have the advantage of employing the counts of the monitor which are less suffering from the statistical errors than those of samples.

Numerical computation of Eq. (12) has been done by employing the values obtained by the present experiment as follows:

λ = decay constant of $Cu^{62} = 0.0657 \pm 0.0017\ \text{min}^{-1}$,

$[C_g]_s$ = correction factor concerning the geometrical conditions of activity measurement of sample $= 2.1 \pm 0.1$,

$[C_\beta]_s$ = correction factor for the absorption of positrons of Cu^{62} from the sample in a mica window of the counter $= 1.04_7$,

ε_{ff} = counting efficiency of the gamma-ray counter for 17.6 Mev $h\nu = 0.21_7$,

ω = solid angle subtended by effective space of the gamma-ray counter at the gamma-ray source $= 2 \times 3.3/29.4^2$ steradians,

μ_γ = practical absorption coefficient of the lead cylinder covering the gamma-ray counter for the gamma-rays of Li $(p, \gamma) = 0.53\ \text{cm}^{-1}$,

x = wall thickness of the lead cylinder covering the gamma-ray counter $= 1.05$ cm,

m = number of Cu^{63} atoms per cc in copper sample = (Avogadro's number $\times$ abandance ratio* of Cu^{63} $\times$ density of copper, ρ.)/atomic weight of normal copper $= 6.48_6 \times 10^{21} \times \rho$,

* The value of abundance ratio of Cu^{63} used here is 68 % (J. Mattauch, *Kernphysikalische Tabellen*, Springer-Verlag, Berlin, 1942).

$[a]_s$ = distance between the sample and the gamma-ray source = 1.3_5 mm,

$[r_0]_s$ = radius of the sample = 11.4 mm,

$Q = \lim_{w_S \to 0} (N_s/N_m \cdot w_s) = 2.9_2$,

N_m = observed net counts of the activities of the monitor (summation from 6 runs), as shown in Table II,

$n_{\gamma i}$ = observed net counts of the gamma-ray counter for each half minute interval in 8 minutes of the irradiation (summation from 6 runs), as shown in Table II.

Thus we have obtained the result that $\sigma = 7.7_5 \times 10^{-26}\,\mathrm{cm}^2$ with a probable error of about 15 percent.

TABLE II. Experimental data

	n_{γ_i}							
i / Run No.	1	2	3	4	5	6	7	8
1	244	304	408	368	348	364	332	376
2	324	364	324	324	344	292	272	260
3	192	394	368	352	304	284	260	272
4	256	356	392	368	288	336	296	268
5	256	324	312	160	268	296	328	284
6	252	336	308	316	288	296	244	248
Total	1524	2080	2112	1888	1840	1868	1732	1708
Natural counts	43.8	43.8	43.8	43.8	43.8	43.8	43.8	43.8
$n_{\gamma i}$	1480.2	2036.2	2068.2	1844.2	1796.2	1824.2	1688.2	1664.2
$\exp[-\lambda(9-0.5\,i)]$*	0.5718	0.5910	0.6108	0.6313	0.6525	0.6740	0.6963	0.7196
$n_{\gamma i}\exp[-\lambda(9-0.5i)]$	846.38	1203.39	1263.26	1164.24	1172.02	1129.51	1175.49	1197.56
								$\sum_{i=1}^{16} 2n_{\gamma i}\exp[-\lambda(9-0.5\,i)]$

* $\lambda = 0.0657 \pm 0.0017\ \mathrm{min}^{-1}$.

V. Results and Discussions

In the present experiment a new method of eliminating the effect of self-absorption of beta-rays induced in the sample was introduced and

various careful experiments for determining many important and necessary factors have been carried out. The cross section of $Cu^{63}(\gamma, n)\, Cu^{62}$ has been then found to be

$$\sigma_{Cu(17)} = 7.7_5 \times 10^{-26}\ \text{cm}^2 \pm 15\ \%\ \text{for}\ 17.6\ \text{Mev}\ h\nu\ \text{of}\ \text{Li}\,(p, \gamma).$$

This result, however, has been obtained on the assumption that the gamma-rays of Li (p, γ) constitute themselves of the quanta of 17.6 Mev monochromatically. But, according to the determination of energy of the radiation by several workers such as Delsasoo, Fowler and Lauritsen[15] and Walker and McDaniel,[16] there are probably two lines instead of a single line, namely, one line at 17.6 Mev and another at 14.8 Mev. And the ratio of intensities of the lower energy line to the higher energy line was found to be approximately 0.5_0 for the protons of $n_{\gamma t}$ and N_m.

9	10	11	12	13	14	15	16	N_m
328	284	316	344	308	296	312	292	1273
260	280	248	252	248	252	252	236	1042
204	204	232	256	240	252	224	228	1070
260	212	260	236	216	232	216	235	1107
260	228	224	180	232	208	200	203	1091
232	224	220	204	224	200	228	200	1082
1544	1432	1500	1472	1468	1440	1432	1394	6665
43.8	43.8	43.8	43.8	43.8	43.8	43.8	43.8	1725.9
1500.2	1388.2	1456.2	1428.2	1424.2	1396.2	1388.2	1350.2	
0.7438	0.7687	0.7945	0.8212	0.8487	0.8767	0.9057	0.9361	
1115.85	1067.11	1156.95	1172.84	1208.72	1224.05	1257.29	1263.92	$N_m = 4939.1$
= 37437.36								

of 460 Kev bombarding energy.

Therefore the value of $\sigma_{Cu(17)}$ obtained from this experiment should

15. L. A. Delsasoo, W. A. Fowler, and C. C. Lauritsen, Phys. Rev. **51** (1937), 391.
16. R. L. Walker and B. D. McDaniel, Phys. Rev. **74** (1948), 315.

be increased by a factor, α, which is given by

$$\alpha = \left(1 + \frac{\varepsilon_{14}}{\varepsilon_{17}} R\right) \Big/ \left(1 + \frac{\sigma_{\mathrm{Cu}(14)}}{\sigma_{\mathrm{Cu}(17)}} R\right),$$

where R is the ratio of intensities of the line at 14.8 Mev to that at 17.6 Mev, and ε_{17} and ε_{14} are the counting efficiencies of the gamma-ray counter for each of the components of the rays respectively, and are given by M. Sonoda[11] as $\varepsilon_{17} = 0.21_7$ and $\varepsilon_{14} = 0.17_2$ respectively. According to the theory of Weisskopf[17] the cross section is proportional to $(h\nu)^3$, so the ratio of cross sections for 14.8 Mev $h\nu$ and 17.6 Mev $h\nu$, $\sigma_{\mathrm{Cu}(14)}/\sigma_{\mathrm{Cu}(17)}$, is considered to be $(14.8/17.6)^3 = 0.595$. Recently, by the measurements with high voltage X-rays, however, the ratio is given as about 0.61 by McElhinney *et al.*[8] and as about 0.17 by Baldwin and Klaiber.[7] If R is taken to be 0.5, α's should be given from the above relation, according as the three different values of $\sigma_{cu(14)}/\sigma_{cu(17)}$, as

$$\alpha = \begin{cases} 1.07_6 \text{ for } \sigma_{\mathrm{Cu}(14)}/\sigma_{\mathrm{Cu}(17)} = (14.8/17.6)^3 = 0.595, \\ 1.07_1 \text{ for } \sigma_{\mathrm{Cu}(14)}/\sigma_{\mathrm{Cu}(17)} = 0.61, \\ 1.28_8 \text{ for } \sigma_{\mathrm{Cu}(14)}/\sigma_{\mathrm{Cu}(17)} = 0.17. \end{cases}$$

Then the corrected values of the cross section of the reaction under consideration are given as

$$\sigma_{cu(17)} = \begin{cases} 8.3_5 \times 10^{-26}\,\mathrm{cm}^2 \text{ for } \alpha = 1.07_6, \\ 8.3_0 \times 10^{-26}\,\mathrm{cm}^2 \text{ for } \alpha = 1.07_1, \\ 9.9_8 \times 10^{-26}\,\mathrm{cm}^2 \text{ for } \alpha = 1.28_8, \end{cases}$$

respectively. Since, however, the theory of Weisskopf is based on several assumptions and is not yet complete while the measurements of the relative yield of these reactions carried with X-rays from betatrons involve several uncertainties because of the lack of the accurate knowledge of the spectral distribution of quanta in them, the value $\sigma_{\mathrm{Cu}(14)}/\sigma_{\mathrm{Cu}(17)}$ is fairly ambiguous. Though, therefore, we can not ascertain which of these three different values is most reliable, we may yet conclude that $\sigma_{\mathrm{Cu}(17)}$ lies between $7.2 \times 10^{-26}\,\mathrm{cm}^2$ and $10.8 \times 10^{-26}\,\mathrm{cm}^2$ as is shown in Fig. 5, in which $\sigma_{\mathrm{Cu}(17)}$ is given as a function of $\sigma_{\mathrm{Cu}(14)}/\sigma_{\mathrm{Cu}(17)}$.

In this way, we arrive at the conclusion that the cross section of Cu^{63} (γ, n) Cu^{62} is to be taken as

$$\sigma_{\mathrm{Cu}(17)} = 8.5 \times 10^{-26}\,\mathrm{cm}^2 \pm 15\ \% \text{ for } 17.6 \text{ Mev } h\nu.$$

17. V. F. Weisskopf, Phys. Rev. **59** (1941), 318.

However, if the ratio of cross sections for 14.8 Mev $h\nu$ and 17.6 Mev $h\nu$ is precisely determined, one can easily find a more accurate value of $\sigma_{Cu(17)}$ by inspecting the curve shown in Fig. 5.

The historical value of Bothe and Gentner[9] obtained in 1937, 5×10^{-26} cm^2, may be considered to be too small, since the contribution of 14.8 Mev $h\nu$ on the reaction was neglected in their measurements.

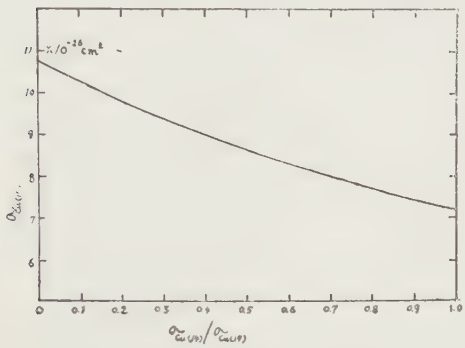

Fig. 5.

$\sigma_{Cu(17)}$ as a function of $\sigma_{Cu(14)}/\sigma_{Cu(17)}$. This curve is given by

$$7.7_5 \times \frac{1 + \frac{\varepsilon_{14}}{\varepsilon_{17}} R}{1 + \frac{\sigma_{Cu(14)}}{\sigma_{Cu(17)}} R} \times 10^{-26}\,\text{cm}^2,$$

where $\varepsilon_{17} = 0.21_7$, $\varepsilon_{14} = 0.17_2$, and $R = 0.5_0$.

Recent measurements by Wäffler and Hirzel[10] gave a value of 12×10^{-26}cm^2. This value was obtained from the experiments with the gamma-rays of Li (p, γ) and was corrected to 16×10^{-26}cm^2 by taking into account the existence of 14.8 Mev line. However, as it is discussed above, this value may be presumably too large.

Since the energy levels of heavier nuclei are not precisely determined, there is, so far, no theoretical way to calculate the cross section. Notwithstanding, under some simplified assumptions Weisskopf[17] calculated that the cross section is proportional to $(h\nu)^3$, and he obtained the proportionality constant from the measurements of Bothe and Gentner[18] of relative yields of (γ, n) reactions for the gamma-rays produced by Li (p, γ) and B (p, γ) reactions. According to his theory the cross section is expected to be about 3.5×10^{-26}cm^2 or less. On the other hand, the behavior of resonance phenomena of (γ, n) reactions was observed for the high voltage X-rays. Baldwin and Klaiber[7] observed such a resonance in carbon at 30 Mev and in copper at 22 Mev. A theory to account for this phenomenon has been put forward by Goldhaber and Teller[19] in analogy with the "reststrahl frequencies" of polar crystals. According to their theory $h\int \sigma d\nu$ for copper is predicated as about 1 Mev-barn,

18. W. Bothe and W. Gentner, Zeits f. Physik **112** (1939), 45.
19. M. Goldhaber and E. Teller, Phys. Rev. **74** (1948), 1046.

which corresponds to $\sigma_{Cu(17)} = 5 \times 10^{-26}\,cm^2$. Lawson and Perlman[20] have recently measured $h\int \sigma d\nu$ for $C^{12}(\gamma, n)C^{11}$ by using the 50 and 98 Mev X-rays, and deduced the value of $h\int \sigma d\nu$ for $Cu^{63}(\gamma, n)Cu^{62}$ as 1.5 Mev-barns which means that $\sigma_{Cu(17)}$ is about $7.5 \times 10^{-26}\,cm^2$.

Another value of $\sigma_{Cu(17)}$ has been reported by McElhinney *et al*[8]., to be about $6.7 \times 10^{-26}\,cm^2$. On the other hand, $Cu^{63}(e\,;n, e')Cu^{62}$ was studied by Skaggs *et al.*[21] by bombarding electrons of 22 Mev directly upon the target. They obtained the electro-disintegration cross section of this reaction for 17.5 Mev electron as $32 \times 10^{-29}\,cm^2$, from which the photo-disintegration cross section is expected to be about $13 \times 10^{-26}\,cm^2$ by taking the cross section for photo-disintegration by $h\nu$ above threshold energy approximately 400 times that for electro-disintegration.

As mentioned above the values obtained from betatron experiments are considered in general to be rather in large error, and values given so far by several workers differ to a great extent. In the present state of knowledges the value $8.5 \times 10^{-26}\,cm^2$ obtained by the present experiment is, then, considered to be most close to the fact, nevertheless we have a prospect of obtaining a more accurate value when the ratio of cross sections for 14.8 Mev $h\nu$ and 17.6 Mev $h\nu$ would be precisely measured as described in this discussion.

VI. Acknowledgments

The author desires to express his sincere appreciation for the encouragement and many helpful discussions given by Professors Bunsaku Arakatsu and Kiichi Kimura. It is also a pleasure to acknowledge his indebtedness to his colleagues who have been in cooperation during the experiment. Messrs. Y. Uemura and S. Yasumi were particularly responsible for the operation of the high voltage machine. Messrs. Y. Saji, R. Ishiwari and J. Muto have helped greatly in the measurements and the preparation of samples. Mr. M. Sonoda generously informed the author the theoretical values of counting efficiency of the gamma-ray counter before publication. Finally, the work was financially supported by the special fund of the Ministry of Education for the Advancement of Science.

Nuclear Research Laboratory,
Department of Physics,
Faculty of Science, University of Kyoto.

20. J. L. Lawson and M. L. Perlman, Phys. Rev. **74** (1948), 1190.
21. L. S. Skaggs, J. K. Laughlin, A. O. Hanson, and J. J. Orlin, Phys. Rev. **73** (1948), 420.

INDEX OF AUTHORS TO VOLUME XXV

PAGE

Fujiki, Y.—On the Molecular Arrangement of Some Organic Films. 119

Hirata, H., Koyama, M. and **Yasuda, K.**—On the "Precursory Recrystallization" in Copper and Brass Foils prepared by the Mechanical Rolling. 127

Ishiwari, R. and **Yuasa, K.**—A Decade Scaling Circuit. 155

Iwase, K. and **Sano, T.**—Residual Stress in Iron Alloys Variously Heat-Treated. 159

Kabata, M.—On the Structure of Inter-crystalline Boundaries of Metals. I. . . 1

Kabata, M.—On the Structure of Inter-crystalline Boundaries of Metals. II. . . 45

Kanitani, J.—On a Generalization of the Projective Deformation. 23

Kanitani, J.—On a Property of the Conjugate Net in Connexion with Generalized Projective Deformation. 41

Kanitani, J.—On a Method of Plunging of R_2 with Symmetric Projective Connexion into a Projective Space S_4. 87

Kodera, K. (see **Sasaki, N.** and **Kodera, K.**) 83

Koyama, M. (see **Hirata, H., Koyama, M.** and **Yasuda, K.**) 127

Matsumoto, T.—Iteration of Elliptic Functions. 27

Matsushima, S. (see **Miyamoto, S.** and **Matsushima, S.**) 63

Mitani, K. (see **Sasaki, N., Taku, K.** and **Mitani, K.**) 75

Mitani, K. (see **Sasaki, N.** and **Mitani, K.**) 79

Mitani, K. (see **Takahashi, I.** and **Mitani, K.**) 111

Miyamoto, S.—On the Ultra-violet Radiation from the Solar Corona. I. . . . 31

Miyamoto, S. and **Matsushima, S.**—On the Ultra-violet Radiation from the Solar Corona. II. 63

Muto, J. (see **Shimizu, S.** and **Muto, J.**) 61

Nishioka, S.—Thermal Conductivities of Single- and Polycrystalline Bismuth. . 147

Okugawa, K.—Basis-Theorem concerning Differential Polynomials. 93

Okugawa, K.—Linear Conditions at a Point. 99

Sano, T. (see **Iwase, K.** and **Sano, T.**) 159

Sasaki, N.—A New Method for Surface Temperature Measurement. 37

Sasaki, N., Taku, K. and **Mitani, K.**—The Exchange Efficiencies of the Translational and the Internal Energy of Gas Molecules on Solid Surfaces. I. Measurement by Means of Molecular Beams. 75

Sasaki, N. and **Mitani, K.**—The Exchange Efficiencies of the Translational and the Internal Energy of Gas Molecules on Solid Surfaces. II. Measurement by Means of a Vibrating Hot Filament. 79

Sasaki, N. and **Kodera, K.**—On the Direct Measurement of the Effective Collision Radii of Potassium with Chlorine and Other Gases. 83

Shimizu, S. and **Muto, J.**—A Note on the Angular Distribution of Pair-electrons of 17 Mev γ-Rays. 61

Shimizu, S.—Photo-induced Reaction Cu^{63} (γ, n) Cu^{62} produced by the Gamma-Rays of Lithium bombarded with High Speed Protons. 193

Sododa, M.—A Type of Geiger-Müller Counter suitable for the Measurement of High Energy Gamma-Rays. 175

Sonoda, M.—On the Proportional Counter. 185

PAGE

Takahashi, I.—One Possibility of Oscillation caused by Electrons in a Constant Magnetic Field. 11

Takahashi, I.—On the Possibility of Barkhausen-Kurz Oscillation. I. 15

Takahashi, I.—On the Possibility of Barkhausen-Kurz Oscillation. II. 55

Takahashi, I.—A Wave-mechanical Treatment of the Electron Oscillation . . . 103

Takahashi, I. and **Mitani, K.**—On the Electronic Admittance in Reflex Klystron. I. 111

Takasu, K.—Microclimatic Study. I. A New Type Self-Recorder. 69

Taku, K. (see **Sasaki, N., Taku, K.** and **Mitani, K.**) 75

Yasuda, K. (see **Hirata, H., Koyama, M.** and **Yasuda, K.**) 127

Yuasa, K. (see **Ishiwari, R.** and **Yuasa, K.**) 155

昭和二十四年十二月二十五日　印刷
昭和二十四年十二月三十一日　發行

編輯兼發行者　京都大學理學部

印刷者　河北印刷株式會社
代表者　河北喜四良
京都・二條・堺町

CONTENTS

On a Method of Plunging of R_2 with Symmetric Projective Connexion into a Projective Space S_4

BY *Joyo Kanitani* 87

Basis-Theorem concerning Differential Polynomials

BY *Kôtaro Okugawa* 93

Linear Conditions at a Point

BY *Kôtaro Okugawa* 99

A Wave-mechanical Treatment of the Electron Oscillation

BY *Isao Takahashi* 103

On the Electronic Admittance in Reflex Klystron. I

BY *Isao Takahashi* AND *Kenji Mitani* 111

On the Molecular Arrangement of Some Organic Films

BY *Yoshibumi Fujiki* 119

On the "Precursory Recrystallization" in Copper and Brass Foils prepared by the Mechanical Rolling

BY *Hideki Hirata, Masashige Koyama* AND *Katsuyuki Yasuda* 127

Thermal Conductivities of Single- and Polycrystalline Bismuth

BY *Shigeka Nishioka* 147

A Decade Scaling Circuit

BY *Ryutaro Ishiwari* AND *Kazunori Yuasa* 155

Residual Stress in Iron Alloys Variously Heat-Treated

BY *Keizo Iwase* AND *Tadao Sano* 159

A Type of Geiger-Müller Counter suitable for the Measurement of High Energy Gamma-Rays

BY *Masateru Sonoda* 175

On the Proportional Counter

BY *Masateru Sonoda* 185

Photo-induced Reaction Cu^{63} (γ, n) Cu^{62} produced by the Gamma-Rays of Lithium bombarded with High Speed Protons

BY *Sakae Shimizu* 193